Radiosynthesis and Optimization of ^{18}F-Fluorinated GW2580 Derivatives as A Dual Trk/CSF-1R Radiotracer for Potential Use in PET Imaging

by

Sang Ho Choi

A thesis submitted in partial fulfillment of the requirements for the degree of

Master of Science

in

Experimental Oncology

Department of Oncology

University of Alberta

Abstract

As one of the medical imaging modalities applied in clinical diagnosis of various diseases, positron emission tomography (PET) is used to non-invasively visualize cellular and molecular changes that are occurring in the human body. Fluorine-18 [^{18}F] is the most widely used radionuclide for development of radiotracers due to its favorable decay properties. A key process in developing radiotracers for PET imaging is selecting a target with a particular set of cellular and molecular properties that is expected to have therapeutic utility. As a member of the tyrosine kinase family, tropomyosin receptor kinase (Trk) and colony stimulating factor-1 receptor (CSF-1R) have been demonstrated to be valuable for cancer prognosis and are potential therapeutic targets for cancer treatment due to their diverse involvement in tumor regulation. As a result, development of radiotracers for these targets would allow identification of patients suitable for Trk/CSF-1R targeted therapy, improve prognosis, and offer a non-invasive method for *in vivo* visualization of treatment response. Being able to differentiate patients based on tumor characteristic, such as *NTRK* gene fusion, would ultimately lead to an improved personalized therapy reducing toxic side effects and low drug responses that are often associated with generalized chemotherapy.

In this M.Sc thesis, two new fluorinated analogues **3.0** and **3.1** were synthesized based on the structure of a selective pan-Trk and CSF-1R inhibitor, GW2580. Initial molecular docking studies of **3.0** and **3.1** against TrkB crystal structure suggested similar binding potency as GW2580 (TrkB: IC$_{50}$ = 56 nM). However, *in vitro* binding assay demonstrated a 2-fold decrease in binding potency for **3.0** (TrkB: IC$_{50}$ = 123 nM) and a 30-fold decrease in binding potency for **3.1** (TrkB: IC$_{50}$ = 1690 nM). The decrease in binding potency for both **3.0** and **3.1** was attributed to unfavorable electrostatic interactions between the methyl/fluorine substituents and amino acid residues within the binding site. However, when the binding potency of **3.0** was compared to a previously studied derivative of GW2580, **1.23** (TrkB: IC$_{50}$ = 132 nM), by the Schirrmacher Group, both compounds demonstrated a similar binding potency.

Due to the significant decrease in binding potency of **3.1**, only **3.0** was considered for radiosynthesis. The boronic ester precursor **4.8a** was synthesized and subjected to a Cu-catalyzed

two-step (labelling/deprotecting) radiofluorination method to access $[^{18}F]$**3.0**. However, unfavorable steric interactions between the *ortho*-methoxy substituent and the Cu-catalyst prevented radiofluorination of **4.8a**, therefore preventing the development of $[^{18}F]$**3.0**.

In order to avoid a methoxy substituent *ortho* to the boronic ester, radiosynthesis of $[^{18}F]$**1.23** lacking the *ortho*-methoxy group was chosen. Even though radiosynthesis of $[^{18}F]$**1.23** was previously achieved by the Schirrmacher Group, it was accessed via a multi-step radiosynthesis unsuitable for automatic synthesis. In order to avoid the multi-step radiosynthesis, boronic ester precursor **4.8b** was utilized. Radiofluorination of **4.8b** and subsequent Boc-deprotection led to a two-step radiosynthesis of $[^{18}F]$**1.23**. Due to inseparable protodeboronated side product **4.21** and unexpected Boc-deprotection during the initial radiofluorination, radiosynthesis $[^{18}F]$**1.23** afforded radiochemical yields (RCY) of only $2.5 \pm 0.5\%$, $> 99\%$ radiochemical purity (RCP), and molar activity (A_m) of $3.4 - 4.5$ GBq/µmol. Even though radiosynthesis of $[^{18}F]$**1.23** was successfully developed for potential use in preliminary studies such as autoradiography, further investigation to improve the RCY and A_m is required for human studies.

AKNOWLEDGEMENT

I wish to express my sincerest gratitude my supervisor Prof. Ralf Schirrmacher for all his guidance, support and encouragement. Prof. Schirrmacher's immense patience and unyielding support were crucial to completion of this thesis. Also thank you to the members of my MSc committee, Prof. Frank Wuest and Prof. Dennis Hall for their scientific inquiry and advice.

I am also greatly indebted to Dr. Justin Bailey for always taking time to explain new concepts and guiding me during my initial exposure to radiochemistry.

I would also like to thank Dr. Vadim Bernard-Gauthier for providing intellectual support and always engaging me in helpful discussion. The thoughtful suggestions have helped me to improve the quality of this thesis.

I thank my lab mate Sheldon Burke for always creating a pleasant working environment and thoughtful inputs towards this thesis.

I would like to further thank Alberta Cancer Foundation for providing the Antoine Noujaim Scholarship and FGSR Graduate Travel Awards for enabling me to attend the 99th Canadian Chemistry Conference and Exhibition in Toronto.

Finally, and most importantly, I would like to thank my family and friends for their support during my study and always being there for me when I need them.

Table of Content

List of Table

List of Figures

List of Schemes

List of Abbreviation

^{18}F-FDG	[^{18}F]2-fluorodeoxyglucose
Ac	acetyl
Akt	protein kinase B
A_m	molar activity
BDNF	brain derived neurotropic factor
B_{max}	total receptor density
Boc	*tert*-butyloxycarbonyl
BP	binding potential
Bpin	boronic ester
CD	chopper domain
CRD	cysteine-rich domain
CSF-1R	colony stimulating factor-1 receptor
Cu(OTf)$_2$(py)$_4$	tetrakis(pyridine)copper(II) triflate
DCM	dichloromethane
DFG	asp-phe-gly
DD	death domain
DMA	dimethylacetamide
DMF	*N,N*-dimethylformamide
DMSO	dimethyl sulfoxide
DMT	dimethoxytrityl
EDG	electron donating group
E_{max}	maximum energy
Et$_4$NHCO$_3$	tetraethylammonium bicarbonate
EtOH	ethanol
EtOAc	ethyl acetate
FMIP	Fms-interacting protein
HPLC	high performance liquid chromatography
HRMS	high resolution mass spectrometry
IC$_{50}$	half-maximal inhibitory concentration

IgL	immunoglobulin-like domain
IL-34	interleukin-34
K_{222}	Kryptofix 2.2.2
K_2CO_3	potassium carbonate
K_d	dissociation constant
KOTf	potassium trifluoromethanesulfonate
$LiAlH_4$	lithium aluminum hydride
LRR	leucine-rich repeat
Log D	distribution coefficient
Log P	partition coefficient
LOXO-101	larotrectinib
MAPK	mitogen activated protein kinase
MeCN	acetonitrile
MOM	methoxymethyl
MScore	molecular score
NaOMe	sodium methoxide
n-BuOH	*n*-butanol
NGF	nerve growth factor
NMR	nuclear magnetic resonance
Ns	nosylate
NT-3	neurotrophin-3
NT-4	neurotrophin-4
NT-5	neurotrophin-5
OMe	methoxy
OTf	triflate/trifluoromethanesulfonate
Pd	palladium
PET	positron emission tomography
PI3K	phosphoinositide 3-kinase
PLC	phospholipase C
PLC-γ2	phosphoinositide phospholipase C
PMTs	photomultiplier tubes

py	pyridine
QMA	quaternary methyl ammonium anion
RCC	radiochemical conversion
RCP	radiochemical purity
RCY	radiochemical yield
RMSD	root mean square deviation
R_f	retention factor
RT	room temperature
RXDX-101	entrectinib
SPECT	single photon emission computed tomography
SnAr	nucleophilic aromatic substitution
TAM	tumor associated macrophage
TEA	triethylamine
TFA	trifluoroacetic acid
TKD	tyrosine kinase domain
TKI	tyrosine kinase inhibitor
TLC	thin layer chromatography
TNF	tumor necrosis factor
TPM3	tropomyosin gene 3
TrkA	tropomyosin receptor kinase A
TrkB	tropomyosin receptor kinase B
TrkC	tropomyosin receptor kinase C
Ts	tosylate

1.0   Introduction

1.1   Nuclear Imaging

Nuclear imaging is based on the usage of biological probes that are labeled with a radionuclide. Emissions from the radioactive decay of the radionuclide is then detected by external cameras to visualize the distribution in the body.[1] With recent advances in nuclear imaging, visualization of radionuclides in picomolar amounts are possible.[2] In particular, the low positron energy of ^{18}F allows for detection of small tumor sizes resulting in early cancer detection and medical intervention, thus reducing the potential for tumor metastasis. In addition to early tumor detection, nuclear imaging also provides a non-invasive method for *in vivo* visualization of biological processes occurring at a molecular and cellular level.[1] As a result, information gathered by nuclear imaging benefits patient care by directing patients to appropriate therapies, measuring early treatment responses, and improved prognoses.[1] A common method of nuclear imaging is by positron emission tomography (PET).

1.1.1   Positron emission tomography (PET)

PET imaging utilizes radiopharmaceuticals labeled with a positron emitting radionuclide. Once the radiopharmaceuticals are injected into the body, they are distributed according to their molecular properties and interaction with the target site. As a function of the nuclide's half-life, the proton (p) inside the radionuclide nucleus decays into a neutron (n), a positron (β^+) and an electron neutrino (v_e) (**1**).[3]

$$\mathbf{p \rightarrow n + \beta^+ + v_e} \tag{1}$$

Once the positron is released and depending on its energy, it travels a finite distance in the tissue before being annihilated by combining with an electron from the surrounding tissue. The movement of the positron away from the original source location results in a decrease of PET

imaging spatial resolution.[4] The annihilation process results in emission of two 511 KeV photons (gamma rays) emitted at an angle of 180°. These gamma rays are then detected in coincidence by scintillator detectors, to produce a PET image after image reconstruction (Figure 1).[5]
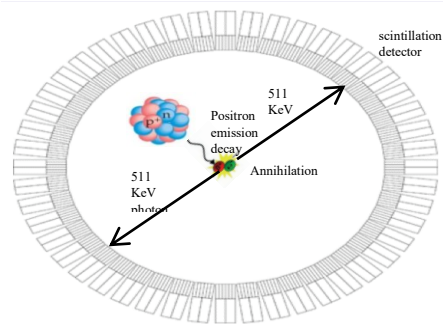
Figure 1. Schematic representation of PET imaging principle

Following the line of response drawn between two independent detectors reading a detection event at the same time, the location of the source radioisotope can be pinpointed to be somewhere on that line. However, not all lines of response correspond to the actual annihilation event of a positron decay. Materials surrounding the radioisotopes can cause the lines of response to be scattered or absorbed, resulting in incorrect determination of radioisotope origin or a loss of signal. The different types of coincidence that can be detected are: true coincidence, scatter coincidence, spurious coincidence, and random coincidence (Figure 2).[6]
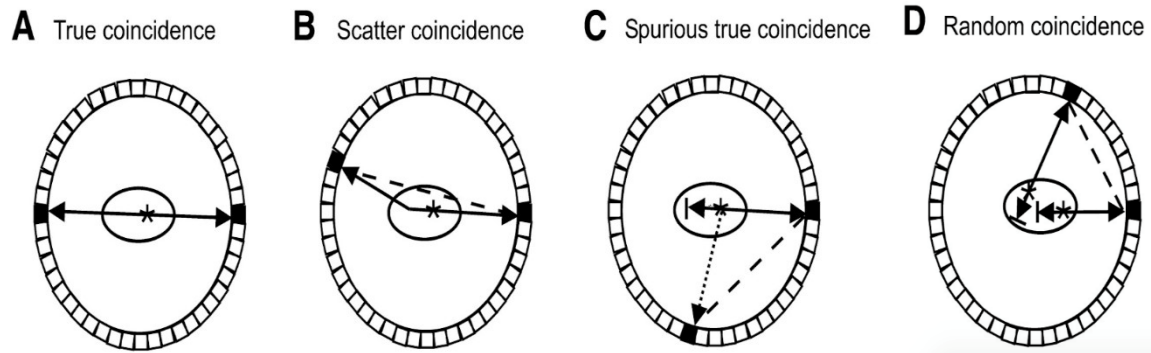
Figure 2. Illustration of the 4 major coincidences in PET imaging: true coincidence, scatter coincidence, spurious coincidence, and random coincidence. (A) True coincidence occurs when two opposite photons emitted from the positron annihilation arrive at the detector at the same time, without any scattering or absorption by the tissue. (B) Scatter coincidence is caused by one of the photons undergoing Compton scattering or electron absorption in the tissue, changing the trajectory of the photons. (C) Spurious coincidence is produced when a photon from the original radionuclide source is detected at the same time as gamma rays from a non-positron annihilation event (gamma ray from the radionuclide). (D) Random coincidence is produced when two distinct photons from different radionuclides are detected at the same time. (This image was originally published in *JNM*. Reference 6)

1.2 Radioisotope production for PET imaging

Table 1. Common organic isotopes produced from a cyclotron; and the different physical properties of radioisotopes: natural abundance, cyclotron energy range requirement, and mode of decay

Isotope	Half-life	Nuclear Reaction	Target Abundance (%)	E_{max} (MeV)	Mode of Decay (%)
^{11}C	20.4 min	$^{14}N(p,\alpha)^{11}C$	99.6	0.96	β^+ (100)
^{13}N	9.96 min	$^{16}O(p,\alpha)^{13}N$	99.8	1.19	β^+ (100)
^{15}O	2 min	$^{14}N(d,n)^{15}O$	99.6	1.72	β^+ (100)
^{18}F	109.8 min	$^{18}O(p,n)^{18}F$	0.2	0.635	β^+ (97), EC (3)

Cyclotrons are composed of three main components: an electromagnet (1.5 – 2.0 tesla), D-shaped hollow copper electrodes (*dees*), and a negative ion source for the production of H⁻ (also possible with alpha particles or deuterium ions).[7] For the production of radioisotopes such as ^{18}F, the negative ion source ionizes hydrogen gas and injects the ionized hydrogen into the center of the two dees, at which point they are accelerated by the dees due to the alternating potential generated by an oscillator.[7] Due to the oscillating potential and the magnetic field, the ions travel outwards in a spiral pattern.[8] Once the H⁻ ions reach a certain kinetic energy level (10 – 30 KeV), they pass through a thin foil of carbon (graphite) where their electrons are stripped from the nucleus and a proton (H⁺) is generated that can now engage in a nuclear reaction with the target material. The H⁺ is then directed to the target material in order to produce the desired radioisotope (Figure 3).[9] There are a wide range of radioisotopes that can be produced by cyclotrons.[8] Crucial aspects to consider include the energy of the ion required for radionuclide production and the abundance of the target material.[10,11]
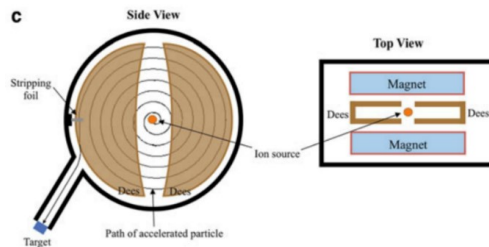
Figure 3. Schematic representation of a cyclotron. The two main components of the cyclotron are shown: two large electromagnets; and two semi-circular electrodes (*dees*) (Image reproduced from Reference 7 with permission of Springer-Verlag Berlin and Heidelberg GmbH & Co. K in the format Thesis/Dissertation via Copyright Clearance Center)

1.2.1   Fluorine-18 (^{18}F) production

The most common method of fluorine-18 production is based on the irradiation of a [^{18}O]H$_2$O liquid target with protons, according to the following nuclear reaction ^{18}O(p,n)^{18}F producing an aqueous solution of [^{18}F]fluoride.[12] Another method of production involves the usage of a ^{20}Ne gas target containing 0.1% cold [^{19}F]fluorine gas. ^{20}Ne(d,α)^{18}F reaction yields [^{18}F]F$_2$ gas at low specific activities.[13] There are other methods of ^{18}F production however, due to high energy consumption and uncommon ion sources they are rarely used (Table 2).

Table 2. Multiple nuclear reactions of ^{18}F production

Nuclear reaction	Useful energy range (MeV)	Natural abundance (%)
^{18}O(p, n)^{18}F	14-4	0.2
^{16}O(^{3}He, p)^{18}F	15-1	99.7
^{16}O(^{3}He, n)^{18}Ne: ^{18}F	40-15	99.7
^{16}O(α, np)^{18}F	40-20	99.7
^{16}O(α, 2n)^{18}Ne: ^{18}F	52-10	99.7
^{20}Ne(d, α)^{18}F	15-0	90.5
^{20}Ne(p, 2pn)^{18}F	40-30	90.5

1.3 [^{18}F]2-Fluorodeoxyglucose (^{18}F-FDG)

The most commonly used PET imaging agent is [^{18}F]2-fluorodeoxyglucose (^{18}F-FDG), a fluorinated glucose analogue used in oncology for tumor localization, tumor size detection, and assessment of treatment response.[14] In addition to usage in oncology, ^{18}F-FDG has demonstrated to be extensively involved in neurology. By observing ^{18}F-FDG uptake in the brain, cerebral glucose metabolism can be non-invasively observed and morphological changes identified.[15] In this regard, ^{18}F-FDG is commonly used in clinical settings for evaluation of epilepsy and Alzheimer's disease.[16] Increased glucose transporter 1 (Glut-1) in tumor cells up-regulates the uptake of glucose and ^{18}F-FDG in tumor cells. Once in the tumor cell, the ^{18}F-FDG is converted to ^{18}F-FDG-6-phosphate by hexokinases. Due to the fluorine present in the glucose derivative, the compound is unable to be further metabolized and accumulates in the tumor cells (Figure 4), allowing for the imaging of tumor cells via metabolic trapping. However, a major limitation of ^{18}F-FDG is found when imaging tumors in the brain; the high metabolic activity of the brain in its natural state causes a high background uptake of ^{18}F-FDG, resulting in low tumor-to-background contrast.[17]
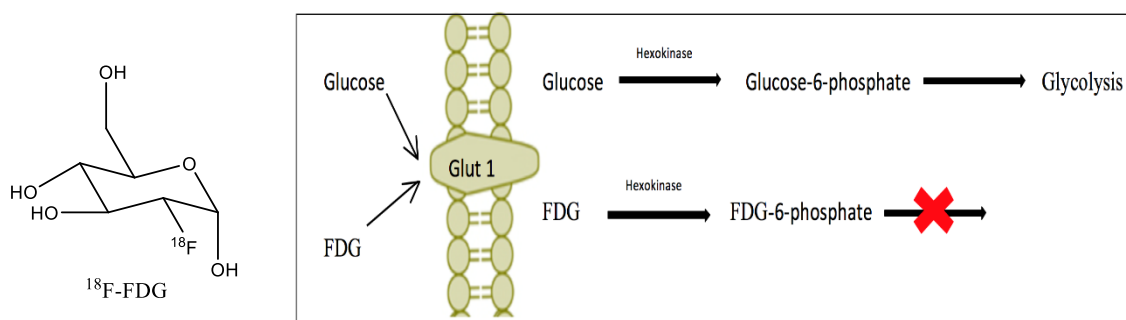
Figure 4. Chemical structure of ^{18}F-FDG and metabolic trapping mechanism of FDG. Comparison of Glucose and FDG metabolic pathway. FDG remains in the intracellular matrix unable to be utilized in the mitochondria for glycolysis. However, glucose remains unhindered and undergoes glycolysis.

1.4   Development of receptor-ligand based radiotracer: rationale design

When developing PET imaging tracers different properties have to be taken into consideration such as tumor selectivity, binding affinity, *in vitro* absorption, distribution, metabolism, and excretion.[18] While these vast libraries may provide multiple leads for PET imaging, it is impractical to develop all compounds into radiotracers. It is essential to be able to distinguish compounds with the most potential to become suitable radioligands for PET imaging from those that are unlikely to succeed. Some of the factors that must be taken into considerations for radiotracer development are lipophilicity, binding affinity/potency, and binding selectivity

1.4.1   Lipophilicity

Lipophilicity is used to determine the ability of a compound to dissolve in a hydrophobic environment. When designing a receptor-ligand based radiotracer, it is crucial to look at the lipophilicity of the compound. The lipophilicity of a drug contributes to membrane permeability, potency, selectivity, and metabolism/pharmacokinetic. The lipophilicity of a compound is commonly reported as either the partition coefficient (log P) or distribution coefficient (log D). Log P is determined by the partition coefficient of unionized species between the aqueous (water) and lipophilic (octanol) phase, and log D is expressed as the partition coefficient of all species (unionized and ionized) at physiological pH 7.4. It has been found that compounds with low lipophilicity often display problems with membrane permeability in tumor tissues and are cleared rapidly by the kidneys, reducing the availability of drug for its target receptor.[19] On the other hand, compounds with high lipophilicity are often associated with high binding towards plasma proteins such as serum albumin leading to decreased drug concentration in the blood plasma and increased non-specific binding.[20] As a result, log P or D values between 1 and 3 yield the most optimal radiotracer properties with reduced clearance rate, increased drug availability for target-specific binding, and decreased non-specific binding to plasma proteins.[20]

7

1.4.2   Binding affinity and binding potency

Binding affinity is another essential property of a radiotracer and is used to describe the strength with which a ligand binds to a receptor. One of the ways to report the binding affinity of a ligand is through the dissociation constant (K_d). K_d is used to quantify the noncovalent interaction between the desired ligand and its target proteins. The dissociation constant is defined as K_d = [L][P]/[LP] where the ligand-protein complex (LP) concentration is in an equilibrium with free ligand (L) and free protein (P).[21] Observing this equation, it can be inferred that for low binding affinity ligands, the K_d value would be high due to higher concentrations of [L] and [P]. Ligands with high binding affinity would have higher ligand-protein concentrations resulting in lower K_d value.[21]

The half maximal inhibitory concentration (IC_{50}) is also commonly used to measure the potency of a desired substance in inhibiting protein function. While IC_{50} is not a direct indicator of binding affinity, it is a useful value for the relative comparison of drug molecules inhibition strength. The evaluation of an IC_{50} value of a ligand-receptor system depends on the concentration of the competitive inhibitor.[22] IC_{50} values are determined *in vitro* by inhibition assays in constructing a dose-response curve.[22] A ligand with high binding potency would result in a low IC_{50} value since minimal amounts of the ligand is required to inhibit 50% of the protein's activity. Hence, a ligand with low potency would require high concentration of the ligand to observe the same inhibition resulting in a high IC_{50} value.

Even though a high binding affinity is beneficial for a PET radiotracer, it is not the only important factor. An essential property that must also be optimized for radiotracer development is its binding potential (BP).[23] BP takes into account both the total biological target density (B_{max}) and the K_d value to measure *in vivo* radiotracer-target interaction. BP is defined as B_{max}/K_d and it is generally accepted that a BP of at least 5 is suitable for PET imaging. Also in a clinical setting, it is suggested that a BP with a minimal value of 10 is required to develop a site-specific radiotracer for PET imaging.[24] Therefore, BP suggests that radiotracers with low binding affinity can still be used for

PET imaging as long as the target receptor is expressed in high density. For the successful development of radiotracers, the target protein should be expressed with high B_{max} and demonstrate a significant change in density or occupancy as a tumor characteristic.[23]

1.4.3 Binding selectivity

Another property of an ideal radiotracer would be having selectivity towards only the desired target. In order to determine the binding selectivity, binding affinity of a ligand has to be tested against the target receptor and any other potential targets. Selective ligands would only have binding affinity towards the desired target while non-selective ligands would have binding affinity towards numerous targets. In addition, drug selectivity also depends on the density of the target proteins vs off-target proteins.[23] Also in cases where the off-target protein expression has minimal anatomical overlap with the target protein expression, selectivity may not be an issue.[23] Even in situations where there is an anatomical overlap, if the receptor density of the target protein greatly exceeds the off-target protein density, radiotracers with low selectivity may still be used for PET imaging.[23]

1.5 Radiofluorination

After determining the lead compound for potential PET imaging, a suitable method of radiolabeling must be identified. The favorable half-life of ^{18}F isotopes (109.8 min) compared to ^{11}C (20.4 min) makes it the more prominent radionuclide used for PET imaging.[25] Also, the positron released from ^{18}F isotopes has lower maximum energy (0.64 MeV), compared to ^{11}C (0.97 MeV), allowing for less energy deposits into tissues and a smaller positron range (max 2.4 mm). This results in a PET image with a higher spatial resolution.[26] When reviewing radiolabeled compounds, it is important to take three factors into consideration: radiochemical yield (RCY), molar activity (A_m) and radiochemical purity (RCP).[27] The RCY is defined by the amount of radioactivity recovered in the purified radiolabeled compound in comparison to the initial starting amount of radioactivity. RCY can be reported as isotopic decay corrected yield or the uncorrected yield. The A_m, on the other hand, is defined by the ratio of the amount of radioactivity of the ^{18}F-

labeled compound to the total number of molecules (any isotopic species) and reported for example as GBq/μmol. Typical A_m value of PET radiotracers are in the order of 50-500 GBq/μmol.[28] Also since PET imaging only requires tracer doses (low or sub-micro gram levels) of the radiolabeled compound, distribution of radiotracers can be studied *in vivo* without any pharmacodynamic effect.[28] A_m is especially important when dealing with toxic compounds or human studies.[28] Lastly, RCP is defined by the ratio of radioactivity from the desired radiolabeled species versus the total radioactivity present in a sample. High RCP is important for producing an accurate PET imaging since signals should only be produced by the desired radiolabeled species.

1.5.1   Electrophilic fluorination

Electrophilic fluorination was commonly used during the development of the first fluorine-18 labeled radiotracers. However, in recent years, many of these reactions have been replaced by newer nucleophilic fluorination methods. A crucial problem with electrophilic fluorination stems from the addition of carrier $[^{19}F]F_2$ when extracting the radioactivity from the cyclotron target. As a result of an ^{19}F atom being present in every $[^{18}F]F_2$ molecule only half of the fluorinated compounds would contain ^{18}F while the remaining half would contain ^{19}F. Therefore, the maximum theoretical yield of electrophilic radiofluorination is limited to 50%. Due to problems such as non-specific reaction and side-product formation resulting in low RCY and A_m, recent methods prefer the use of nucleophilic fluorination.

1.5.2   Nucleophilic fluorination

The irradiation of $[^{18}O]H_2O$ is a non-carrier (no fluorine-19 added) reaction, resulting in a high A_m (maximum possible A_m of 63.3 TBq/μmol). The final radioactive product is ^{18}F-fluoride dissolved in water. However, when fluoride ions are in an aqueous environment, the ions become poor nucleophiles due to interactions with hydrogen ions and thus hinder chemical reactivity. To isolate the $^{18}F^-$ ions from the aqueous environment, quaternary ammonium anion (QMA) exchange cartridges are used. First, the water-containing $^{18}F^-$ ions are run through the QMA cartridge to trap

the [18]F⁻ ions. The trapped fluoride ions are then eluted with a solution containing a cryptand, such as Kryptofix 2.2.2 (K$_{222}$), and an alkaline metal salt—most commonly, potassium carbonate (K$_2$CO$_3$).[29] The residual water must be fully removed by azeotropic drying with acetonitrile *in vacuo* under a stream of inert gas such as argon, helium, or nitrogen. The dried ^{18}F-fluoride ion can then be used for an array of radiolabeling methods, such as aliphatic nucleophilic fluorination, nucleophilic aromatic fluorination, and transition metal-mediated fluorination.[29] Most ^{18}F radiofluorination work best in aprotic solvents such as *N,N*-dimethylformamide (DMF), acetonitrile (MeCN), or dimethyl sulfoxide (DMSO), since protic solvents reduce the nucleophilicity of [^{18}F]fluoride due to hydrogen bonding and interactions with a partial positive charge of the solvents.[30] However, there have been cases where radiofluorination was carried out in the presence of polar protic solvents without the need to remove [^{18}O]H$_2$O.[31-34] For example, Chun *et al* (2013) have demonstrated radiofluorination of diaryliodonium salts using a mixture of [^{18}O]H$_2$O and [^{18}F]F⁻ resulting in RCYs up to 50%.

Also, it has been demonstrated that using K$_{222}$ and K$_2$CO$_3$ for [18]F⁻ processing is detrimental to novel radiofluorination approaches involving transition-metal catalysis such Cu(OTf)$_2$.[35] Although it is unclear as to why K$_{222}$ and K$_2$CO$_3$ is detrimental to Cu-catalyzed radiofluorination, Mossine *et al* (2017) have suggested that formation of copper adducts might contribute to the problem.[35] For example, Mossine *et al* (2017) have also demonstrated that using [18]F⁻ eluted using either potassium trifluoromethanesulfonate (KOTf) or dimethylaminopyridine (DMAP) without the use of cryptands (K$_{222}$) resulted in significant improvements in RCY of Cu-catalyzed radiofluorination of boronic acid derivatives.[35]

1.5.2.1   Aliphatic nucleophilic fluorination

Aliphatic nucleophilic fluorination is a method of radiolabeling with [^{18}F]fluoride by an S$_N$2 mechanism. Aliphatic nucleophilic fluorination is often a one-step synthesis without the use of protecting groups and standard leaving groups such as tosylate, halides, triflate, and mesylate are applied.[29] However, the precursors often require one or more protecting groups, such as tert-

butyloxycarbonyl (Boc), dimethoxytrityl (DMT), nosylate (Ns), acetyl (Ac), trifluoromethanesulfonate (OTf), methylester (OMe), tosylate (Ts), and methoxymethyl ether (MOM), which result in a two-step synthesis (Figure 5).
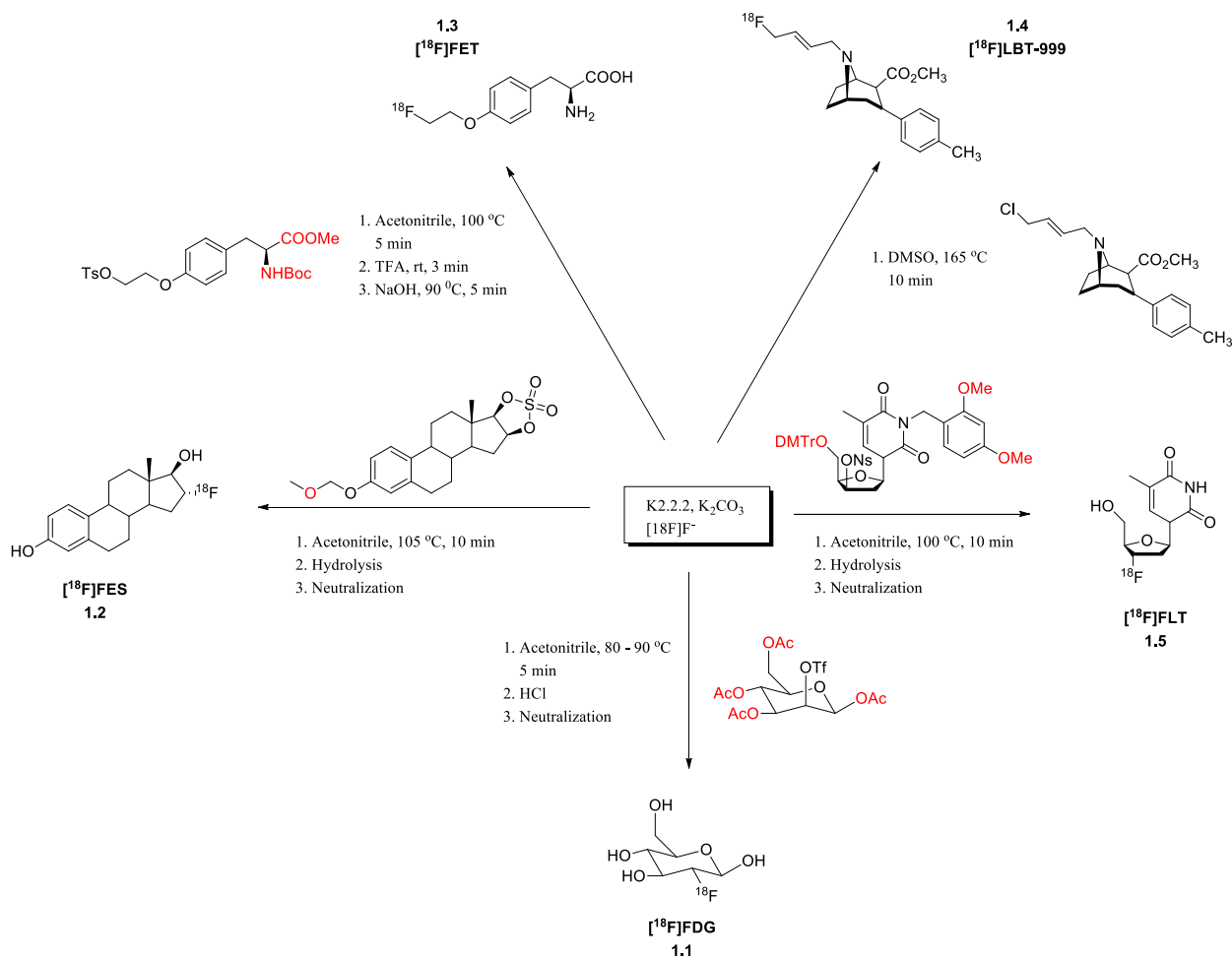
Figure 5. Different leaving groups used for aliphatic nucleophilic radiofluorination. The scheme illustrates the synthesis of radiotracers from a variety of precursors with protecting groups and good leaving groups, such as halide (e.g. [18F]LBT-999), nosylate (e.g. [18F]FLT), triflate (e.g. [18F]FDG), cyclic sulfonate (e.g. [18F]FES), and tosylate (e.g. [18F]FET).[36-40]

1.5.2.2   Nucleophilic aromatic fluorination

Traditionally, for aromatic fluorination to occur, it is essential to have an electron withdrawing group located either in the ortho or para position to the leaving group within the aromatic system. Without the electron withdrawing group, the aromatic ring is generally not reactive enough to undergo an nucleophilic aromatic substitution (S_NAr) reaction.[27] Several methods have been developed for labeling [18F]-fluoroarenes from [18F]F-. Early methods of aromatic fluorination did not utilize electron withdrawing groups; instead, they directly labeled aromatic rings. Such methods involved Balz-Schiemann reactions, which utilized diazonium tetrafluoroborate salt[41], or a Wallach reaction, which utilized triazene-based arenes (Figure 6).[42] However, both the Balz-Schiemann reactions and the Wallach reaction are seldom used in the present because of their low RCY.[43]
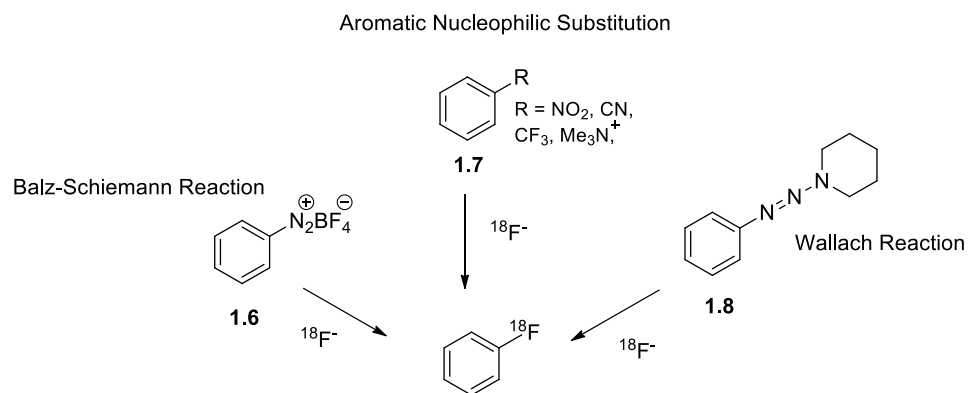
Figure 6. Traditional radiosynthetic approaches of nucleophilic aromatic fluorination.

Another method of nucleophilic aromatic fluorination utilizes the activation of aromatic rings by electron withdrawing groups such as –NO_2, -CN, -CF_3, or carbonyl groups in the *ortho* or *para* position to the leaving group. The most commonly used leaving groups for nucleophilic aromatic substitution are trimethylammonium or nitro groups (**1.7**).[44] However, the formation of the side product, [18F]methyl fluoride, might causes the overall RCY to decrease significantly.[45] Both trimethylammonium and nitro leaving groups require the reaction to occur at high temperatures in a polar aprotic solvent. As a result, this condition limits the types of precursors that can be utilized

13

due to potential decomposition of target molecules.[44] Regardless of these drawbacks, trimethylammonium and nitro groups are still commonly used to produce many different PET tracers.[44]

1.5.2.3   Radiofluorination of non-activated aromatic systems

In recent years, there has been an increase in the study of novel methods of "late-stage fluorination," of non or only weekly activated aromatic systems. This is the concept of introducing fluorine to complex molecules with chemo and stereoselectivity, near the end of the synthetic process has gained much attraction lately.[46] To address the problem to efficiently radiolabel non-activated aromatic systems, one of the earliest experiments were done using strong electrophiles such as diaryliodonium salts to introduce $^{18}F^-$ (Figure 7A). These experiments produced RCY between 30% and 70%.[47] However, the difficult precursor synthesis and the necessity for high reaction temperatures limited diaryliodonium salts' practical usage at first.[47] To improve the use of diaryliodonium salt chemistry, different types of precursors, such as iodonium ylides, were employed (Figure 7B).[48] However, the instability of the precursor led to the development of a more stable iodonium ylide precursor with spirocyclic structures (Figure 7C).[49]
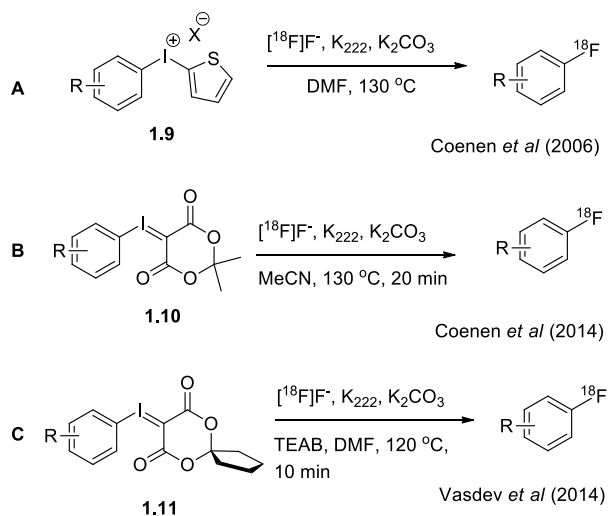
Figure 7. Examples of different diaryliodonium precursors that have been used for nucleophilic radiofluorination.

Another method for the nucleophilic [^{18}F]fluorination of designated electron-rich aromatic rings employs transition metal catalysts. Initial work by Hooker and Ritter employed palladium (Pd) complexes to accelerate the rate of radiofluorination.[50] Unlike common methods of nucleophilic fluorination, which involve [^{18}F]KF for fluorination, Hooker and Ritter developed an electrophilic fluorinating reagent based on [^{18}F]fluoride and Pd(IV) complexes.[50] Afterwards, the [^{18}F]Pd(IV)F complex was used to fluorinate Pd(II) aryl compounds to achieve the desired radiolabeled compound.[50] However, the instability of the [^{18}F]Pd(IV)F complex when exposed to air and moisture has limited its usage in the radiochemistry community.[51] To avoid problems resulting from Pd catalysts, Hooker and Ritter utilized aryl nickel (Ni) complexes for radiofluorination.[52] The authors developed a one-step electrophilic fluorination method from [^{18}F]Fluoride, Ni(II) aryl complex, oxidant, and 18-crown-6.[52]

Even though improvements have been made with aryl radiofluorination mediated by Ni and Pd catalysts and precursors, these compounds are still difficult to synthesize, and they are not commercially available.[53] In another study, Gouverneur and co-workers developed a simpler method of direct nucleophilic ^{18}F fluorination to (hetero)arenes from easily prepared precursors.[53] This newly developed method converts pinacol-derived aryl boronic esters (Bpin) into ^{18}F arylfluoride by using copper complex [Cu(OTf)$_2$(py)$_4$] (py = pyridine), [^{18}F]KF/K$_{222}$, DMF, heated

at 110 °C for 20 minutes (Figure 8A).[53] Also, even though the mechanism of the Cu-catalyzed radiofluorination is not well understood based on mechanisms proposed by Sanford Group, the hypothesized mechanism is shown in Figure 8B.[54-55]
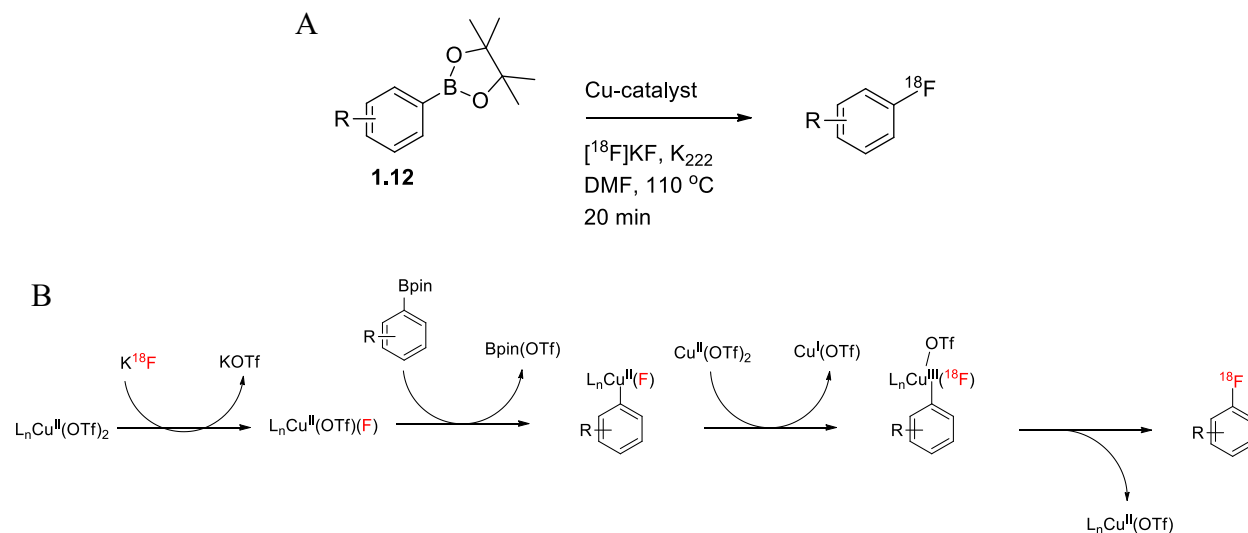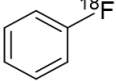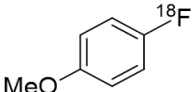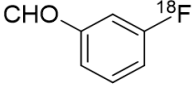
Figure 8. General scheme of Cu-catalyzed radiofluorination of aryl boronic ester and the hypothesized Cu-catalyst radiofluorination mechanism.

Using this method of radiofluorination, a series of Bpin precursors were tested with RCY ranging from 5% to 83%.[53] However, a study conducted by Zlatopolskiy *et al* demonstrated that the conventional elution of $^{18}F^-$ using high amounts of K_2CO_3 from QMA cartridges has a detrimental effect on copper-mediated radiofluorination reactions.[56] The radiofluorination of Bpin precursors based on low base conditions had RCY of 41% - 64% versus high base conditions with RCYs of 5% - 7% (Table 3).[56]

Table 3. Comparison of RCYs between high and low base conditions of different [^{18}F]aryl fluorides synthesized from Neumaier Group's Bpin precursors.

	RCY (%)	
Product	High base (2.8 mg)	Low base (0.06 mg)
1.13	5	64
1.14	7	42
1.15	7	41

To avoid strong basic radiofluorination environment that arise from the use of K_2CO_3, Scott's Group developed a different method for ^{18}F$^-$ elution from QMA via potassium trifluoromethanesulfonate (KOTf) with a minimal addition of K_2CO_3 (50 µg).[57] The use of commercially available Cu-catalyst, Cu(OTf)$_2$(py)$_4$, is prone to degradation; therefore, to avoid complications that might arise from using degraded catalyst, the Cu-catalyst was synthesized by combining Cu(II)OTf$_2$ with pyridine (1:25 ratio) *in situ*.[57] Using (4-acetylphenyl)boronic acid (**1.16**) as an example, Scott's Group was able to demonstrate that the newly optimized radiofluorination obtained an RCY of 51%, whereas the Gouverneur method of radiosynthesis obtained 0% RCY (Table 4).[57] This study also demonstrated that the synthesized Cu-catalyst catalyzed the reaction as effectively as the commercially available Cu-catalyst.[57]

Table 4. Study done by the Scott's Group comparing the RCYs between KOTf vs K_2CO_3, and commercially available Cu-catalyst vs Cu-catalyst formed during radiosynthesis.
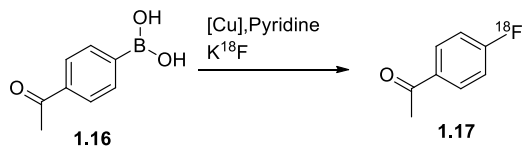
QMA eluent	[Cu]	RCY (%)
K_2CO_3	$Cu(OTf)_2$ [1]	0
K_2CO_3	$Cu(OTf)_2(py)_4$ [2]	0
KOTf/ K_2CO_3	$Cu(OTf)_2$ [1]	61 ± 8
KOTf/ K_2CO_3	$Cu(OTf)_2(py)_4$ [2]	51 ± 7

1. *In-situ* synthesized Cu-catalyst
2. Commercially available Cu-catalyst

1.6   Tropomyosin Receptor Kinase (Trk)

1.6.1   Neurotrophins

Neurotrophins are a family of closely related proteins that are responsible for the regulation of the central nervous system.[58] The four neurotrophins characterized in mammals are the nerve growth factor (NGF), the brain-derived neurotropic factor (BDNF), neurotrophin-3 (NT-3), and neurotrophin-4/5 (NT-4/5) (Figure 9).[59]
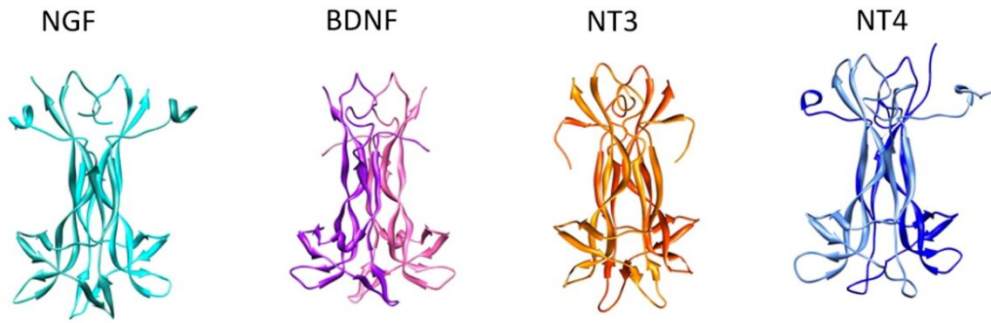
Figure 9. X-ray crystal structures of four different neurotropic factors. NGF (cyan) is taken from 1WWW.pdb; the BDNF structure is a modeled homodimer using 1BND.pdb template; NT3 (orange) is from 1BUK.pdb in complex with two p75 receptors; and NT4 (blue) is taken from 1HCF.pdb, in complex with TrkB. (Image adapted from reference 58 with permission from Elsevier)

These neurotrophins are responsible for neurogenesis, differentiation, cell migration, synaptic plasticity, neuronal survival, and synaptogenesis.[60] The target organs release these neurotrophins in limited quantities, which maintains a balance between the size of the organs and the number of neuronal innervations.[61] The first neurotrophin, NGF, was discovered when it was isolated and observed to support the survival of spinal neurons in a cell culture.[62] Following the discovery of NGF, a second neurotrophin, BDNF, was discovered when a certain portion of neuronal population responded to a neurotrophin homologous to NGF.[63] Neurotrophins NT-3 and NT-4/5 were discovered by analyzing the conserved sequences and comparing them to other proteins with the same amino acid sequences.[64,65] Similar to other growth factors, the neurotrophins are initially synthesized from a single codon exon as proneurotrophins (31-35 kDa),[66] which are composed of a hydrophobic N-terminal pro-domain and C-terminal mature domain.[67] Once the proneurotrophins are translated, the mature domains interact to form a non-covalent dimer due to their cysteine knot-like structures.[68] The proneurotrophins are converted into mature neurotrophins (~13 kDa) by intracellular proteases such as proconvertase furin, plasmin in the Golgi or organelles such as endoplasmic reticulum and secretory vesicles.[66] Formation of endogenous mature neurotrophins are able to bind to Trk receptors with high affinity, potentially competing against the radiolabeled small molecule Trk inhibitors.

1.6.2   Neurotrophin receptor—Trk

The Trk receptors are the primary binding sites for the neurotrophins.[69] The *NTRK1* (*trkA*) oncogene was first identified in colon carcinoma patients due to somatic rearrangement, which caused tropomyosin and protein tyrosine kinase domains to fuse.[70] By using a *NTRK1* derived probe, two other *trk* oncogenes, namely *NTRK2* (*trkB*) and *NTRK3* (*trkC*), were found.[71] The Trk family is composed of three homologous transmembrane receptors: TrkA, TrkB, and TrkC.[72] These Trk receptors are then preferentially bound by their primary neurotropic ligands to become activated. Nerve growth factor binds to TrkA, while BDNF and NT-4 bind to TrkB, and NT-3 binds to TrkC.[72] However, binding of these ligands to their non-primary receptors does occur depending on the cell-type, receptor structure, receptor-receptor interaction, and neurotrophin concentrations.[73-74] For example, there have been studies that demonstrated that TrkA/TrkB receptors may also be activated by NT-3.[74]

1.6.3   The Trk receptor structure

The Trk receptors are composed of two distinct domains: extracellular and intracellular.[75] The extracellular domain consists of the N-terminus region of the amino acid sequence, and it is divided into five subdomains: one leucine-rich motif (three tandem repeats), two cysteine clusters, and two immunoglobulin-like subdomains (Figure 10).[76] The binding specificity and affinity of neurotrophins to Trk are mainly determined by the second immunoglobulin-like subdomain.[77] The intracellular domain contains the C-terminus region, and it is mainly composed of the tyrosine kinase subdomain. The tyrosine kinases in the intracellular domain are highly conserved between the three Trk receptors (~80% amino acid similarity), unlike the extracellular domain (~30% amino acid similarity).[78]
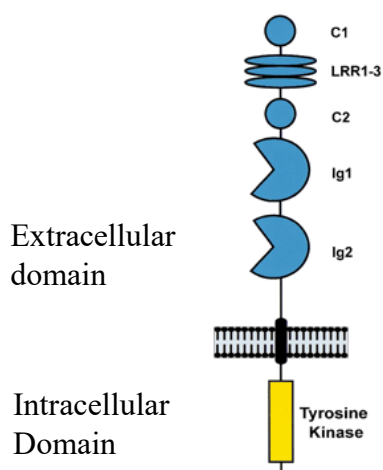
Figure 10. Schematic representation of Trk structures. The abbreviations used are as follows for the following terms: cysteine-rich domain (C), leucine-rich domain (LRR), immunoglobulin-like domain (Ig), tyrosine kinase domain (TKD). (Image adapted from reference 78)

1.6.3.1   TrkA isoforms

The *NTRK1* gene encodes two major isoforms of TrkA receptors with amino acid residues with lengths of 790(TrkA-I) and 796(TrkA-II).[79] The six amino acid residues that differentiate the two isoforms occur in the extracellular domain, near the transmembrane region. However, these residues do not affect the binding of neurotrophin NGF.[79] Also, the binding of NGF to the two different isoforms of TrkA receptors does not affect the receptor's binding specificity or its ability to initiate a signaling cascade in response to NGF.[80] The main difference between the two isoforms is their differential expression throughout the human tissue. In humans and rats, the longer 796 residue TrkA receptor is primarily expressed in the neuronal tissues, while the shorter 790 residue TrkA receptor is expressed mainly in the non-neuronal tissues.[80]

1.6.3.2   TrkB isoforms

There are four different isoforms of TrkB receptors that can occur in the central nervous system: a full-length TrkB.TK+ and three truncated TrkB.TK- receptors—T1, T2, and T-shc.[81] . These isoforms arise because of alternative splicing of the *NTRK2* gene; however, the truncated forms T1, T2, and T-sch lack a tyrosine kinase domain, which results in a loss of signaling during ligand binding. As a result, only the full-length TrkB receptors with tyrosine kinase domains are able to producing cellular signaling.[81] The formation of truncated TK- receptors have a significant impact on TrkB signaling due to their inhibitory effect. There are two main hypotheses on the inhibitory effect of truncated TrkB receptors.[82] The first hypothesis suggests that TK- receptors restrict the availability of neurotrophins to TK+ receptors, by acting as ligand traps.[82] This results in a lower concentration of unbound BDNF in the cell, thereby reducing the signaling cascade through the TK+ receptors.[82] Another hypothesis suggests that TK- receptors inhibit TK+ receptors by undergoing dimerization during the ligand activation of the TK+ receptors. This would ultimately lead to the inhibition of tyrosine kinase autophosphorylation and halt the cellular signaling.[82] These isoforms are important to take into consideration when developing small molecule inhibitors or radiotracers since most compounds are only able to bind to the non-truncated TrkB isoform.

1.6.3.3   TrkC isoform

There are many different isoforms of TrkC receptors that can be identified. Similar to TrkB receptors, some of the TrkC receptors have isoforms that lack the tyrosine kinase domain.[79] These truncated TrkC receptors play a similar role to TrkB receptors in inhibition and heterodimer formation.[83] However, there are three different TrkC receptor isoforms that have varying amounts of amino acid residue insertion at the tyrosine kinase domain. These isoforms are TrkC K14, TrkC K25, and TrkC K39, with the addition of an extra 14, 25, and 39 amino acids respectively.[84] Although all three isoforms were demonstrated to exhibit similar binding to the NT-3 neurotrophin, the signaling cascade initiated by each isoform differs from the original Trk C receptor.[84]

1.6.4   Trk signaling pathway

Tropomyosin receptor kinase-mediated signaling is initiated by the binding of the neurotrophin to the receptors, resulting in dimerization and kinase activity.[85] In the vertebrae Trk receptors, there are 10 evolutionarily conserved tyrosine residues (three of which are Y670, Y674, and Y675) in the cytoplasmic domain. These tyrosines are in the autoregulatory loop located in the tyrosine kinase domain. The phosphorylation of these tyrosines further activates the receptor and increases kinase activity.[61] Two other tyrosine residues (Y490 and Y785) are not located in the tyrosine kinase domain; instead, the phosphorylation of these residues creates additional binding sites for adaptor proteins.[86] Tyrosine residue 490 is demonstrated to interact with SH2-containing collagen-related proteins (Shc), while tyrosine residue 785 interacts mainly with the phospholipase C-γ1 (PLC-γ1).[85] The activation of Trk receptors affects numerous downstream proteins; however, the three major pathways activated by Trk receptors are the Ras, phatidylinositol-3-OH kinase (PI3-kinase), and PLC-γ1 pathways. The Ras pathway is mainly involved in the regulation of neuronal differentiation, while PI3-kinase is involved in neuronal survival. Lastly, the PLC-γ1 pathways induces the release of Ca^{2+} into the cytoplasm, further activating the signaling pathways controlled by Ca^{2+}.[85]

1.7   Trk and Cancer

Involvement of *NTRK* gene fusions in cancer was first identified more than 30 years ago. The first *NTRK1* gene fusion with non-muscle tropomyosin gene (*TPM3*) was identified in colorectal cancer.[87] Also with advances in genetic sequencing, more *NTRK* gene fusion products being identified as tumor drivers.[87] With the growing use of next-generation sequencing (NGS), a wide range of tumor types have been discovered to express *NTRK* gene fusion. Oncogenic fusion of *NTRK* gene typically involves 3' region (kinase domain) of the proto-oncogene juxtaposed with the 5' region of an unrelated gene through intra-or interchromosomal rearrangement.[74] As a result, the fusion of *NTRK* genes are implicated in the pathogenesis of many cancer types due to their ability to overexpress oncogenic proteins which are independent of ligand activation.[88] There are numerous cases with *NTRK* gene fusion in tumors such as glioblastoma, non-small cell lung cancer,

colorectal cancer, papillary thyroid carcinoma, spitzoid tumors, congenital fibrosarcoma, secretory breast carcinoma, acute myeloid leukemia.[89-95] Even though *NTRK* gene fusions are low frequency events, it is counter-balanced by a diverse involvement in numerous different tumor types. This may result in a significant fraction of patients who may be eligible for treatment with pan-Trk inhibitors for cancer treatment.[96] Due to diverse involvement of *NTRK* gene fusion in cancer development, there are a growing number of Trk inhibitors targeting such fusion proteins as a method of cancer treatment.

In addition to the involvement of *NTRK* gene fusion in cancer, overexpression of certain Trk receptors have been demonstrated as a useful prognostic tool. In the case of neuroblastoma, a common solid tumor in children, different levels of TrkA/B/C expression in neuroblastoma can lead to varied prognostic values.[97] Neuroblastoma with TrkA expression often indicates a good prognostic value, however, expression of TrkB leads to a poor prognosis.[83] With high levels of TrkA expression, the activation of TrkA by NGF leads to the differentiation of neuroblastoma into ganglion cells. On the other hand without NGF activation, TrkA expressing tumor cells initiates a programmed cell death allowing spontaneous regression of neuroblastoma to occur.[98] However, in cases with high TrkB expression, an aggressive tumor behavior was seen due to TrkB's ability to suppress cell death, promote angiogenesis, and increase drug resistance.[98-99] Even though TrkC is not as well correlated with prognosis as TrkA, the expression of TrkC is suggested to have favorable biological effects.[97] There are also other cases where Trk receptors have been shown to influence pro-tumorigenic behaviors such as in breast cancer[100] and prostate cancer.[101]

1.7.1   Personalized medicine

Current approaches to the treatment of cancer primarily involve the targeting of certain organs or the tumor microenvironment with surgical procedures, radiotherapy, and chemotherapy. As a result, most traditional methods of cancer treatment involve a "shotgun" approach where both the healthy cells and the tumor cells are killed off.[102] In many cases, standard cancer therapy results in low response rates and significant side effects due to systemic toxicity.[103] Due to the limitations of the traditional approaches to cancer therapy, there is a growing interest in personalized therapy/medicine.[103] In the context of Trk therapy, there is a heavy focus on targeting differential

genomic characterization such as *NTRK* fusion. This has led to employing a "basket design" as a new clinical trial paradigm where patients are identified for certain treatments based on precise genomic alteration regardless of tumor histology.[104] A major factor in determining the success of a small molecule inhibitor is to identify the biomarkers in tumor cells for selecting patients that would benefit from small molecule inhibitor treatment.[105] In addition, it is also imperative to monitor early treatment response to avoid ineffective treatment, reducing the risk of chemotoxicity.[105] Even though methods for tumor characterization such as next generation sequencing (NGS) exists, such methods often employ invasive procedures. However, there are many cases where surgery cannot be performed due to medical reasons or the location of the tumor. As a result, it is essential to develop a non-invasive method to identify biomarkers in tumor cells using target specific radiotracer such as PET imaging.

1.7.2   Trk inhibitors

There are numerous Trk inhibitors that are currently being developed, of which some are in various clinical stages ranging from research stage to phase II clinical trial stage. Even though there are 3 different isoforms of Trk receptors, due to their high level of sequence homology, many of the advanced Trk inhibitors are pan-Trk inhibitors targeting all three isoforms.[106] Some of the more advanced pan-Trk inhibitors in phase 1 or phase 2 studies are larotrectinib (LOXO-101), LOXO-195, entrectinib (RXDX-101), TPX-0005 (Table 5).

Table 5. Trk inhibitor targeting *NTRK* fusion in different clinical phase

Drug	Company	Target fusion	Phase
Larotrectinib (LOXO-101)	Loxo Oncology	NTRK1/2/3	2
Entrectinib (RXDX-101)	Ignyta, Inc	NTRK1/2/3, ROS1, ALK	2
TPX-0005	TP Therapeutics, Inc.	NTRK1/2/3, ROS1, ALK	1/2
LOXO-195	Loxo Oncology	NTRK1/2/3	1/2

In the past few months LOXO-101 has shown promising drug efficacy for treating cancer patients expressing *NTRK* gene fusions in diverse tumor types. LOXO-101 is a highly potent (IC_{50} = 5-11 nM) and > 100 times selective over other kinases (NCT02576431).[107] LOXO-101 was demonstrated to be effective in both children and adults with ages ranging from 4 months to 76 years old.[108] Out of the 55 patients that were involved in a phase 2 study, there was a 75% overall response rate.[108] Also, when observing for potential toxicity, the authors reported no drug-related

adverse effect and minimal central nervous system toxicity.[107] However, drug resistance against LOXO-101 was observed resulting in cancer relapse. As a result, researchers are starting to test a new drug, LOXO-195, on patients that have developed drug resistance towards LOXO-101 (NCT03215511).[109] In addition to LOXO-195, TPX-0005 has also demonstrated to be effective in overcoming drug resistance towards LOXO-101[110] and entrectinib has demonstrated a promising drug efficacy.[111]

1.7.3   Trk radiotracer development

In order to aid and accelerate the drug development process for small molecule tyrosine kinase inhibitors (TKI) for clinical use, PET has demonstrated to be promising.[112-113] Being able to develop TKI-PET allows for the visualization and quantification of radiolabeled molecules *in vivo*.[114] Development of a PET radiotracer during drug development can allow for biodistribution studies to answer several fundamental questions[114]:

1) The location and existence of the desired target expression
2) The localization of drug to target site
3) *In vivo* kinetic binding
4) Uptake in normal organs which allows the prediction of potential toxicity

Even though there is numerous evidence demonstrating the benefit of nuclear imaging in relation to drug development, there are limited number of PET radiotracers that target Trk and *NTRK* fusion expressing tumors. With recent clinical advances in Trk inhibitor such as LOXO-101 and RXDX-100 entering phase 2 clinical study, research groups such as the Schirrmacher Group have developed Trk radiotracers for PET imaging.

1.7.4   Trk development by the Schirrmacher Group

The Schirrmacher Group is extensively involved in the development of Trk radiotracers for PET imaging. A selection of examples such as **1.18**, **1.19**, **1.20** and **1.21** are shown in Figure 11.
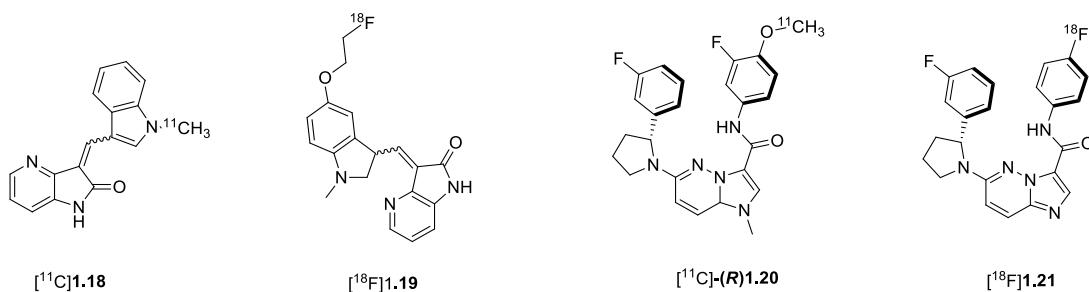
Figure 11. Examples of radiotracers developed by the Schirrmacher Group

Initial studies in rat brain and human neuroblastoma using ^{11}C labelled **1.18** demonstrated high metabolic stability and high brain uptake. However, further mice PET studies displayed high non-specific binding of [^{11}C]**1.18** (IC_{50} = TrkA: 29.6 nM, TrkB: 6.7 nM, TrkC: 4.6 nM) in the rodent brain.[115] Following the development of [^{11}C]**1.18,** the Schirrmacher Group also developed [^{18}F]**1.19** (IC_{50} = TrkA: 28.3 nM, TrkB: 4.1 nM, TrkC: 3.7 nM) to improve Trk specific binding. Initially, *in vitro* studies of [^{18}F]**1.19** revealed increased Trk specific binding, however, *in vivo* studies revealed metabolic and isomeric instability of [^{18}F]**1.19**. As a result, this led to nonspecific distribution of [^{18}F]**1.19** in the brain. Further development of Trk radiotracers led to the discovery of compound [^{11}C]**-(R)-1.20**, highly potent and selective towards TrkB/C (IC_{50} = TrkA: 4.0 nM, TrkB: 0.2 nM, TrkC: 0.1 nM).[116] Using [^{11}C]**-(R)-1.20** as a Trk radiotracer, the Schirrmacher Group were able to demonstrate the first in-human PET imaging of TrkB/C receptors (Figure 12).[116] However, due to the P-gp efflux liability of [^{11}C]**-(R)-1.20**, the Schirrmacher Group also developed [^{18}F]**1.21** (IC_{50} = TrkA: 4.21 nM, TrkB: 0.15 nM, TrkC: 0.31 nM) by replacing the methoxy group with fluorine and removing a methyl group from an anime group. These structural modification led to a decrease in P-gp liability and brain kinetic improvement in non-human primates.[117]
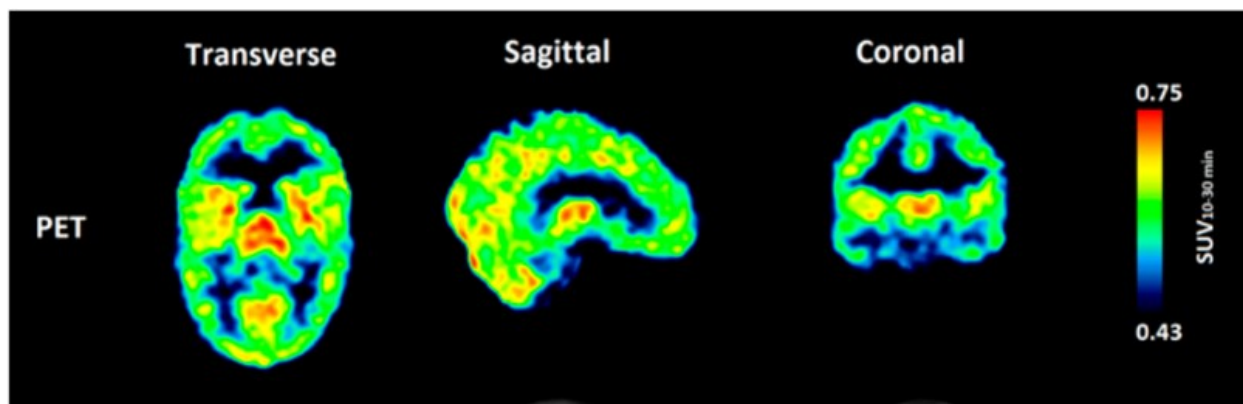
Figure 12. First *in vivo* PET imaging of Trk receptors in the human brain. PET images were produced with [^{11}C]-**(R)-1.20**. (Image adapted with permission from Reference 116. Copyright (2017) American Chemical Society)

1.8 GW2580

1.22
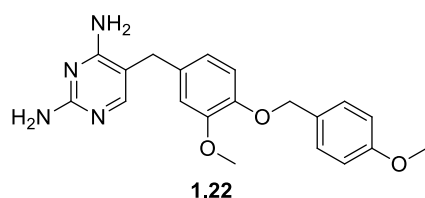
Figure 13. Structure of GW2580

In addition to previous Trk inhibitors, the Schirrmacher Group also continuously studying new Trk inhibitors such as GW2580 (**1.22**). In order to develop a radiotracer for Trk receptors, a lead structure such as GW2580 (Figure 13) with high binding potency and selectivity towards Trk is required. Even though GW2580 isn't designed for use in the brain, other Trk inhibitors that target the brain require binding potency (IC$_{50}$ value) in the picomolar range such as compounds **1.20** and **1.21**. Due to the broad expression of Trk receptors in the brain high binding potency is required to differentiate between tumor cells and normal cells. However, for tumors such as neuroblastoma, outside the central nervous system, it was hypothesized that the nanomolar binding potency of GW2580 was acceptable for PET imaging purposes. GW2580 was originally identified by Shewchuk *et al.* (2004) as a small molecule inhibitor for colony stimulating factor -1 receptor (CSF-1R).[118] Conway *et al* (2005) also demonstrated the use of GW2580 as an orally bioavailable

inhibitor of CSF-1R.[119] When 10 µM of GW2580 was used to perform binding potency assay, GW2580 had an IC_{50} value of 0.03 µM *in vitro* against CSF-1R.[120] The initial kinase selectivity assay of GW2580 against 186 other kinases demonstrated that there was no other significant off-target binding.[120] In this initial screen IC_{50} value, GW2580's binding potency to CSF-1R was more than 100-fold greater than the next closest IC_{50} value of 4.8 µM.[120] However, further kinase selectivity tests showed that GW2580 also revealed a strong binding affinity towards Trk receptors (*vide infra*).

1.8.1   CSF-1R involvement in cancer

Increased levels of CSF-1 and its receptor, CSF-1R, are found in various types of tumors such as breast[121], ovarian[122], endometrial[122], and adenocarcinoma tumors.[122] The CSF-1R is responsible for the regulation of mononuclear phagocyte/macrophage development, morphology, and function.[123] Some examples of the major pathways involved in the CSF-1R-induced macrophage regulation are phosphoinositide 3-kinase/protein kinase B (PI3K/Akt), phospholipase C (PLC), Fms-interacting protein (FIMP), phosphoinositide phospholipase C (PLC-γ2) pathways, and mitogen activated protein kinase (MAPK).[124] These CSF-1R signaling pathways play a critical role in the regulation of tumor-associated macrophages (TAMs) in a tumor microenvironment. Tumor-associated macrophages are inflammation infiltrates with a distinct phenotype seen in primary and secondary tumors, and they are one of the major factors of poor prognosis for cancer patients.[125] In more than 80% of cancer cases, high levels of TAMs are associated with a poor prognostic value.[126] This is due to TAMs' ability to provide tumors with an immunosuppressive microenvironment, resulting in tumor cell proliferation, chemo-resistance, and metastasis.[127] CSF-1R inhibition has also been demonstrated to be affective in combined therapy due to increased CSF-1 secretion during chemotherapy or radiotherapy.[128] The upregulation of CSF-1 induces TAM infiltration which provides increased growth and viability of the tumor cells.[128] Clinical trials of CSF-1R inhibition by small molecules or monoclonal antibodies have shown promising results when used for both monotherapy and combined therapy.[128] However, adverse events such as fatigue, elevated liver enzyme, asthenia, rash, nausea/vomiting, headache have been associated with the use of CSF-1R inhibitor.[128] As a result, a key question of which type of cancer patients will most likely respond to CSF-1R treatment remains to be addressed.[128] Therefore, due to the

diverse involvement of CSF-1R/TAM in tumor cells, developing GW2580 as a dual Trk/CSF-1R PET imaging agent has the potential to be a unique tool for selective assessment of Trk and CSF-1R levels *in vivo*.

1.8.2   GW2580 and Trk

In addition to binding to CSF-1R receptor (K_d = 1.6 nM), GW2580 also displays high binding potency towards TrkA (630 nM), TrkB (36 nM), and TrkC (120 nM).[129] As a result GW2580 is a potential candidate for a dual PET imaging radiotracer study. Recently it has also been demonstrated that potency measured with recombinant proteins may underestimate the real binding potency *in vivo*.[130] Previous measurements of binding potency of GW2580 to Trk receptors were done by using recombinant proteins extracted from an *E. coli* host.[131] However, by measuring binding potency in recombinant proteins many *in vivo* factors such as cellular localization, intramolecular interaction between protein-protein, post-translational modification, and active metabolites are not taken into consideration.[130] As a result, it is possible that the binding potency of GW2580 towards Trk or CSF-1R could potentially improve during *in vivo* analysis.

1.8.2.1   TrkB-GW2580 binding interaction

X-ray crystallography between GW2580 and TrkB demonstrated that the hydrogen bonding is achieved in the tyrosine kinase domain (Figure 10) by interacting with the Asp-Phe-Gly (DFG) motif and amino acid residues Met 636 and Glu 634.[132] The DFG motif is located on the activation loop, and it is a highly conserved catalytic domain between kinases. Conformational changes in the DFG motif are able to regulate the kinase ability to phosphorylate.[133] In the DFG-in (type 1) conformation the Phe residue of DFG motif is positioned behind the gatekeeper residue opening the catalytic site for adenosine triphosphate (ATP).[133] However, in the DFG-out (type 2) conformation, the Phe residue is rotated out of its position behind the gatekeeper preventing ATP binding but reveals a large allosteric hydrophobic pocket.[133] When analyzing the interaction

31

between GW2580 and TrkB (PDB code: 4AT5) in a DFG-out conformation, there are three distinct regions of GW2580 that interact with TrkB receptor, as illustrated in Figure 14: 1) diaminopyrimidine moiety (hinge region) ; 2) central dimethoxy-benzyl moiety (DFG-motif); and 3) methoxy-phenyl moiety (allosteric hydrophobic pocket). The 2,4-diaminopyrimidine moiety interacts with the Met 636 and Glu 634 residue to form hydrogen bonds while the central dimethoxy-benzyl moiety interacts with the Asp 710 backbone in the DFG motif.
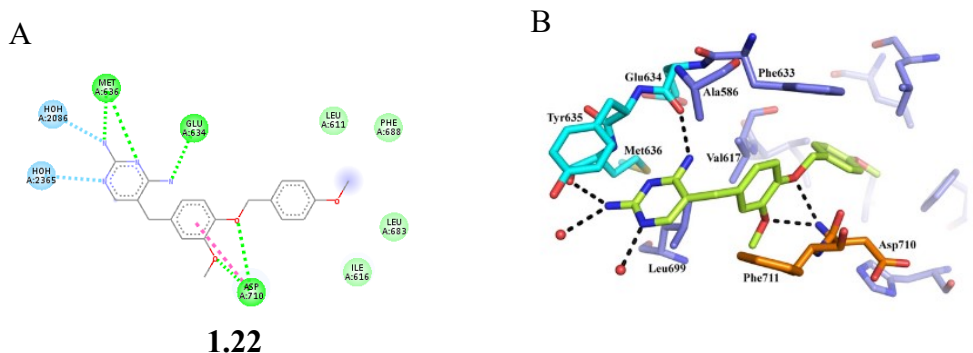
Figure 14. (A) A 2-D diagram of the key interaction between TrkB and GW2580. Image was obtained using Discovery Studios 3.5. (B) Crystal structure of a GW2580-TrkB co-crystallized system. (Image adapted from reference 132)

Since the diaminopyrimidine moiety and the central dimethoxy-benzyl moiety are crucial for the hydrogen bonding between GW2580 and TrkB, fluorine had to be inserted into regions that would have minimal effect on the hydrogen binding interactions. A visualization of the receptor's binding pocket, presented in Figure 15, demonstrates two regions of hydrophobicity—one located in the central DFG region (position 1) and another in the right allosteric region, where modification to the structure could be accommodated (positions 2-3).
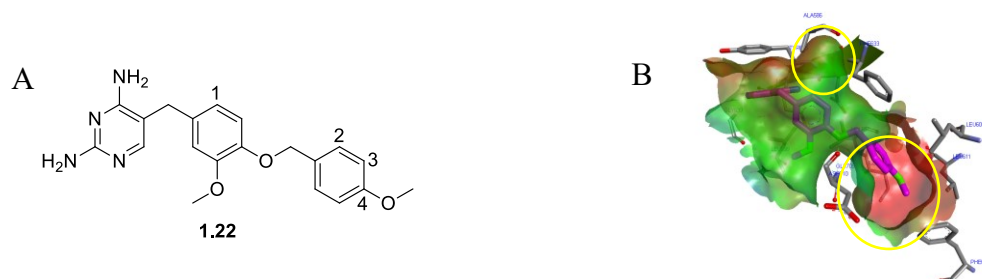
Figure 15. (A) The numbering of different positions that can be modified on the GW2580 structure. (B) Visualization of a TrkB binding pocket. The yellow circle indicates the two regions of the hydrophobic pocket. Green represents less hydrophobic region while red represents a more hydrophobic region.

1.9   Radiolabeling of GW2580

As previously mentioned, the high selectivity and high binding affinity of GW2580 towards Trk and CSF-1R make it a promising compound for PET imaging. To develop GW2580 as a potential ^{18}F-labelled PET imaging agent, fluorinated analogues and labeling precursors needed to be synthesized. Initial attempts to develop the GW2580 as a PET radiotracer were done by the Schirrmacher Group[134]

1.9.1   Previously synthesized fluorinated derivatives of GW2580

In a previous study by the Schirrmacher Group, three different fluorinated derivatives were synthesized based on the TrkB-GW2580 co-crystal structure (Figure 16).[134]
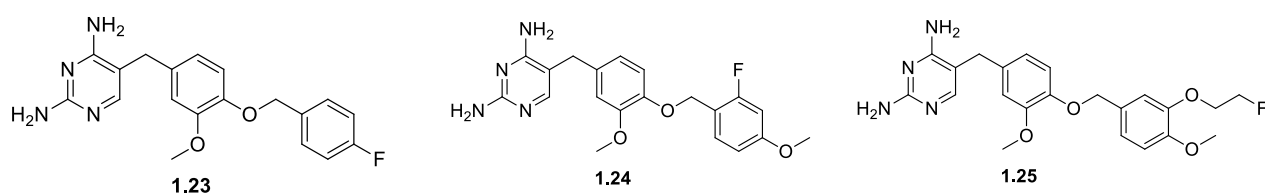
Figure 16. Chemical structures of previously synthesized fluorinated derivatives

A competitive binding assay demonstrated that **1.23** (TrkA: IC$_{50}$ = 663 ± 19.8 nM, TrkB: IC$_{50}$ = 132 ± 12.0 nM, TrkC: IC$_{50}$ = 135 ± 5.66 nM) obtained a similar binding potency as GW2580

(TrkA: $IC_{50} = 338 \pm 29.0$ nM, TrkB: $IC_{50} = 119 \pm 38.7$ nM, TrkC: $IC_{50} = 69.1 \pm 0.99$ nM).[134] Also further analysis of **1.23** demonstrated that **1.23** maintained high selectivity towards Trk and CSF-1R when tested in an enzymatic assay on a panel of 342 full, wild-type kinases.[134] However, fluorination at position 2 (**1.24**) resulted in a loss of binding potency towards Trk. The loss of binding potency for **1.24** was attributed to unfavorable electrostatic interaction distorting the methoxy-phenyl moiety into a disfavored orientation.[134] For **1.25**, the binding potency decreased by 2-4.5 fold (TrkA: $IC_{50} = 674 \pm 79.2$ nM, TrkB: $IC_{50} = 409 \pm 3.54$ nM, TrkC: $IC_{50} = 309 \pm 31.2$ nM), suggesting that the fluoro ethoxy group might be too large for the allosteric pocket.

1.9.2 Radiolabeling of **1.23**

A previous approach by the Schirrmacher Group to synthesize [^{18}F]**1.23** involved a multi-step approach (Scheme 1).[134]
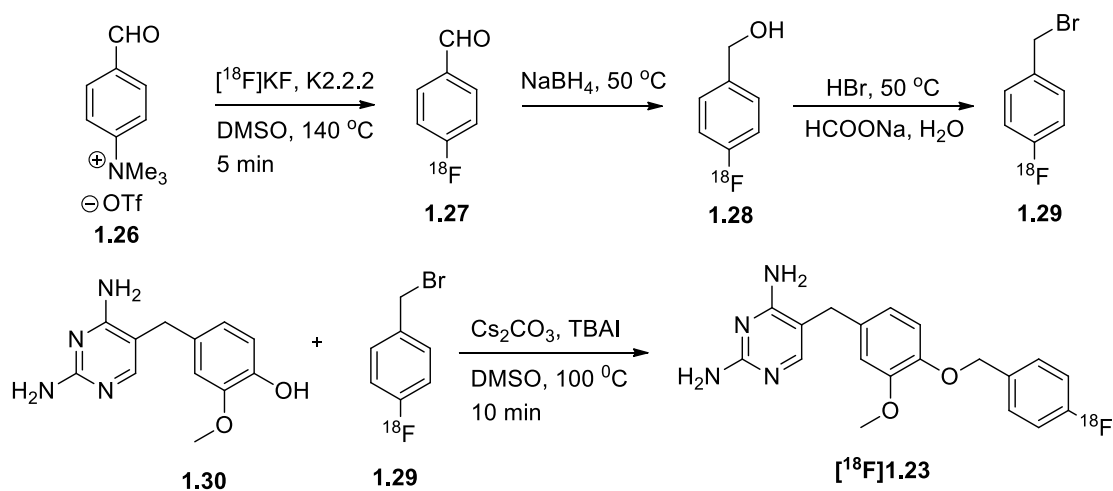
Scheme 1. Multi-step approach for the radiosynthesis of [^{18}F]**1.23**

Using this approach [^{18}F]**1.23** was synthesized with RCY of 13% (non-decay corrected).[134] Even though the multi-step synthesis was able to successfully synthesize [^{18}F]**1.23** for evaluation purposes, this method was unsuitable for automated synthesis.[134] Due to the limited number of radiosynthesis steps that the automated processes can accommodate, a simpler method of [^{18}F]**1.23** radiosynthesis was required. Following the previous study done by the Schirrmacher Group, this

thesis focused on developing other radio-fluorinated analogues of GW2580 and utilizing a more straightforward method to synthesize [^{18}F]**1.23** for automated synthesis and routine production.

2.0   Objectives of the Thesis

The objectives of the thesis were: (1) to develop radio-fluorinated analogue of GW2580, **3.0**, that maintains the high selectivity and high binding potency towards Trk and CSF-1R. (2) To radiolabel a previously studied fluorinated analogue of GW2580, [^{18}F]**1.23**, using a two-step radiosynthesis method.

The specific objectives of the studies were as follows:

1.   To develop new fluorinated analogues of GW2580 (**3.0** and **3.1**) and evaluate the biological data to identify the binding potency towards Trk A, B and C.

2.   To compare and analyze the data of the newly synthesized analogues **3.0** and **3.1** to the previously developed compounds **1.23-1.25** for comparison of Trk A, B and C binding potency

3.   To establish and optimize a two-step radiosynthetic procedure to develop [^{18}F]GW2580 analogues [^{18}F]**3.0** and [^{18}F]**1.23** with high RCY (non-decay corrected), A_m and RCP.

3.0   Results and Discussion

3.1   Designing new fluorinated analogues of GW2580, **3.0** and **3.1**

Combining the information gathered from the GW2580-TrkB co-crystal structure and the previous study by the Schirrmacher Group, two new fluorinated derivatives, **3.0** and **3.1,** were designed and synthesized (Figure 17).
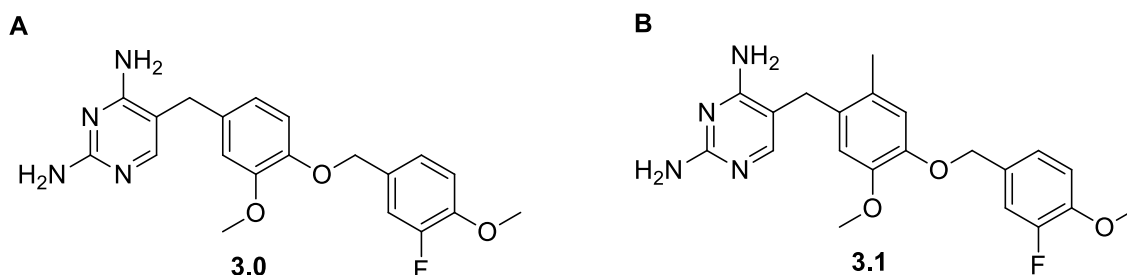
Figure 17. Chemical structure of newly proposed fluorinated derivatives of GW2580, **3.0** and **3.1**.

Compound **3.0** was based on the designs of compound **1.24** and **1.25** (Figure 16)**.** Since it was previously demonstrated that the addition of a large fluoro ethoxy group lowered the binding potency towards all three Trk isoforms, it was hypothesized that by direct C-F bond formation at the *meta* position, the smaller group size would result in an improved binding potency. Also, by leaving the methoxy group located at the *para* position unaltered (Figure 17A), possible improvements in the binding potency were hypothesized due to increased hydrophobic interaction and a closer structural resemblance to GW2580. Compound **3.1** is structurally similar to **3.0**, except for the addition of a methyl group *ortho* to the diaminopyrimidine ring in the central dimethoxy-benzyl moiety (Figure 17B). It was hypothesized that by adding a methyl group it would improve the binding potency through increase Van Der Waals interaction and lipophilicity.

3.1   Molecular docking study

To visualize the binding conformation of **3.0** and **3.1** towards TrkB, a molecular docking study was conducted using FITTED Forecaster with a TrkB-GW2580 co-crystal structure (PDB code:

4AT5). The low root mean square deviation (RMSD) (0.42Å) validated that the docking study was able to produce a similar conformation to the co-crystalized structure of GW2580.

3.1.1 Docking study of **3.0** to TrkB

When visualizing the interaction of **3.0** with the TrkB receptor, the hydrogen bonds at the hinge and the DFG motif was maintained as expected (Figure 18A), however a slightly different conformation can be observed in the allosteric region. Even though the methoxy-phenyl moiety maintains a similar perpendicular orientation relative to the central methoxy region, there is a slight change in the angle (Figure 18B). More importantly, the distance (2.69Å) between the *meta*-hydrogen and the oxygen atom from the carbonyl group from Val617 suggests unfavorable electrostatic interaction between the *meta*-fluorine and oxygen. Due to the *van der* Waals radii of fluorine and oxygen (2.99Å) being greater than the distance provided, this prevents orientation of the fluorine towards back of the allosteric pocket (Figure 18B). However, when the fluorine orients away from the Val617 residue, favorable hydrophobic interactions form and accommodation in the allosteric pocket can be observed (Figure 18C).
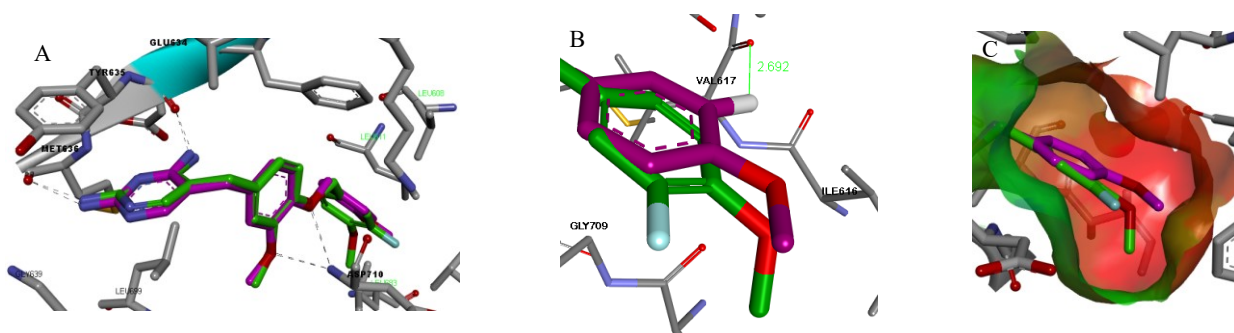
Figure 18. Binding poses of **3.0** (green) and the crystalized structure of GW2580 (purple) (PDB code: 4AT5). (A) The binding interaction of diaminopyrimidine ring and Met636/Glu634 as well as the binding interaction of the DFG motif with the central dimethoxy moiety. (B) Interaction between oxygen atom from Val617 residue's carbonyl group and *meta*-hydrogen atom. (C) Accommodation of the fluoro methoxy-benzyl moiety in the allosteric pocket. Green represents a less hydrophobic region while red represents a more hydrophobic region.

3.1.2   Docking study of **3.1** to TrkB

Based on the docking study, the addition of a methyl group had no impact on hydrogen bonding in the hinge and DFG motif. (Figure 19A). Initial observations, regarding the hydrophobic binding pocket of TrkB near the central dimethoxy moiety demonstrated accommodation of the methyl group substitution. (Figure 19B). However further analysis of bond lengths demonstrated that the *ortho*-hydrogen atom in the central methoxy ring is near the methyl group from the Ala586 residue (3.11Å) (Figure 19C). This observation suggests that a methyl group might possibly be too large. Despite this observation, it was still hypothesized that if the compound was able to change conformation to accommodate the methyl group insertion, an increase in hydrophobic interaction with the receptor would lead to an increase in binding potency. Lastly, due to presence of the same methoxy-phenyl structure as **3.0** there was no observable change in the conformation at the allosteric pocket region (Figure 19D)
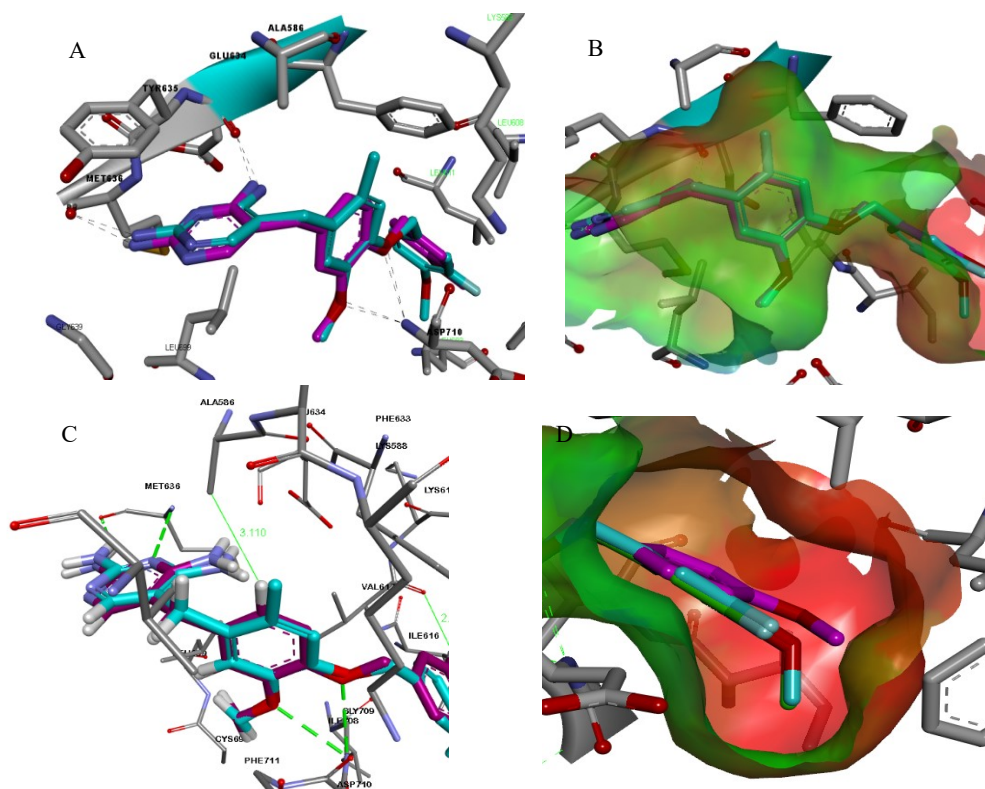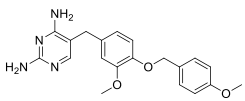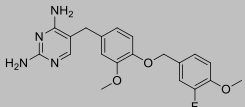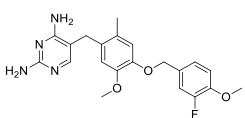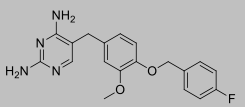
Figure 19. Predicted binding pose of **3.1**(blue), in comparison to a crystallized GW2580 structure (purple). (A) Illustration of the receptor-ligand interaction between the diaminopyrimidine ring

and amino acid residues Met636 and Glu634 as well as the interaction between the DFG motif (Asp710) and the dimethoxy moiety. (B) Housing of the methoxy substituent in the TrkB binding pocket. (C) Distance between the *ortho*-hydrogen and methyl group on Ala586 residue (D) Similar binding conformation of the methoxy-phenyl moiety of **3.0** (green) and **3.1** (blue). Green represents a less hydrophobic region while red represents a more hydrophobic region.

3.2 Biological potency results and molecular property

In vitro binding assays to determine the binding potency of **3.0** and **3.1** against Trk A/B/C was performed by Reaction Biology Corporation using a [γ-33p]ATP-based competitive inhibition enzymatic assay. The binding assay results were compared to compound **1.23** previously studied by the Schirrmacher Group[134] in order to determine if improvements in binding potency were obtained. The IC_{50} values obtained by **3.0** (TrkA: IC_{50} = 455 nM, TrkB: IC_{50} = 123 nM, TrkC: IC_{50} = 137 nM) demonstrated a 2.2-fold to a 2.8-fold decrease in binding potency when compared to GW2580 (Table 6). The slight decrease in binding potency of **3.0** is inferred to be the result of unfavorable electrostatic interaction between the *meta*-fluorine and Val617 as previously demonstrated by molecular docking. When comparing binding potency between **3.0** and **1.23** there were no significant improvements observed. However, **3.1** demonstrated a significant decrease in binding potency (TrkA: IC_{50} = 7220 nM, TrkB: IC_{50} = 1690 nM, TrkC: IC_{50} = 2140 nM) (Table 6). The decrease in potency of **3.1** was attributed to the fact that the van der Waals radii of the two methyl groups (4.0Å) from Ala586 and methyl substituent was too large to be accommodated by the hydrophobic pocket leading to an unfavorable electrostatic interaction.

Table 6. Molecular properties and *in vitro* activity of fluorinated derivatives of GW2580.

Compound	MW (g/mol)	logP [a]	TPSA[b] (Å^2)	In vitro IC$_{50}$ (nM)		
				TrkA	TrkB	TrkC
GW2580	366.41	2.58	105.5	162	56.6	53.3
3.0	384.40	2.70	105.5	455	123	137
3.1	398.5	3.03	105.5	7220	1690	2140
1.23	354.38	2.76	96.3	663 ± 19.8 [c]	132 ± 12.0[c]	169 ± 27.6 [c]

[a] Values were computed with ALOGPS 2.1 program (VCClabs.org)[135-136]

[b] Values were computed with Molinspiration cheminformatics[137]

[c] Previously reported data (Taken from reference 131)

In terms of molecular properties, due to the addition of the methyl group, **3.1** had a slightly higher log *P* prediction (3.03), compared to **3.0** (2.70) and **1.23** (2.76). Also, the methoxy group for **3.0** and **3.1** increased the topological polar surface area (TPSA) values to 105.5 Å^2, compared to the TPSA value of **1.23** (96.3 Å^2). However, the TPSA and log*P* values of **3.0** and **3.1** were still in the favorable range in regards to ideal PET radiotracer physico-chemical properties.[138] In the end, the low potency of **3.1** to Trk prevented the compound from being a suitable candidate for further development into a radiotracer. As a result, **3.0** was chosen as the lead compound for radiosynthesis using the method of radiofluorination reported by the Gouverneur Group[53] and Scott Group.[57] However, in order to use this method, the synthesis of a boronic ester derived precursor was required.

4.0 Chemical Synthesis of Non-radioactive Standards (**3.0**, **3.1**, **4.8a**, **4.8b**), Bpin precursors (**4.17a**, **4.17b**) and Protodeboronated Side Product (**4.21**)

4.1 Chemical synthesis of the non-radioactive standards 5-(4-((3-fluoro-4-methoxybenzyl)oxy)-3-methoxybenzyl)pyrimidine-2,4-diamine (**3.0**) and 5-(4-((3-fluoro-4-methoxybenzyl)oxy)-5-methoxy-2 methylbenzyl)pyrimidine-2,4-diamine (**3.1**)

4.0

4.1 (93%)

4.2 (90%)

4.3a: R_1 = H (66%)
4.3b: R_1 = CH$_3$ (57%)

4.4a: R_1 = H (62%)
4.4b: R_1 = CH$_3$ (88%)

4.5a: R_1 = H (94%)
4.5b: R_1 = CH$_3$ (77%)

3.0: R_1 = H (51%)
3.1: R_1 = CH$_3$ (46%)

4.6

4.7 (61%)
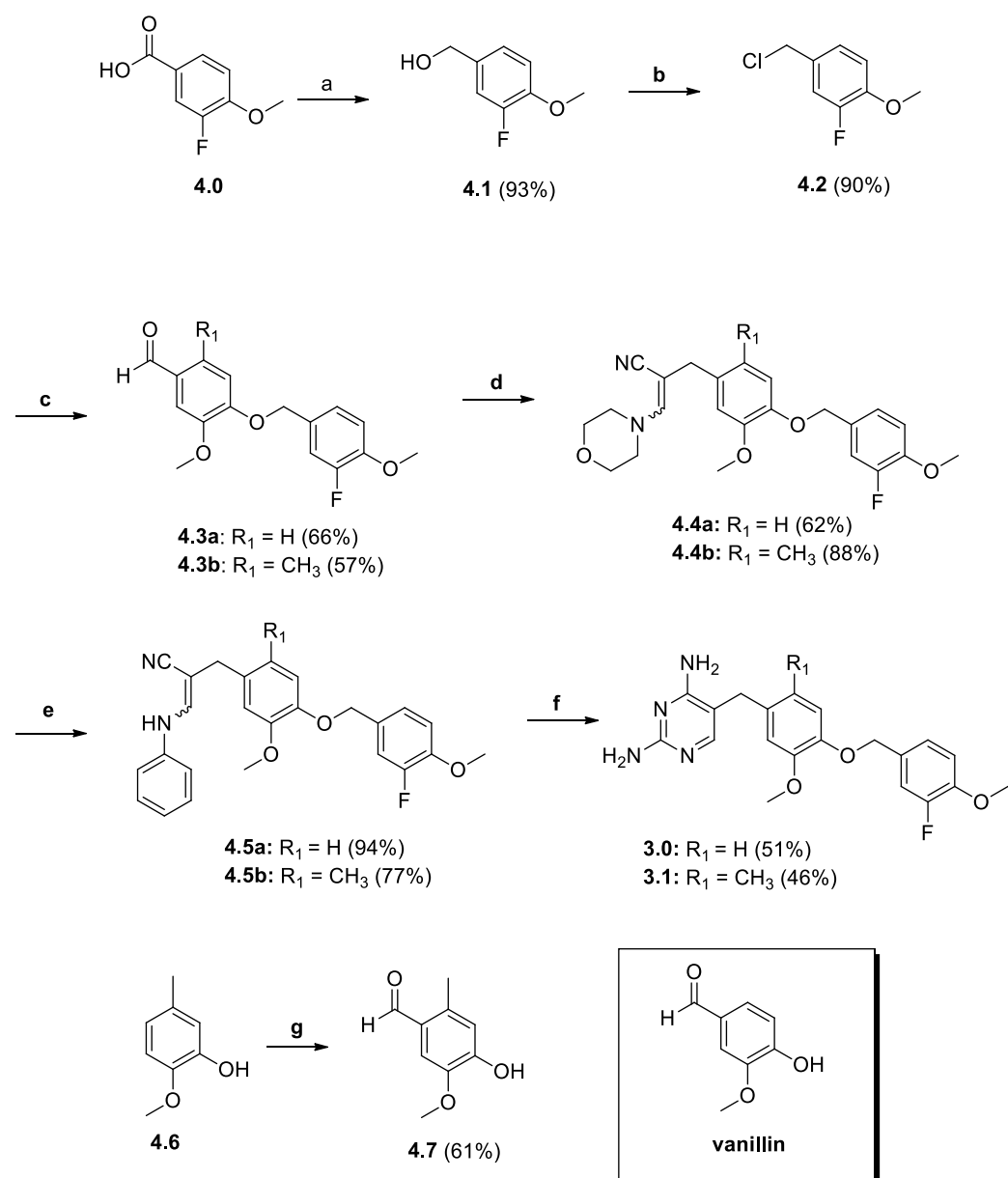
vanillin

Scheme 2. Chemical synthesis of **3.0** and **3.1** (a) LiAlH$_4$, rt, 12 h; (b) cyanuric chloride, rt, 10 min; (c) vanillin or **4.7**, K$_2$CO$_3$, DMF, rt, 12 h; (d) 3-morpholinopropionitrile, NaOMe, DMSO, 75 °C,

42

20 min; (e) anilinium chloride, isopropanol, reflux, 25 min; (f) guanidium chloride, NaOEt, EtOH, reflux, 12 h; (g) titanium tetrachloride, dichloromethyl methyl ether, DCM, 0 °C, 1.5 h.

The method to synthesize **3.0** and **3.1** was adapted from the procedure by Shewchuck *et al*[118] (Scheme 2) and followed a linear synthesis approach starting from a 3-fluoro-4-methoxybenzoic acid **4.0**. The carboxylic acid of **4.0** was reduced using lithium aluminum tetrahydride (LiAlH$_4$) to give 3-fluoro-4-methoxybenzyl alcohol **4.1**. The benzyl alcohol of **4.1** was then treated with cyanuric chloride to give 3-fluoro-4-methoxybenzyl chloride **4.2**. Afterwards, alkylation of vanillin or 6-methylvanillin **4.7** with **4.2** afforded the respective benzaldehyde **4.3a** and **4.3b**. Formylation of 4-methyl-2-hydroxy anisole **4.6** with dichloromethyl methyl ether and titanium (IV) chloride produced **4.7**. Treatment of **4.3a** and **4.3b** with 3-morpholinopropionitrile gave both the *E and Z* isomers of morpholino intermediates **4.4a** and **4.4b**. In order to cyclize of **4.4a** and **4.4b** into their respective 2,4-diaminopyrimidine derivatives, the compounds were initially treated with anilinium chloride to produce **4.5a** and **4.5b**. Finally, the anilinium derivatives were treated with guanidium chloride in the presence of sodium ethoxide to produce the 2,4-diaminopyrimidine derivatives **3.0** and **3.1** (Scheme 2). The overall chemical yield of **3.0** and **3.1** was 16% and 15% respectively.

4.2 Synthesis of tert-butyloxycarbonyl (Boc) rotected standards: di-*tert*-butyl (5-(4-((3-fluoro-4-methoxybenzyl)oxy)-3-methoxybenzyl)pyrimidine-2,4-diyl)bis(*tert*-butoxycarbonylcarbamate) (**4.8a**) and di-*tert*-butyl (5-(4-((4-fluorobenzyl)oxy)-3-methoxybenzyl)pyrimidine-2,4-diyl)bis(*tert*-butoxycarbonylcarbamate) (**4.8b**)

3.0: R$_1$ = F, R$_2$ = OMe
1.23: R$_1$ = H, R$_2$ = F

4.8a: R$_1$ = F, R$_2$ = OMe (67%)
4.8b: R$_1$ = H, R$_2$ = F (40%)
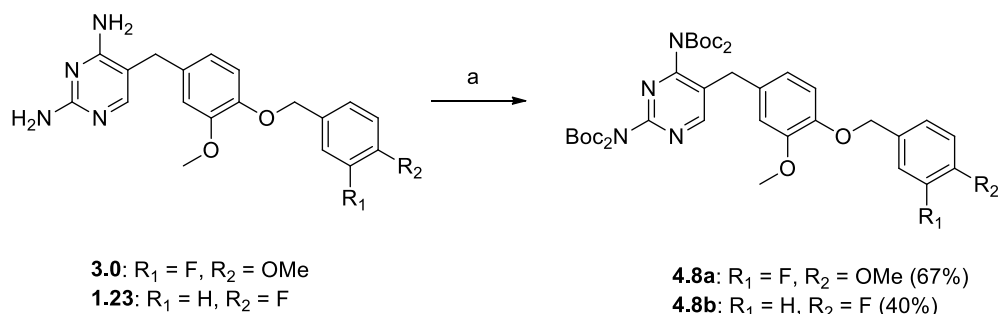
Scheme 3. Synthesis of Boc-protected standards **4.8a** and **4.8b** (a) Boc-anhydride, DMAP, TEA, THF, 4 days

Radiofluorination was planned to be performed in a two-step process including radiofluorination and Boc-deprotection. As a result, Boc-protected standards of **3.0** (**4.8a**) and **1.23** (**4.8b**) were synthesized in order to characterize these intermediates. The Boc-protection procedure was adapted from Chan *et al.*[139] Treatment of **3.0** and **1.23** with excess Boc anhydride in the presence of 4-dimethylaminopyridine (DMAP) and triethylamine (TEA) produced **4.8a** and **4.8b** in chemical yields of 67% and 40% respectively.

4.3   Synthesis of Bpin precursors: di-tert-butyl (5-(3-methoxy-4-((4-methoxy-3-(4,4,5,5-tetramethyl-1,3,2-dioxaborolan-2-yl)benzyl)oxy)benzyl)pyrimidine-2,4-diyl)bis(tert-butoxycarbonylcarbamate) (**4.17a**) and di-tert-butyl (5-(3-methoxy-4-((4-(4,4,5,5-tetramethyl-1,3,2-dioxaborolan-2-yl)benzyl)oxy)benzyl)pyrimidine-2,4-diyl)bis(tert-butoxycarbonylcarbamate) (**4.17b**) for radiofluorination yielding compounds [^{18}F]**4.8a** and [^{18}F]**4.8b**
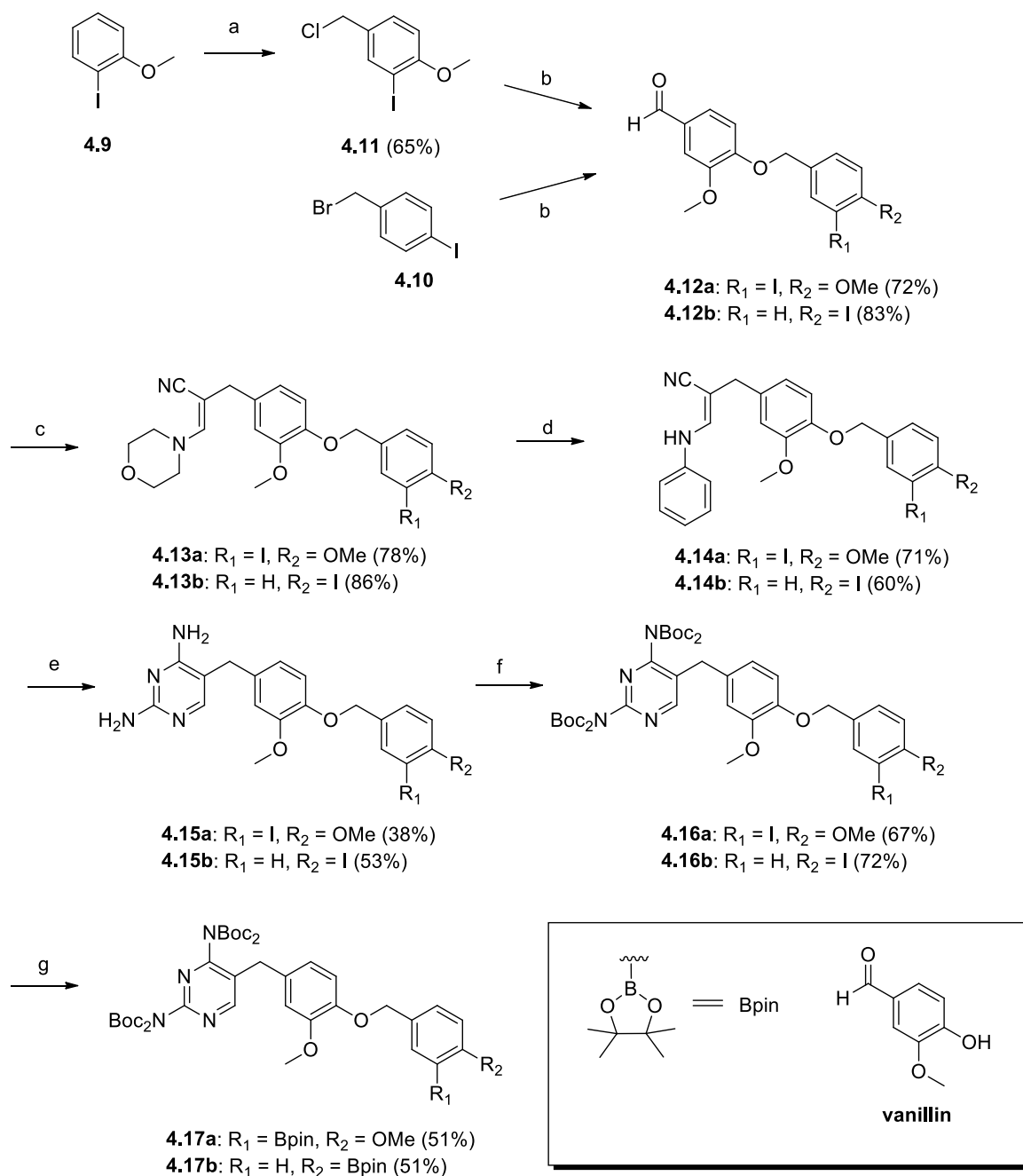
Scheme 4. Chemical synthesis of Boc-protected radiolabeling precursors **4.17a** and **4.17b** (a) chloromethyl methyl ether, acetic acid, 55 °C, 3 days; (b) Vanillin, K_2CO_3, DMF, rt, 12 h; (c) 3-morpholinopropionitrile, NaOMe, DMSO, 75 °C, 20 min; (d) anilinium chloride, isopropanol, reflux, 25 min; (e) guanidium chloride, EtOH, reflux, 12 h; (f) Boc-anhydride, DMAP, TEA, THF, 4 days; (g) bispinacolborane, Pd(dppf)Cl_2, KOAc, DMSO, 80 °C, 12 h

In order to use the radiosynthesis methods developed by the Scott[57] or Gouverneur Group[53], precursors with Bpin functionalities are required. Following a similar linear synthetic approach as for **3.0**, alkylation of vanillin with iodobenzyl halide derivatives **4.10** and **4.11** were accomplished to produce **4.12a** and **4.12b**. Subsequent transformation of the aldehyde **4.12a** and **4.12b**, into the guanidium group proceeded identically as the previously described for the synthesis of **4.8a**. The resulting guanidium intermediates **4.15a** and **4.15b** were protected with Boc groups to produce **4.16a** and **4.16b**. The amino groups present in **4.15a** and **4.15b** were protected with Boc groups to produce **4.16a** and **4.16b**. Finally following Miyaura borylation reaction conditions[140], the iodine substituent was treated with bis(pinacolato)diboron in the presence of palladium catalyst and base to produce the Bpin precursor **4.17a** and **4.17b** (Scheme 4). The overall chemical yield of **4.17a** and **4.17b** was 3.3% and 8.3% respectively.

4.4   Synthesis of expected protodeboronated side-product, 5-(4-(benzyloxy)-3-methoxybenzyl)pyrimidine-2,4-diamine (**4.21**)
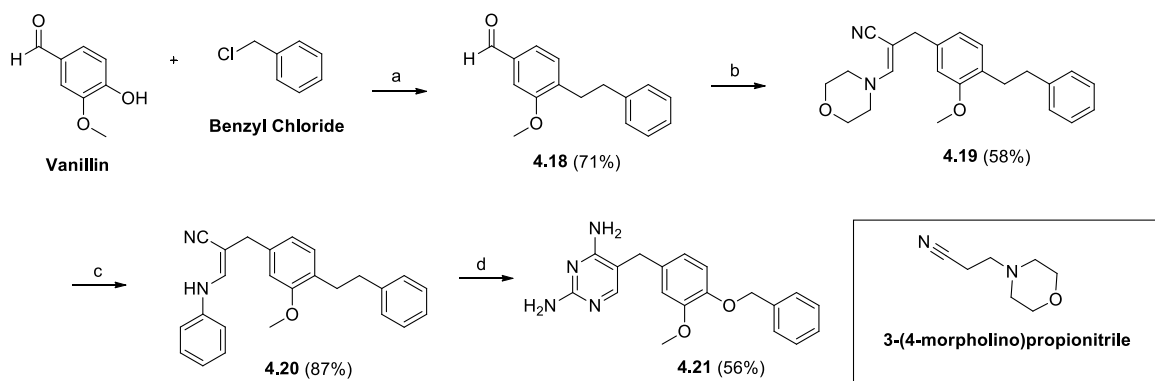
Scheme 5 Chemical synthesis of protodeboronated product **4.21** (a) K_2CO_3, DMF, rt, 12 h; (b) 3-morpholinopropionitrile, NaOMe, DMSO, 75 °C, 20 min; (c) anilinium chloride, isopropanol, reflux, 25 min; (d) guanidium chloride, EtOH, reflux, 12 h

The formation of protodeboronated side product **4.21** was expected during radiosynthesis of [18F]**1.23**. In order to improve the molar activity of [18F]**1.23**, **4.21** was synthesized to compare

46

elution profile against [^{18}F]**1.23** on HPLC and to determine if separation of [^{18}F]**1.23** from **4.21** was possible. Compound **4.21** was synthesized using the same linear synthetic approach as **3.0** (Scheme 5). Also, the protodeboronated product for [^{18}F]**3.0** is the compound GW2580 and this compound was obtained from Vadim Bernard-Gauthier from the Schirrmacher Group and was used as received. The overall chemical yield of **4.21** was 20%.

5.0   Radiosynthesis of [^{18}F]**4.8a**: Intermediate Product During Radiosynthesis of [^{18}F]**3.0**

Utilizing the newly developed boronic ester precursor, **4.17a**, radiosynthesis of [^{18}F]**4.8a** was carried out using the radiofluorination method developed by the Gouverneur Group (Scheme 6).
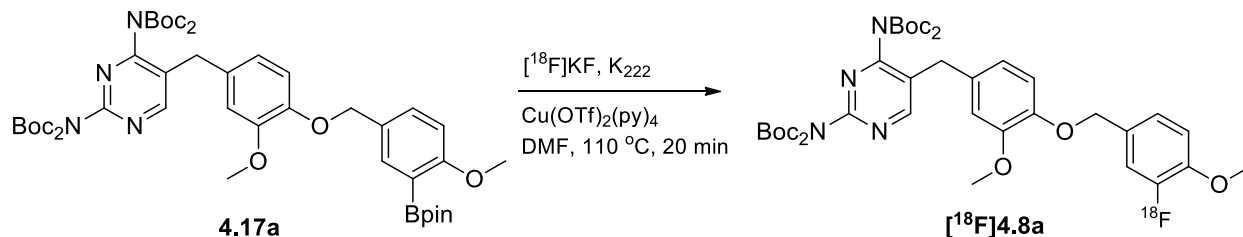
Scheme 6. Radiofluorination of **4.17a**

This method of radiosynthesis involved elution of [^{18}F]F$^-$ from a QMA cartridge using a 1 mL K$_{222}$/K$_2$CO$_3$ solution. After azeotropic drying of [^{18}F]F$^-$, the [^{18}F]KF/K$_{222}$ was re-dissolved in 1 mL of acetonitrile (~1.0 GBq) to form the stock solution of [^{18}F]F$^-$. To optimize and obtain a reasonable radiochemical conversion (RCC, calculated by radio-TLC) of **4.17a** to [^{18}F]**4.8a**, various amounts of the Cu-catalyst and [^{18}F]KF/K$_{222}$ solutions were evaluated. Initially, when varying amounts of Cu-catalyst were employed, the amount of the stock [^{18}F]KF/K$_{222}$ solution used was kept constant at 40 µL. The highest rates of RCC ($3 \pm 1\%$, n=4) were observed when 0.5 equivalents of the Cu-catalyst were used. However, when the amount of Cu-catalyst deviated from the value of 0.5 equivalent, the RCC either decreased or was not observed (Table 7).

Table 7. Varying amounts of Cu-catalyst used in the radiosynthesis of [^{18}F]**4.8a** and the corresponding RCC.

Cu-catalyst used (Equivalent)	RCC (%)
0.1	0.75 ± 0.25 (n=3)
0.2	1.25 ± 0.25 (n=3)
0.5	3 ± 1 (n=4)
1.0	0.75 ± 0.25 (n=2)
5.0	0 (n=1)

In an effort to increase the radioactivity amount of [^{18}F]**4.8a**, increased volumes (60 µL – 500 µL) of the [^{18}F]KF/K$_{222}$ stock solution were used. However, it was found that when the amount of [^{18}F]F$^-$ stock solution was greater than 40 µL, there was a decrease in RCC or no RCC at all (Table 8). As a result of the increased amounts of the [^{18}F]F$^-$ stock volume used, there was an increase in basicity due to the K$_2$CO$_3$ present in the [^{18}F]KF/K$_{222}$ solution. Therefore, the increase in basicity negatively affects the radiofluorination and leads to reduction in RCC. These results were similar to the findings of Neumaier *et al* in regard to the negative influence of basic conditions during radiofluorination with Cu-catalysts due to potential copper adduct formation.[56]

Table 8. Varying amounts of ^{18}F used from a 1 mL stock solution of [^{18}F]F$^-$ (14.0 mg of K$_{222}$, 14 µL of 1M K$_2$CO$_3$ solution)

Volume (µL)	RCC (%)
40	3 ± 1 (n=3)
60	1
100	0
500	0

Even though the radiosynthesis of [^{18}F]**4.8a** demonstrated a low RCC, the following reaction conditions demonstrated to be the most effective for radiofluorination: 1 equivalent of precursor

4.17a (3.5 mg, 0.0039 mmol), (Cu(OTf)$_2$(py)$_4$ (0.5 equiv), and 40 µL of [^{18}F]KF/K$_{222}$ solution, dissolved in 300 µL of DMF heated at 110 $^{\circ}$C for 20 minutes (Figure 20).
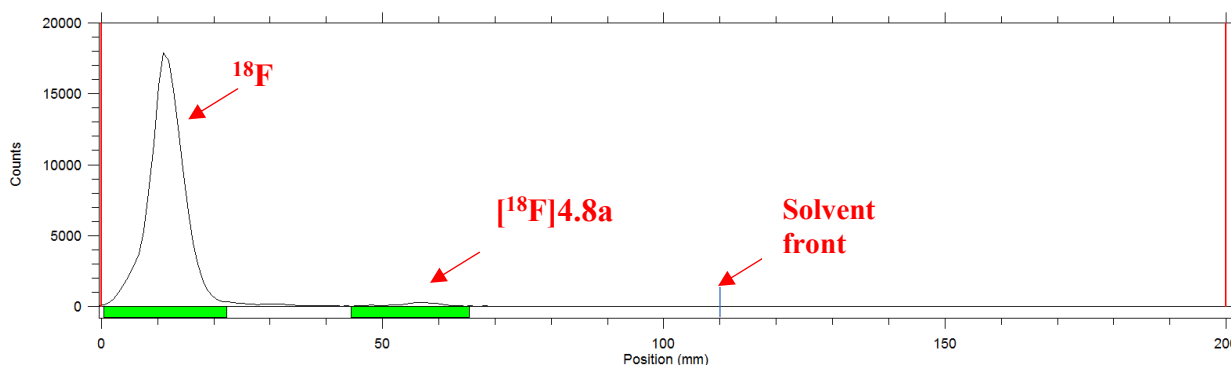
Figure 20. Radio-TLC of [^{18}F]**4.8a** radiofluorination. Reaction conditions: [^{18}F]KF, K$_{222}$, Cu(OTf)$_2$(py)$_4$, DMF, 110 $^{\circ}$C, 20 min. Mixture of 50/50 hexane and ethyl acetate was used as the eluent to develop the radio-TLC.

It was hypothesized that in addition to the basic conditions contributing to the low RCC, the methoxy group present at the *ortho*-position to the Bpin might also negatively influence the RCC. Previously, Gouverneur's Group reported that Cu-mediated radiofluorination was well tolerated with *ortho*-, *para*-, and *meta*-positioned electron donating groups (EDG) relative to the Bpin, although discrepancies in yield could still be observed.[53] Out of the numerous precursors tested by Gouverneur's Group, most of the compounds demonstrated high RCYs, ranging from 27 % to 83 %. However, the two compounds that had an EDG in the *ortho*-position of the boronic ester displayed a significant decrease in radiofluorination, down to 10%-11% RCY (Scheme 7).[53]
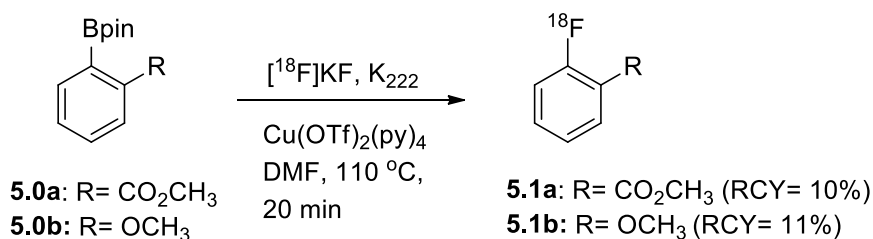
Scheme 7. Two compounds with EDG substituent similar to **4.17a** in the *ortho*-position of the boronic ester and their radiofluorination yield

50

In a similar report by the Scott Group, the authors report that *ortho* substituents lead to reduced RCYs due to slower transmetalation caused by steric hindrance.[57] When arylboronic acids with - *ortho* (**5.2**)*, -para* (**5.3**) *, -meta* (**5.4**) carboxylic ester substituents (Figure 21) were radiofluorinated, only the *ortho* substituted arylboronic acid showed a decrease in RCY (11 ± 2%, n=3).[57]

5.2
11 ± 2% (n=3)

5.3
49 ± 9% (n=3)

5.4
56 ± 1% (n=3)
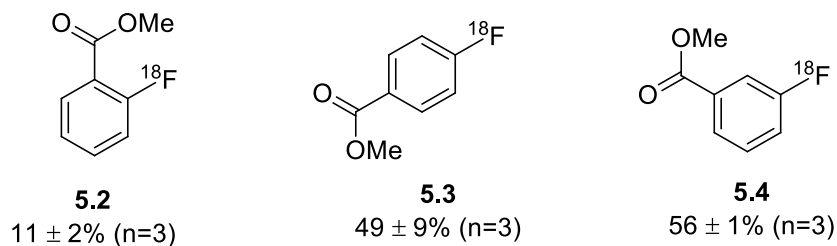
Figure 21. Carboxylic ester substitution at *ortho, para,* and *meta* position. RCYs are dependent on the different substitution positions.

The low RCC of [^{18}F]**4.8a** and previous reports by Gouverneur and Scott suggest that compounds with *ortho* substituents relative to the Bpin are not an ideal candidate for Cu-catalyzed radiofluorination. In order to avoid the *ortho* methoxy group relative to the Bpin, radiosynthesis of [^{18}F]**1.23** lacking an *ortho* methoxy substituent was carried out next.

5.1 Radiosynthesis of Boc-protected [^{18}F]**4.8b**, intermediate product during the radiosynthesis of [^{18}F]**1.23**

In addition to verifying the influence of EDG substituent, synthesizing [^{18}F]**1.23** based on the Gouverneur method would avoid the multi-step radiosynthesis explored previously by the Schirrmacher Group.[134] Unlike **3.0**, **1.23** does not have any substituents located at the *ortho-, para-,* or *meta*-position to the fluorine. From the previous attempts towards the radiosynthesis of [^{18}F]**4.8a**, it was hypothesized the low RCC was obtained due to the *ortho*-positioned EDG group relative to the Bpin. As a result, it was predicted that the radiosynthesis of [^{18}F]**4.8b** should result in an improved RCC of the corresponding Bpin precursor **4.17b**. As a result, in order to test the hypothesis, radiosynthesis of [^{18}F]**4.8b** was carried out using the same conditions as for [^{18}F]**4.8a** (Scheme 8).
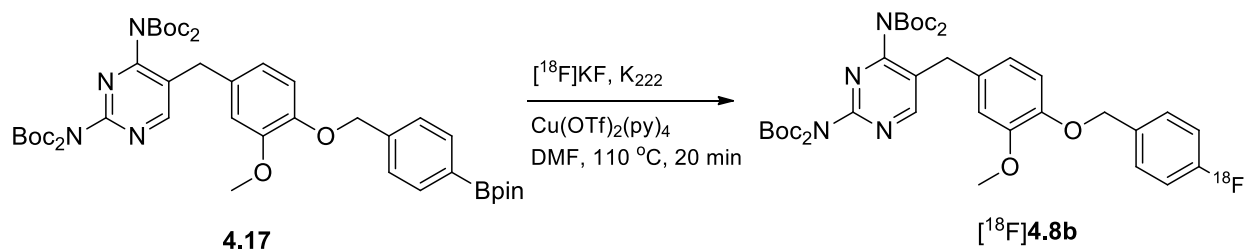
Scheme 8. Radiosynthesis of [^{18}F]**4.8b**

Using the same radiofluorination conditions as for [^{18}F]**4.8a,** improvements in RCYs of **4.17b** to [^{18}F]**4.8b** were observed (8.5 ± 1.5%, n=3).
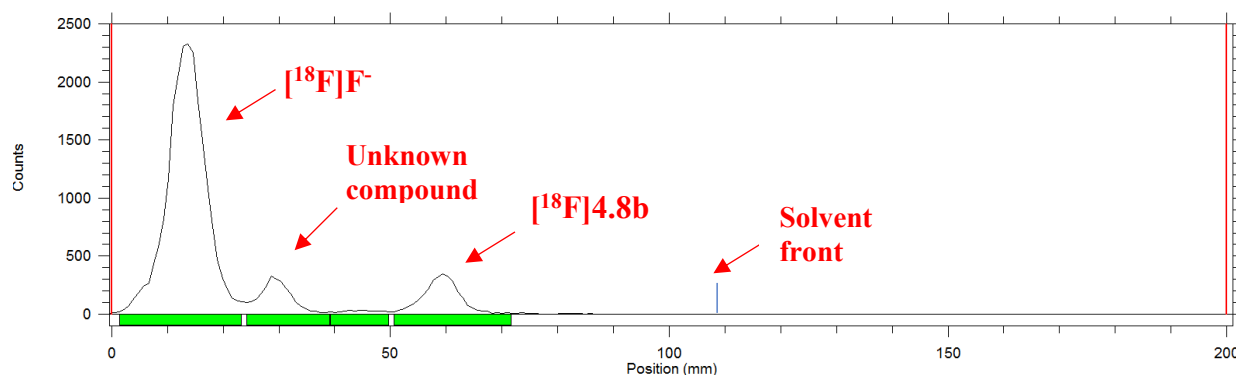
Figure 22. Radio-TLC result of radiofluorination of **4.17b** yielding [^{18}F]**4.8b**. Reaction conditions: [^{18}F]KF, K$_{222}$, Cu(OTf)$_2$(py)$_4$, DMF, 110 °C, 20 min. Mixture of 50/50 hexane and ethyl acetate was used as the eluent to develop the radio-TLC

In addition to the peak with R$_f$ of 0.45, corresponding to [^{18}F]**4.8b**, another peak corresponding to an unknown compound with R$_f$ of 0.2 was observed (Figure 22). It was hypothesized that this additional peak could correspond to a partially Boc-deprotected [^{18}F]**4.8b**. If Boc-deprotection was occurring this would result in an unfavorable reaction condition due to potential Chan-Lam cross coupling by the exposed amine groups. With the discovery of the unknown peak, two major challenges had to be overcome. First, a different radiosynthetic approach had to be utilized to avoid highly basic conditions. Second, characterization of the unknown peak was required. In order to

avoid highly basic radiofluorination conditions, a less basic approach to drying and eluting [^{18}F]F⁻, developed by the Scott's Group, was utilized (*vide infra*).[57]

5.1.1   Radiosynthesis of [^{18}F]**4.8b** using [^{18}F]F⁻ eluted with KOTf (Scott method)

One of the main benefits of using KOTf for drying [^{18}F]F⁻ is the ability to minimize the usage of a strong base such as K_2CO_3.[57] With this method, unlike the Gouverneur's method where only aliquots of [^{18}F]F⁻ stock solution were used, the fully dried [^{18}F]F⁻ stock solution could be used for radiosynthesis. Also, another benefit of the new Scott method was the ability to utilize a freshly formed Cu-catalyst during radiosynthesis. The Cu-catalyst was formed by combining Cu(OTf)$_2$ with pyridine in a 1:25 molar ratio.[57] Due to possible degradation of the Cu-catalyst during storage, *in situ* synthesis of the Cu-catalyst avoids any potential problems that might result from catalyst degradation.

The radiosynthesis of [^{18}F]**4.8b** was performed using 1 equivalent of **4.17b** (4 mg, 0.0046 mmol), 5 equivalents of Cu(OTf)$_2$, 25 equivalents of pyridine, and [^{18}F]KF/K(OTf) (resuspended in 1 mL of DMF, ~ 1 GBq) at 110 °C for 20 minutes (Scheme 9).
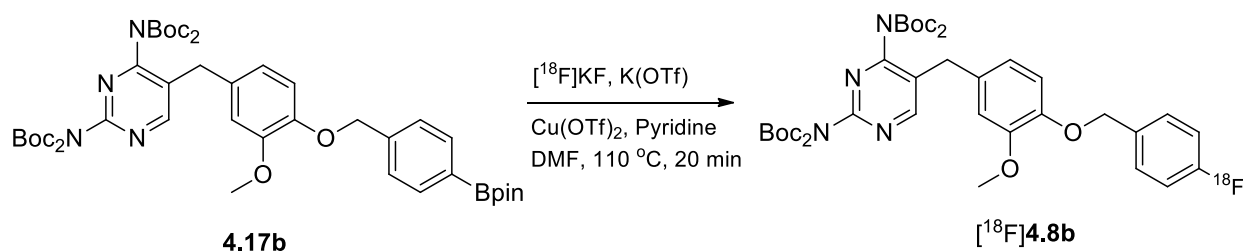
Scheme 9. Radiosynthesis of [^{18}F]**4.8b** using [^{18}F]F⁻ eluted using KOTf.

Utilizing Scott's method of radiofluorination[57], it was possible to obtain 4.5 ± 1.5% (n=4) RCY (non-decay corrected). Even though there were no improvements in RCY compared to Gouverneur's method, significant improvements were observed in terms of absolute yields of [^{18}F]**4.8b** (30-50 MBq) by being able to utilize higher amounts of starting radioactivity (1 GBq).

5.1.2   Unexpected Boc-deprotection during radiosynthesis of [^{18}F]**4.8b**

When the crude reaction mixture of [^{18}F]**4.8b** and [^{18}F]F$^-$ (1.3 GBq) was analyzed by radio-HPLC, multiple peaks were observed. (Figure 23). The four different radiopeaks eluted at 19 minutes (fraction 1), 22 minutes (fraction 2), 33 minutes (fraction 3), and 36 minutes (fraction 4) respectively. Also, each radiopeak had varying amounts of activity: 8.5 MBq, 11.4 MBq, 30.0 MBq, and 20.3 MBq. Based on the radio-HPLC, fraction 4 had the lowest polarity while fraction 1 had the highest polarity. Due to the increase in polarity of the radiopeaks, it was hypothesized that successive Boc-deprotection of [^{18}F]**4.8b** might be occurring.
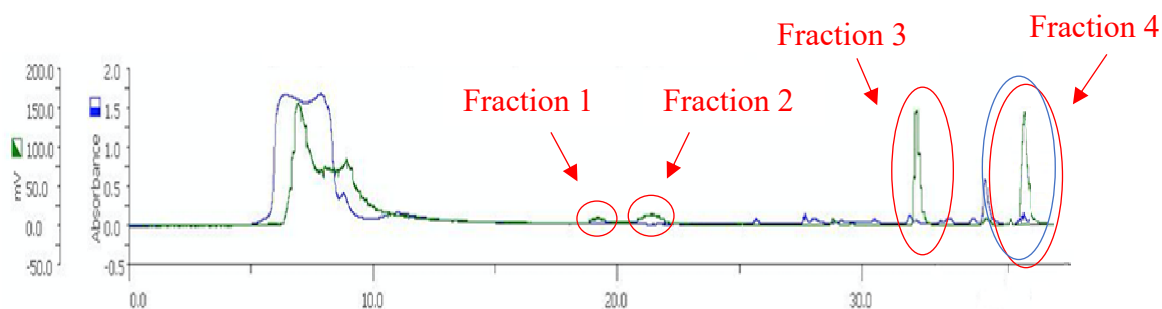
Figure 23. HPLC analysis of the crude radiofluorination reaction of **4.17b** to produce [^{18}F]**4.8b**. Red circles show the four unknown radiopeaks (fractions 1-4). Radioactive signal of [^{18}F]**4.8b** was expected at around 35 min (blue circle). Green line represents the radioactivity signal while the blue line indicates the UV absorbance peak.

Afterwards, each of the fractions from the HPLC separation was collected and further analyzed by radio-TLC. When the radio-TLC was performed, due to the large amounts of [^{18}F]F$^-$ in the crude mixture, this resulted in tailing of [^{18}F]F$^-$ during HPLC analysis, resulting in a radio-signal corresponding to [^{18}F]F$^-$ which can be observed in the radio-TLC analysis of fractions 1 and 2 (Figure 24 A and B). Also, due to tailing of fraction 1 during HPLC separation, the radio-signal corresponding to fraction 1 was observed in the radio-TLC of fraction 2. The radio-TLC results demonstrated that fraction 4 had the same R_f (0.45) as the fully Boc-protected **4.8b** while fraction 1 had the same R_f (0.52) as the fully Boc-deprotected **1.23**. These results suggested that conditions for radiofluorination also resulted in full/partial Boc-de protection of [^{18}F]**4.8b**.
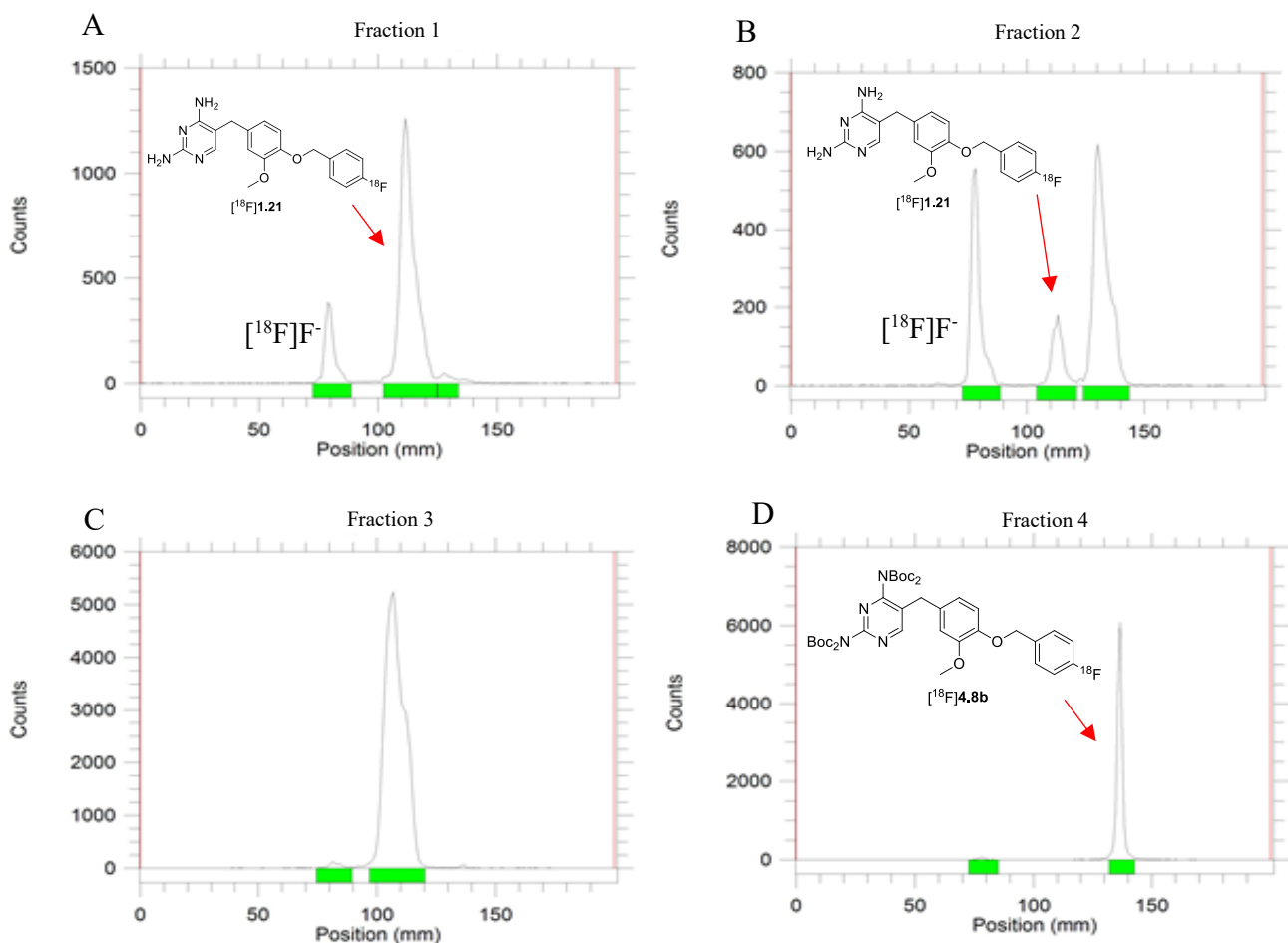
Figure 24. Radio-TLC of the four different fractions collected from HPLC analysis. Fractions 1 corresponds to fully Boc-deprotected ^{18}F-labelled [18F]**1.23**, while fraction 4 corresponds to fully Boc-protected compound [18F]**4.8b**. Fractions 2 and 3 are suspected to be the partially Boc-deprotected ^{18}F-labelled compounds. (A) Fraction 1 and (B) fraction 2 were developed using 50/50 of MeOH/DCM, while (C) fraction 3 and (D) fraction 4 were developed using 50/50 hexane/ethyl acetate.

For further verification, fractions 4 and 1 were co-injected with the ^{19}F standards [19F]**4.8b** and [19F]**1.23** for HPLC analysis. The HPLC analysis demonstrated that fraction 4 with [19F]**4.8b** eluted at the same time (Figure 25A), while fraction 1 eluted at the same time as [19F]**1.23** (Figure 25B). These results suggest that conditions for radiofluorination also resulted in Boc-deprotection of [18F]**4.8b.** As a result**,** fractions 2/3 are hypothesized to be the partially Boc-deprotected derivatives of [18F]**4.8b**. The Boc-deprotection is undesirable since it also suggests that Boc-

deprotection of the precursor **4.17b** might be occuring before it undergoes radiofluorination. This results in an unfavorable reaction environment since presence of unprotected amines or alcohols hinders radiofluorination of Bpin precursors (*vide infra*).
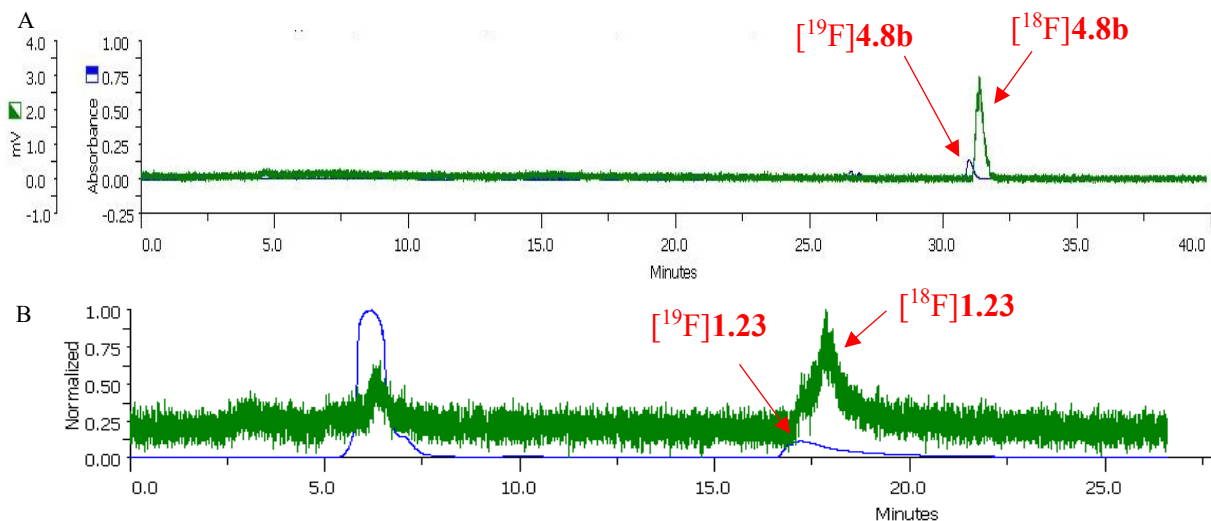
Figure 25. Radio-HPLC chromatograms of co-injection of non-radioactive standards [^{19}F]**4.8b** and [^{19}F]**1.23** with radioactive fractions 4 and 1. (A) Elution of fraction 4 with **4.8b**. (B) Elution of fraction 1 with **1.23**. Green line represents the radioactivity while the blue line indicates the UV absorbance peak.

Also, when the radioactivity amount of each fraction was measured, the combined radioactivity of fraction 2 and fraction 3 was more than 58% of the total combined radioactivity. This result suggested that the majority of the Boc-protected amines might be undergoing partial Boc-deprotection during the labeling reaction. A similar result was reported by Zischler *et al.* (2017) when working with *N,N,O,O*-tetra-boc protected substrates.[141] They reported that almost complete cleavage (> 80%) occurred for one of the *N*-Boc protection groups.

In another report by Gouverneur's Group, the researchers utilized a guanidine-based boronic ester precursor **5.5** for radiofluorination.[142] This guanidine-based structure had four Boc-protecting groups (Scheme 10), similar to the *tetra*-Boc protected diaminopyrimidine ring in compound **4.8b.**
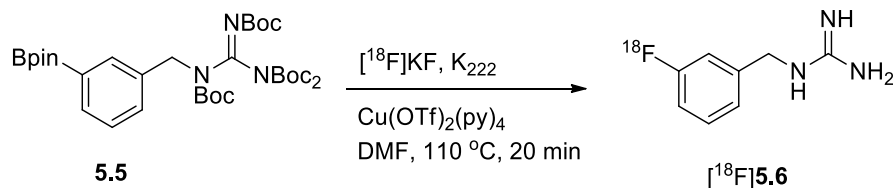
Scheme 10. Radiosynthesis of [¹⁸F]**5.6** using Gouverneur's radiofluorination methodology.

The authors reported a low RCY of 7% for the radiosynthesis of [¹⁸F]**5.6** starting from the boc-protected Bpin precursor **5.5**.[142] These results suggest that having numerous Boc protecting group might be unfavorable for Cu-catalyzed synthesis due to deprotection leading to the presence of amine groups.

In another report by Gouverneur's Group, it was found that the presence of unprotected alcohols or amines results in trace amounts of radiofluorination (RCY < 10%).[53] The authors report that Chan-Lam cross coupling might be a possible explanation for the low yield of radiofluorination for groups with un-protected amines.[53]

5.2   Boc-deprotection of [¹⁸F]**4.8b** using trifluoroacetic acid (TFA)

Since fractions 2-4 corresponded to [¹⁸F]**4.8b** with varying Boc-protection ([¹⁸F]**5.7**, [¹⁸F]**5.8**, [¹⁸F]**5.9)**, these fractions were combined and treated with TFA and heat to completely remove the Boc-protecting groups (Scheme 11).

[¹⁸F]**5.7**: R= NH
[¹⁸F]**5.8**: R= NHBoc
[¹⁸F]**5.9**: R= NBoc₂
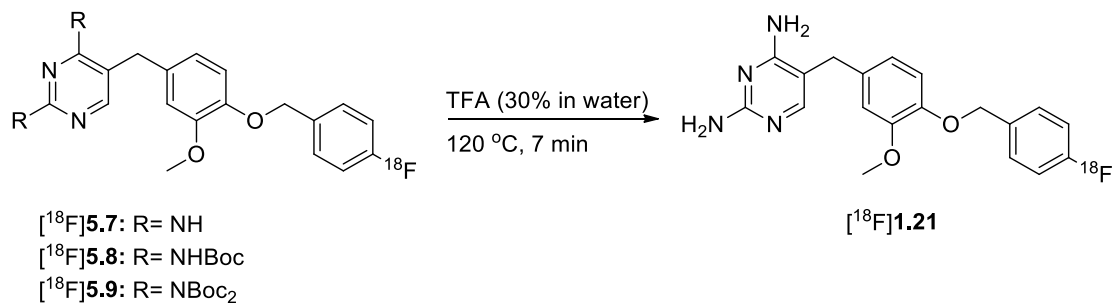
[¹⁸F]**1.21**

Scheme 11. Deprotection of Boc-protecting group on [¹⁸F]**5.7** to produce [¹⁸F]**1.23**

After removal of Boc-protecting groups, the crude mixture containing [^{18}F]**1.23** was co-injected with the [^{19}F]**1.23** standard (Figure 26). As a result, starting from the initial 1.3 GBq of radioactivity, [^{18}F]**1.23** was synthesized with 13 MBq of radioactivity (RCY = 1%, non-decay corrected) Even though [^{18}F]**1.23** was identified by co-injection with non-radioactive standard [^{19}F]**1.23** (Figure 26), due to the tailing of the radioactivity signal, HPLC purification of [^{18}F]**1.23** was difficult to achieve. As a result, improvements in HPLC conditions were made to shorten the elution time and to reduce the radiopeak tailing (*vide infra*).
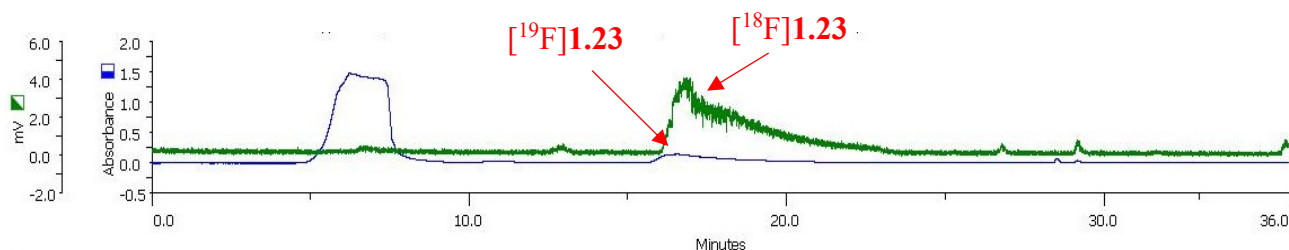
Figure 26. Radio-HPLC analysis of the final crude mixture of [^{18}F]**1.23** after Boc-deprotection of [^{18}F]**5.7**, [^{18}F]**5.8**, [^{18}F]**5.9** using TFA. Reaction condition: 130 µL of 30% TFA solution, 120 °C, 7 min. Green line represents the radioactivity while the blue line indicates the UV absorbance peak.

5.3   HPLC optimization and one-pot radiosynthesis of [^{18}F]**1.23**

One of the major problems in the purification of [^{18}F]**1.23** was the frequently observed tailing of the radioactivity signal and UV signal. Initial studies used TFA to reduce the HPLC tailing by protonating the amines to obtain only one radiochemical species on the HPLC column. However, [^{18}F]**1.23** still eluted over a period of 10 min (Figure 24). On the other hand, when sodium acetate was used as a buffer solution (pH 9), the radiopeak elution broadness was reduced to 1- 1.5 min (refer to experimental section 8.5, condition B). To address solubility issues of [^{19}F]**1.23** in aqueous solutions, 150 µL of DMSO was added to the injection solvent to completely dissolve [^{19}F]**1.23**. As a result, by using a sodium acetate buffer solution and addition of DMSO to injection solvent, HPLC analysis of [^{19}F]**1.23** was significantly improved (Figure 27). These optimized

HPLC conditions reduced the peak broadness of [^{18}F]**1.23**, significantly improving the HPLC purification of [^{18}F]**1.23**.
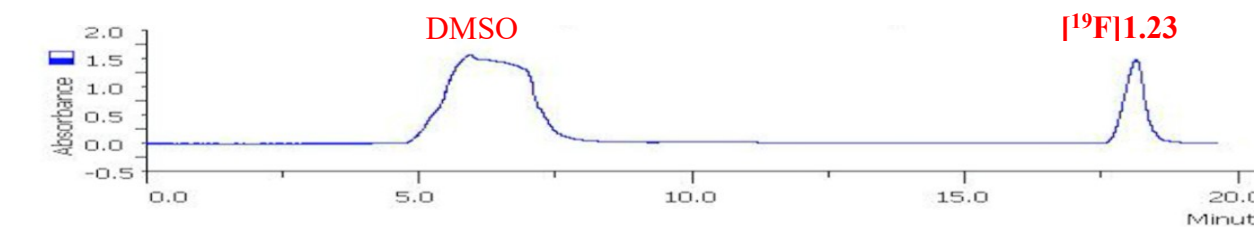
Figure 27. HPLC analysis of non-radioactive [^{19}F]**1.23** using optimized HPLC condition: isocratic 35 % MeCN, 65 % sodium acetate buffer solution (pH: 9)

Synthesis of [^{18}F]**1.23** was successfully carried out in one-pot using a two-step radiosynthesis: 1) radiofluorination of **4.17b** and 2) Boc deprotection of [^{18}F]**5.7**, [^{18}F]**5.8**, and [^{18}F]**5.9** (Figure 28). The reaction conditions were: 1 equivalent of **4.17b** (4 mg, 0.0046 mmol), 5 equivalents of Cu(OTf)$_2$, 25 equivalents of pyridine, and [^{18}F]KF/K(OTf) (resuspended in 1 mL of DMF, ~ 1 GBq) at 110 $^{\circ}$C for 20 minutes followed by treatment with 130 µL of 30% TFA solution, 120 $^{\circ}$C, 7 min. By removing the HPLC purification step between radiofluorination of **4.17b** and Boc deprotection of **[^{18}F]4.8b**, the radiosynthesis duration decreased thus slightly improving the overall RCY from 1% to 2.5% (non-decay corrected).
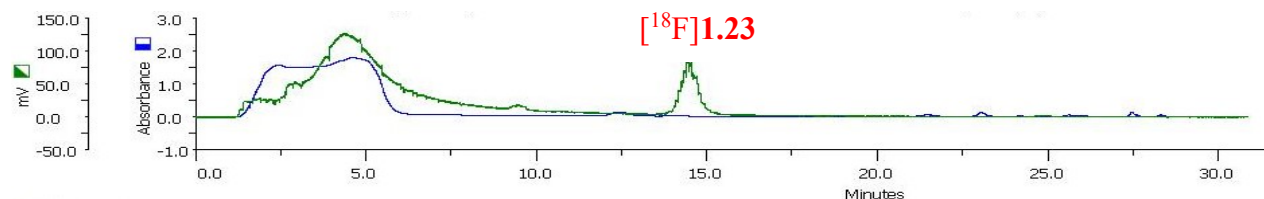
Figure 28. Radio-HPLC analysis of the crude mixture containing [^{18}F]**1.23** from one pot radiosynthesis starting from the Boc-protected Bpin precursor **4.17b**. Green line represents the radioactivity signal while the blue line indicates the UV absorbance peak.

After HPLC purification of the initial crude mixture, the collected eluent containing [^{18}F]**1.23** was further purified by C-18 light Sep-Pak cartridge extraction (Scheme 12).

| Step 1: Radiosynthesis of [^{18}F]**1.23**. | → | Step 2: HPLC purification of [^{18}F]**1.23**. Phenomenex® Luna C-18. Isocratic 35 % MeCN, 65 % sodium acetate buffer solution (pH: 9) | → | Step 3: HPLC purified [^{18}F]**1.23** diluted in 25 mL of water. |

Step 6: Elute the C-18 cartridge dropwise and collect 3 drops of ethanol per Eppendorf tubes (total of 10 Eppendorf tube). ← Step 5: Wash the C-18 light Sep-Pak column containing [^{18}F]**1.23** with 3 mL of water. ← Step 4: Pass the [^{18}F]**1.23** and water mixture through C-18 light Sep-Pak column.

Step 7: Measure the Eppendorf tubes for radioactivity. Combine all Eppendorf tube fractions containing radioactivity from [^{18}F]**1.23**. → Step 8: Transfer EtOH solution containing the [^{18}F]**1.23** into a clean Eppendorf tube. Evaporate the remaining EtOH. → Step 9: Re-dissolve [^{18}F]**1.23** in 100 µL of molecular biology grade EtOH diluted with saline. Ready for use as PET radiotracer.

Scheme 12. Purification process of [^{18}F]**1.23** to obtain an injectable solution.

After the purification process, [^{18}F]**1.23** was eluted in 100 µL of ethanol from the C-18 cartridge as a radiotracer for potential use in PET imaging. When the purified [^{18}F]**1.23** was analyzed by HPLC, the analysis demonstrated complete removal of radioactivity corresponding to [^{18}F]F$^-$ and ^{18}F-labelled partial Boc-protected compounds (**[^{18}F]5.7**). This resulted in an isolated and purified [^{18}F]**1.23** radioactivity signal (Figure 29A). Larger volumes of HPLC purified [^{18}F]**1.23** was injected for HPLC analysis (15 MBq in 1 mL of HPLC solvent) in order to observe UV activity for A_m calculations (Figure 29C). Due to the larger HPLC injection volume of [^{18}F]**1.23** (1 mL), peak broadening is observed (Figure 29C). Furthermore, as a result of the inability to separate

[^{19}F]**1.23** and the expected protodeboronated side product **4.21**, the UV signal was predicted to be produced from both [^{19}F]**1.23** and **4.21** (*vide infra*). In the end, 28 ± 2 MBq of [^{18}F]**1.23** (2.5% ± 0.5% RCY, non-decay corrected), with > 99% RCP, and a A$_m$ of 3.4 – 4.5 GBq/μmol were produced from starting activity of 1 GBq of [^{18}F]F$^-$.
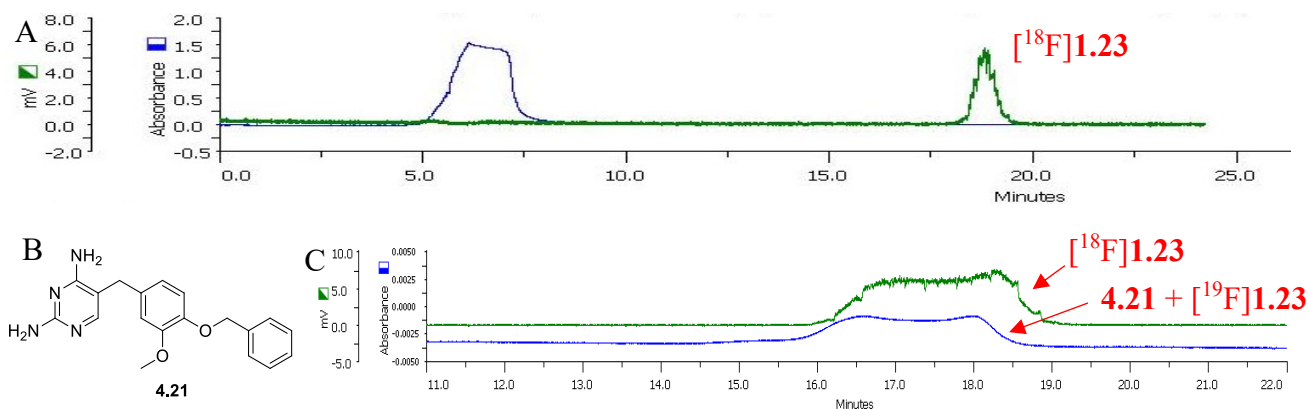
Figure 29. Radio-HPLC analysis of the final HPLC purified compound [^{18}F]**1.23** (A) HPLC analysis demonstrating high RCP of [^{18}F]**1.23,** no other radiopeaks such as [^{18}F]F$^-$ or mixture of [^{18}F]**5.7**/[^{18}F]**5.8**/[^{18}F]**5.9** were observed. (B) Structure of protodeboronated side product **4.21**. (C) HPLC analysis showing trace amounts of UV absorbance assumed to be a mixture of both [^{19}F]**1.23** and **4.21**. Peak broadening is also observed due to large solvent injection onto the HPLC. Green line represents the radiotracer while the blue line indicates the UV absorbance peak.

5.4   Molar activity of [^{18}F]**1.23** under the assumption of occurring protodeboronation

Even though [^{18}F]**1.23** was produced with high RCP, a low A$_m$ (3.4 – 4.5 GBq/μmol) was observed. Two main factors that contribute to this problem are the low RCY and the likely production of protodeboronated side product **4.21**. When the non-radioactive standard [^{19}F]**1.23** and **4.21** were co-injected into the HPLC using the Phenomenex® Luna C-18 column, both compounds co-eluted at the same time (Figure 30).

61
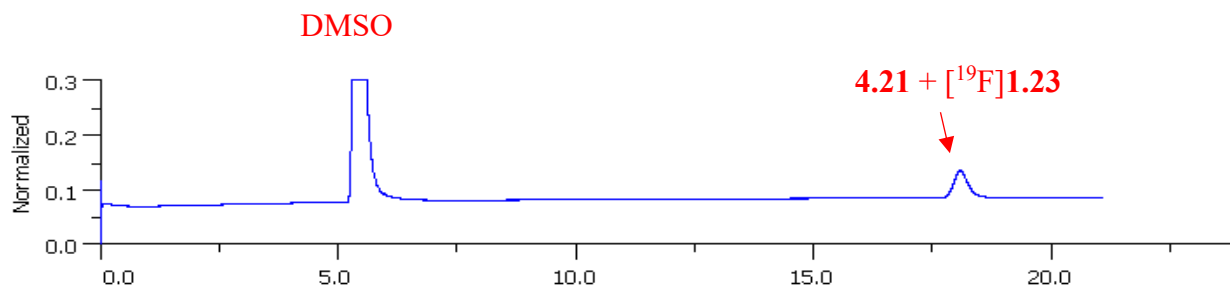
Figure 30. HPLC analysis of non-radioactive standards [^{19}F]**1.23** and **4.21**. When the compounds were co-injected into the HPLC, separation was not achieved resulting in one UV peak corresponding to both [^{19}F]**1.23** and **4.21.** HPLC condition: isocratic 35 % MeCN, 65 % sodium acetate buffer solution (pH: 9)

When the protodeboronated side product **4.21** was co-injected with the ^{18}F-labelled radiotracer, [^{18}F]**1.23,** the HPLC analysis demonstrated that the two compounds eluted at the same time **(**Figure 31).
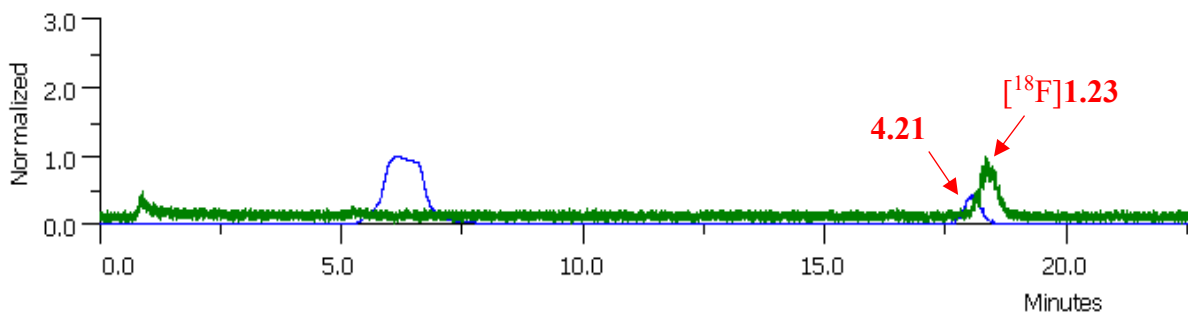
Figure 31. Co-injection of the protodeboronated side product **4.21** and [^{18}F]**1.23** for HPLC analysis using the Phenomenex® Luna C-18 column. The analysis demonstrated that the two compounds elute at the same time (17 min). Green line represents the radiotracer while the blue line indicates the UV absorbance peak.

In an attempt to better separate the protodeboronated side product from [^{18}F]**1.23**, a Phenomenex® Luna PFP(2) column was investigated for separation. Previous research by Mossine *et al* (2017) demonstrated that using the Phenomenex® Luna PFP(2) column, the researchers were able to get a better separation of the protodeboronated side product from their ^{18}F-labelled product.[143]

However, when the mixture of [^{19}F]**1.23** and **4.21** was co-injected with [^{18}F]**1.23** into the HPLC, the HPLC analysis demonstrated a broad tailing UV peak corresponding to both [^{19}F]**1.23** and **4.21** (Figure 32).
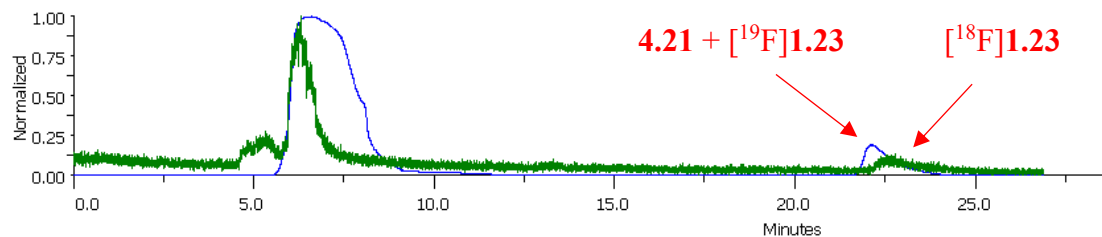
Figure 32. HPLC analysis of [^{18}F]**1.23** co-injected with mixture of the non-radioactive standard [^{19}F]**1.23** and **4.21**. Only a single UV peak indicating overlap of the [^{19}F]**1.23** and **4.21** UV signal. HPLC condition: isocratic 35 % MeCN, 65 % sodium acetate buffer solution (pH: 9). Green line represents the radiotracer while the blue line indicates the UV absorbance peak.

HPLC analysis was also performed with varying solvent gradients and without the addition of DMSO in the injection solvent. However, only minimal separation of the non-radioactive [^{19}F]**1.23** and **4.21** was achieved and tailing of the UV signal was consistently observed (Figure 33). As a result, it was concluded that the separation of [^{19}F]**1.23** and **4.21** was not achievable with the Phenomenex® Luna PFP(2) column, due to tailing of **4.21** into the [^{19}F]**1.23** peak.
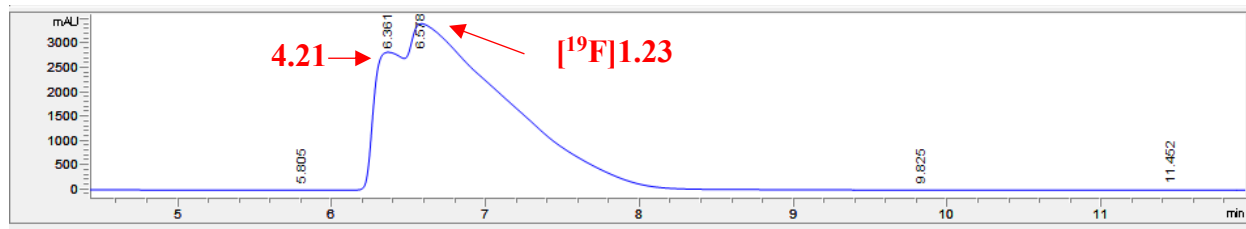
Figure 33. HPLC-analysis of non-radioactive [^{19}F]**1.23** co-injected with **4.21**. HPLC analysis was done using the non-radioactive compounds and demonstrates minimal separation of the two compounds. HPLC condition: isocratic 45 % MeCN, 55 % sodium acetate buffer solution (pH: 9)

As it is not possible to collect [^{18}F]**1.23** without the protodeboronated contaminant **4.21**, A_m was calculated using the molar mass of [^{19}F]**1.23** (354.38 g/mol). However, the molar mass of **4.21** (336.39 g/mol) should also have been taken into consideration since the UV trace contains both [^{19}F]**1.23** and **4.21**. As a result, due to the inability to determine the ratio between [^{19}F]**1.23** and **4.21**, it was not possible to determine the exact A_m during radiosynthesis.

Due to the formation of protodeboronated side product when using Bpin precursors, the ability to utilize the Bpin precursors for radiofluorination crucially depends on the ability to separate the protodeboronated product from the ^{18}F-labelled radiotracers. Inability to separate the protodeboronated side product results in low A_m and leads to detrimental effects when performing PET studies. For example, a study done by the Schirrmacher and the Scott Group demonstrated that when ^{18}F-labelled compound, [^{18}F]**1.21** was not separated from the protodeboronated product **5.8** (Figure 34), resulting in a low A_m (15 GBq/μmol).[117] However, when [^{18}F]**1.21** was separated from **5.8** significant improvements in A_m were observed (245 Gbq/μmol).[117] As a result the quality of corresponding PET images in non-human primates varied significantly depending on A_m.[117]
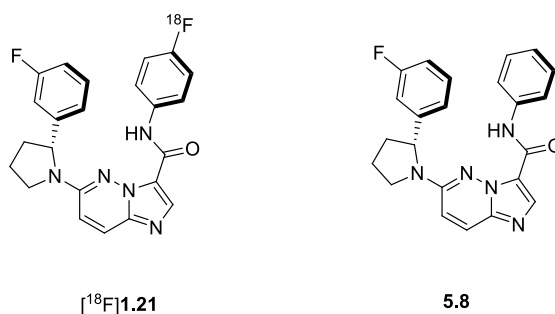
Figure 34. Chemical structure of [^{18}F]**1.21** and the respective protodeboronated product **5.8**

When the low A_m or high A_m versions of [^{18}F]**1.21** was injected into non-human primates for PET imaging, the high A_m [^{18}F]**1.21** demonstrated higher uptake in TrkB/C-rich regions compared to the low A_m [^{18}F]**1.21** (Figure 35).[117] These results demonstrate the importance of a method to separate protodeboronated side product when using Bpin precursors for radiosynthesis or avoid protodeboronation during the radiosynthesis.
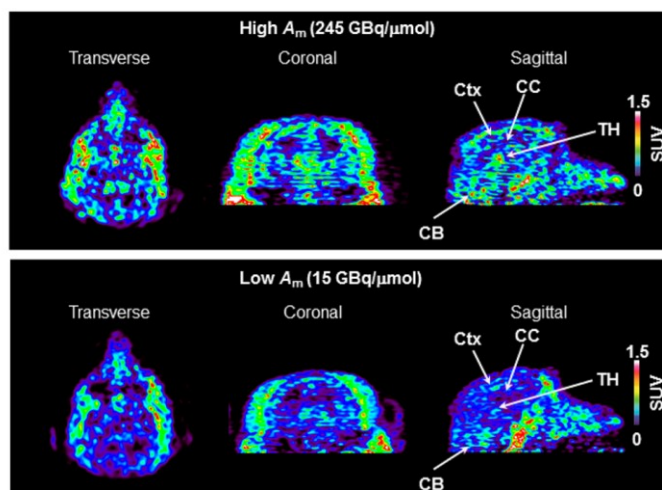
Figure 35. *In vivo* PET imaging of $[^{18}F]$**1.21** in the rhesus monkey brain. Top panel: PET image developed using a high A_m $[^{18}F]$**1.21**. Bottom panel: PET image developed using a low A_m $[^{18}F]$**1.21**. CB= cerebellum; CC= corpus callosum; Ctx= cortex; TH= thalamus. (Image adapted with permission from Reference 117. Copyright (2018) American Chemical Society)

In conclusion, $[^{18}F]$**1.23** was synthesized starting from the Bpin precursor **4.17b** with high RCP **(> 99%)** using the Scott method of Cu-catalyzed radiofluorination. Even though the Gouverneur method of Cu-catalyzed radiofluorination has been demonstrated to be effective, the highly basic condition during $[^{18}F]F^-$ elution proved detrimental for radiofluorination of **4.17b.** Scott's method of radiofluorination employed milder basic conditions, however, the high reaction temperature led to Boc-deprotection of **4.17b,** exposing free amines. It was predicted that the low overall RCY (2.5% non-decay corrected) of $[^{18}F]$**1.23** is the result of the exposed free amines during radiofluorination. Also, the low A_m (3.4 – 4.5 GBq/μmol) of $[^{18}F]$**1.23** was conluded to be the result of the inseparable protodeboronated side product **4.21** formed in the reaction.

6.0   Summary and Conclusion

With recent advances in NGS and identification of *NTRK* gene fusion involvement in cancer, numerous Trk inhibitors have been developed. Some of these Trk inhibitors are in clinical phase with promising results and potential for future usage in clinical setting. As a result, it is crucial to develop a method to non-invasively image and quantify Trk receptors using PET. Research groups such as the Schirrmacher group have previously developed numerous Trk radiotracers and have performed first in-human PET imaging of Trk receptors in the human brain. In order to further develop PET imaging of Trk receptors, two new Trk inhibitors **3.0** and **3.1** were synthesized based on the structure of GW2580 and previous work done by the Schirrmacher Group.

Initial molecular docking studies predicted that **3.0** and **3.1** had the potential to bind TrkB in a favorable conformation. However, an *in vitro* binding assay of **3.0** demonstrated an approximate two-fold decrease in the nanomolar binding potency towards Trk A, B and C, while **3.1** demonstrated a 30- to 44-fold decrease in binding potency for Trk A, B and C. Further analysis of molecular docking studies revealed that unfavorable steric interaction might be responsible for the decrease in binding potency. Even though **3.0** showed a decrease in binding potency versus GW2580, it maintained a similar binding potency as the previously studied GW2580 derivative, **1.23** reported by the Schirrmacher Group.

Radiosynthesis of [^{18}F]**3.0** was attempted starting from the Bpin precursor **4.17a**. The radiosynthesis followed a two-step approach: 1) radiofluorination of **4.17a** to form [^{18}F]**4.8a**, 2) Boc-deprotection of [^{18}F]**4.8a** to form [^{18}F]**3.0**. Radiofluorination of **4.17a** followed the method developed by the Gouverneur Group. However, during the radiofluorination step to synthesize [^{18}F]**4.8a,** low RCC (3%) was observed. The low RCC was predicted to be the result of the *ortho*-methoxy group leading to steric hindrance during transmetalation of the Cu-catalyst to the boronic ester. In order to avoid the *ortho*-methoxy substituent, attempts were made to achieve radiosynthesis of [^{18}F]**1.23** lacking an *ortho*-methoxy substituent. **1.23** is a fluorinated derivative of pan-Trk/CSF-1R inhibitor GW2580 and has previously been studied by the Schirrmacher Group. When **3.0** and **1.23** were compared with regard to their binding affinities to all three Trk sub-types, both compounds demonstrated similar binding potencies towards Trk A, B, and C. Even though

66

the Schirrmacher Group previously developed[^{18}F]**1.23** as a PET imaging agent, the previous radiosynthesis utilized a multi-step radiosyntheic procedure and required a simpler method of radiofluorination for possible clinical introduction as a Trk PET tracer.

The radiosynthesis of [^{18}F]**1.23** followed a two-step one-pot radiosynthesis: 1) radiofluorination of the Bpin precursor **4.17b** to form Boc-protected [^{18}F]**4.8b** and 2) Boc-deprotection of [^{18}F]**4.8b** to form [^{18}F]**1.23**. When attempts were made to radiofluorinate **4.17b,** improvements in RCC (8%) was observed. Even though improvements in RCC were achieved, Gouverneur Group's method of radiofluorination limited the amount of starting initial activity that could be used (40 MBq). As a result, radiosynthesis was carried out using the method developed by Scott Group. Scott Group's method of [^{18}F]F$^-$ elution involved usage of KOTf instead of the K_2CO_3. When Scott Group's method of radiofluorination was employed, the RCY (4%, non-decay corrected) remained similar to the previous RCY while using Gouverneur Group's method. However, based on Scott Group's method, the reaction was amenable with increased radioactivity (1 GBq) compared to the Gouverneur's method (40 MBq). Furthermore, during HPLC analysis of the crude radiofluorinated mixture of [^{18}F]**4.17b** several different radiopeaks were observed. By comparing each radiopeaks with the known non-radioactive standards [^{19}F]**4.17b** and **1.23**, it was concluded that Boc-deprotection is occurring during radiofluorination. This resulted in formation of partially Boc-protected radiofluorinated compounds [^{18}F]**5.7**, [^{18}F]**5.8**, and [^{18}F]**5.9** in addition to [^{18}F]**4.17b** and [^{18}F]**1.23**. The Boc-deprotection is might be detrimental to the radiofluorination since the presence of free amines and alcohols during Cu-catalyzed radiofluorination leads to low RCY. As a result, it was concluded that the unwanted Boc-deprotection might contribute to the low RCY observed during radiofluorination.

Starting from a 1 GBq of [^{18}F]F$^-$, 28 MBq of [^{18}F]**1.23** could be synthesized (2.5% RCY, non-decay corrected) with high RCP (> 99%). However, the formation of the protodeboronated side product **4.21** contributed to the low A_m of [^{18}F]**1.23** (3.4 – 4.5 GBq/μmol). In order to separate the side product **4.21** and [^{18}F]**1.23,** Phenomenex® Luna PFP(2) column was employed. However, even when using the Phenomenex® Luna PFP(2) column a separation of **4.21** and [^{19}F]**1.23** was not achieved. As a result, in addition to improving the RCY, separating the protodeboronated side

product **4.21** from the radiotracer [^{18}F]**1.23** is crucial for future studies using [^{18}F]**1.23** for PET imaging.

Lastly, even though using the Cu-catalyzed "late stage" radiofluorination of inactivated aromatic compounds increase the number of radiofluorinated compounds that can be developed, there are still several crucial problems that must be overcome. Initially, the use of boronic acid or ester derived precursors are an attractive compound due to their chemical stability and readily available method of synthesis. However, a major problem with working with boronic acid/ester is the formation of protodeboronated side product. In some cases, the formation of protodeboronated side product formation can be overcome through HPLC purification however, there are still limitations to using such a method as seen in this thesis. As a result, it is critical to identify alternate radiofluorination methods, such as lowering reaction temperature to decrease/abolish the formation of protodeboronated side product. Also, even though Gouverneur[53] and Scott[57] have previously reported high RCY for wide variety of aromatic compounds, there are still limitations when using compounds with multiple Boc-protected amines. For compounds with multiple Boc-protecting groups, the Cu-catalyzed radiofluorination condition leads to unwanted Boc deprotection exposing free amines. These free amines have the potential to undergo Chan-Lam cross coupling contributing to the low RCY. Finally, although limitations and problems still exist for Cu-catalyzed radiofluorination reactions, if these problems can be resolved, this method would prove to be a promising tool to develop a wide variety of ^{18}F-labelled PET tracers that will aid in improving personalized medicine for future cancer patients.

7.0   Materials and Methods

7.1   General materials and methods

All reagents and solvents were obtained from Sigma-Aldrich, ThermoFischer Scientific, and Alfa-Aesar, used as received. **1.23** and GW2580 were obtained from Vadim Bernard-Gauthier and used as received.[144] NMR data was collected by either Agilent/Varian DD2 MR two channel 400 MHz spectrometer or Agilent/Varian Inova four-channel 500 MHz spectrometer. ^{1}H-NMR and ^{13}C-NMR chemical shifts are recorded in ppm relative to deuterated chloroform ($CDCl_3$ 7.26 ppm) or dimethyl sulfoxide (DMSO 2.50 ppm). Peaks are reported as: s = singlet, d = doublet, t = triplet, q = quartet, p = quintet, m = multiplet, b = broad; coupling constants in Hz; integration. High Resolution Mass Spectra (HRMS) were obtained from the Regional Center for Mass Spectrometry of The Chemistry Department of the Université de Montréal (LC-MSD-TOF Agilent). Radio-TLC was performed using Merck silica gel F-254 aluminum plates and detected by Eckert & Ziegler AR-2000 Radio-TLC Imaging Scanner. High performance liquid chromatography (HPLC) purifications and analysis were performed using a Phenomenex LUNA® C18 column (100 Å, 250 Å~10 mm, 10 μm) using a Gilson 322 Pump module fitted with a 171 Diode Array and a radio detector

7.2   Biological evaluation

3.0 and **3.1** were tested in a [γ ^{33}P]ATP based enzymatic assay by Reaction Biology Corporation (Malvern, PA). The compounds were tested in a 10-concentration IC_{50} curve with a 3-fold serial dilution starting at 10 μM. The reactions were performed with 10 μM ATP and initially profiled against TrkA/B/C. Reagent used in the assay are base reaction buffer; 20 mM Hepes (pH 7.5) , 10 mM $MgCl_2$, 1 mM EGTA, 0.02% Brij35, 0.02 mg/mL BSA, 0.1 mM Na_3CO_4, 2 mM DTT, 1% DMSO.

7.3   Docking analysis

Molecular docking simulations were done using FITTED 3.5 program (FORECASTER platform)[145-147] The results were visualized using Discovery Studios 4.5.[148]

7.4 General radiosynthesis procedure

[^{18}F]Fluoride was produced by $^{18}O(p,n)^{18}F$ nuclear reaction through proton irradiation of enriched (98%) ^{18}O water (3.0 mL, Rotem ,Germany) using a TR19/9 cyclotron (Advanced Cyclotron Systems, Inc., Richmond, BC, Canada).

7.4.1 [^{18}F]F$^-$ elution using K_{222}/K_2CO_3

A Sep-Pak Light carbonate QMA cartridge (Waters) was preconditioned with 15 mL of water. Afterwards [^{18}F]fluoride (1.5 Gbq) in 1.5 mL [^{18}O]water was passed through the cartridge to trap the [^{18}F]fluoride. The trapped [^{18}F]fluoride was eluted with K_{222}/K_2CO_3 solution (14.0 mg of K_{222}, 14 µL of 1M K_2CO_3 solution, in 1 mL of acetonitrile/water (95/5)) into a graduated borosilicate v-vial. The eluted solution was azeotropically dried twice with 1.0 mL of anhydrous acetonitrile under stream of N_2 gas in vacuum at 90 $^{\circ}$C. After completion of the azeotropic drying, [^{18}F]fluoride was re-dissolved in anhydrous MeCN (1000 µL) to form the [^{18}F]KF/K_{222} stock solution.

7.4.1.1 Radiosynthesis of [^{18}F]4.8a and [^{18}F]4.8b using [^{18}F]F$^-$ eluted with K_2CO_3 (Gouverneur method)

Cu(OTf)$_2$(py)$_4$ (3.1 nmol, 0.5 equiv) was added to the Bpin precursor (**4.17a** or **4.17b)** (6 nmol, 1 equiv) and dissolved in 300 µL of DMF. The mixture was sealed under ambient air using a silicone septum cap. Using a syringe, 40 µL of the [^{18}F]KF/K_{222} stock solution was added into the reaction vial. The sealed vial was heated at 110 $^{\circ}$C for 20 minutes. The reaction was quenched with 100 µL of water and observed for RCC using radio-TLC.

7.4.2 [^{18}F]F$^-$ elution using KOTf

QMA-light Sep-Paks were flushed with 10 mL of ethanol, 10 mL of 90 mg/mL KOTf solution, and 10 mL of sterile water. [^{18}F]fluoride (1.5 GBq) in 1.5 mL [^{18}O]water was trapped on a QMA-light Sep-Pak (Waters) to remove [^{18}O]water and other impurities. The [^{18}F]fluoride was eluted into a reaction vial using 550 µL of aqueous solution containing 5 mg of KOTf. Then 1 mL of acetonitrile (MeCN) was added to the reaction vial and azeotropically dried at 100 $^{\circ}$C under argon stream for 8 minutes. An additional 1 mL of acetonitrile was added and dried for another 8 minutes. Generally, 70% of the radioactivity remained after azeotropic drying. After drying, the reaction vial was directly used for further radiosynthesis.

7.4.2.1 Radiosynthesis of [^{18}F]**1.23** using [^{18}F]F$^-$ eluted with KOTf (Scott method)

Prior to the radiosynthesis, copper (II) trifluoromethanesulfonate (CuOTf) (20 µmol, 5 equiv) in 100 µL of DMF, was added to pyridine (500 µmol, 25 equiv) in an Eppendorf tube. The mixture was briefly agitated using a vortex shaker (ThermoFischer Analog Vortex Mixer). To this mixture, boronic ester precursor **4.17b** (4 µmol, 1 equiv) dissolved in 100 µL of DMF was added. The reaction mixture was briefly agitated again using the vortex shaker. The combined reaction mixture was added to the glass vial containing the dried [^{18}F]fluoride with additional 600 µL of DMF, bringing the total solution volume to 800 µL. The reaction vial was sealed under an atmosphere of ambient air with a plastic cap and heated to 110 $^{\circ}$C for 20 minutes. Afterwards, the slight amount of remaining DMF was evaporated under argon gas for 8 minutes. A solution of 30 µL of TFA in 100 µL of water was added to the reaction vial and heated for another 7 minutes at 120 $^{\circ}$C. Finally, the reaction was allowed to cool to room temperature and the crude mixture was diluted with 150 µL of dimethyl sulfoxide (DMSO) and 350 µL of sodium acetate buffer (pH adjusted to 9 using ammonium hydroxide). afterwards, the mixture was injected in to HPLC using a 1 mL injection loop for purification.

7.5 Purification of [^{18}F]**1.23** with C-18 light Sep-Pak column

After HPLC purification of the crude mixture containing [^{18}F]**1.23**, the HPLC fraction containing the [^{18}F]**1.23** was collected and mixed with 25 mL of water. After washing the C-18 light Sep-Pak column with 5 mL of water, the mixture containing HPLC purified [^{18}F]**1.23** and water was injected into the C-18 light Sep-Pak column. Afterwards, the C-18 light Sep-Pak column was eluted with ethanol in a dropwise and the ethanol was collected into an Eppendorf tube. Finally, Eppendorf tube fractions containing [^{18}F]**1.23** were combined and heated to 90 ^{0}C to evaporate any remaining ethanol.

7.6 HPLC conditions

HPLC Condition A.

Condition: 35 % MeCN, 65 % TFA buffer (0.05 % TFA in water)

Flow Rate: 0.8 ml/min

Column: Phenomenex® Luna C-18 Column 150 x 4.6 mm. 5 µm.

HPLC Condition B

Condition: 35 % MeCN, 65 % sodium acetate buffer solution (pH: 9)

Flow Rate: 1 mL/min

Column: Phenomenex® Luna C-18 Column 250 x 10 mm. 10 µm

HPLC Condition C

Condition: 35 % MeCN, 65 % sodium acetate buffer solution (pH: 9)

Flow Rate: 1 mL/min

Column: Phenomenex® Luna PFP(2) Column 250 x 10 mm. 5 µm

Bibliography

1.   Pantel, A. R.; Mankoff, D. A., Molecular imaging to guide systemic cancer therapy: Illustrative examples of PET imaging cancer biomarkers. *Cancer Lett* **2017,** *387*, 25-31.

2.   Wehrl, H. F.; Judenhofer, M. S.; Wiehr, S.; Pichler, B. J., Pre-clinical PET/MR: technological advances and new perspectives in biomedical research. *Eur J Nucl Med Mol Imaging* **2009,** *36 Suppl 1*, S56-68.

3.   Turkington, T. G., Introduction to PET instrumentation. *Journal of Nuclear Medicine Technology* **2001,** *29* (1), 4-21.

4.   Shukla, A. K.; Kumar, U., Positron emission tomography: An overview. *Journal of Medical Physics / Association of Medical Physicists of India* **2006,** *31* (1), 13-21.

5.   Townsend, D. W., Physical principles and technology of clinical PET imaging. *Annals Of The Academy Of Medicine, Singapore* **2004,** *33* (2), 133-145.

6.   Verel, I.; Visser, G. W.; van Dongen, G. A., The promise of immuno-PET in radioimmunotherapy. *J Nucl Med* **2005,** *46 Suppl 1*, 164s-71s.

7.   Jacobson, M. S.; Steichen, R. A.; Peller, P. J., PET Radiochemistry and Radiopharmacy. In *PET-CT and PET-MRI in Oncology: A Practical Guide*, Peller, P.; Subramaniam, R.; Guermazi, A., Eds. Springer Berlin Heidelberg: Berlin, Heidelberg, 2012; pp 19-30.

8.   Das, B. K., Basic Principles of Cyclotron and Production of Positron-Emitting Isotopes. In *Positron Emission Tomography: A Guide for Clinicians*, Das, B. K., Ed. Springer India: New Delhi, 2015; pp 175-180.

9.   Production of Radionuclides. In *Molecular Imaging: Radiopharmaceuticals for PET and SPECT*, Vallabhajosula, S., Ed. Springer Berlin Heidelberg: Berlin, Heidelberg, 2009; pp 45-58.

10.   Schmor, P., Review of Cyclotrons for the Production of Radioactive Isotopes for Medical and Industrial Applications. *Reviews of Accelerator Science and Technology* **2011,** *04* (01), 103-116.

11.   Saha, G. B., *Basics of PET Imaging: Physics, Chemistry, and Regulations*. Springer New York: 2005.

12.   AGENCY, I. A. E., *Cyclotron Produced Radionuclides: Physical Characteristics and Production Methods*. INTERNATIONAL ATOMIC ENERGY AGENCY: Vienna, 2009.

13.   Chirakal, R.; Firnau, G.; Garnett, E. S., Sequential production of electrophilic and nucleophilic fluorinating agents from [18F]fluorine gas. *International Journal of Radiation Applications and Instrumentation. Part A. Applied Radiation and Isotopes* **1988,** *39* (10), 1099-1101.

14.   Miele, E.; Spinelli, G. P.; Tomao, F.; Zullo, A.; De Marinis, F.; Pasciuti, G.; Rossi, L.; Zoratto, F.; Tomao, S., Positron Emission Tomography (PET) radiotracers in oncology – utility of 18F-Fluoro-deoxy-glucose (FDG)-PET in the management of patients with non-small-cell lung cancer (NSCLC). *Journal of Experimental & Clinical Cancer Research : CR* **2008,** *27* (1), 52-52.

15.   Zhuang, H.; Codreanu, I., Growing applications of FDG PET-CT imaging in non-oncologic conditions. *Journal of Biomedical Research* **2015,** *29* (3), 189-202.

16.   Hoh, C. K., Clinical use of FDG PET. *Nuclear Medicine and Biology* **2007,** *34* (7), 737-742.

17.   Herholz, K.; Langen, K.-J.; Schiepers, C.; Mountz, J. M., Brain Tumors. *Seminars in nuclear medicine* **2012,** *42* (6), 356-370.

18.   Zhang, L.; Villalobos, A., Strategies to facilitate the discovery of novel CNS PET ligands. *EJNMMI Radiopharmacy and Chemistry* **2016,** *1* (1), 13.

19.   Varma, M. V. S.; Feng, B.; Obach, R. S.; Troutman, M. D.; Chupka, J.; Miller, H. R.; El-Kattan, A., Physicochemical Determinants of Human Renal Clearance. *Journal of Medicinal Chemistry* **2009,** *52* (15), 4844-4852.

20.   Arnott, J. A.; Planey, S. L., The influence of lipophilicity in drug discovery and design. *Expert Opinion on Drug Discovery* **2012,** *7* (10), 863-875.

21.   Papaneophytou, C. P.; Grigoroudis, A. I.; McInnes, C.; Kontopidis, G., Quantification of the Effects of Ionic Strength, Viscosity, and Hydrophobicity on Protein–Ligand Binding Affinity. *ACS Medicinal Chemistry Letters* **2014,** *5* (8), 931-936.

22.   Hein, P.; Michel, M. C.; Leineweber, K.; Wieland, T.; Wettschureck, N.; Offermanns, S., Receptor and Binding Studies. In *Practical Methods in Cardiovascular Research*, Dhein, S.; Mohr, F. W.; Delmar, M., Eds. Springer Berlin Heidelberg: Berlin, Heidelberg, 2005; pp 723-783.

23.   Van de Bittner, G. C.; Ricq, E. L.; Hooker, J. M., A Philosophy for CNS Radiotracer Design. *Accounts of Chemical Research* **2014,** *47* (10), 3127-3134.

24.   Patel, S.; Gibson, R., In vivo site-directed radiotracers: a mini-review. *Nuclear Medicine and Biology* **2008,** *35* (8), 805-815.

25.   Gillis, E. P.; Eastman, K. J.; Hill, M. D.; Donnelly, D. J.; Meanwell, N. A., Applications of Fluorine in Medicinal Chemistry. *Journal of Medicinal Chemistry* **2015,** *58* (21), 8315-8359.

26.   Stehouwer, J. S.; Goodman, M. M., Fluorine-18 Radiolabeled PET Tracers for Imaging Monoamine Transporters: Dopamine, Serotonin, and Norepinephrine. *PET clinics* **2009,** *4* (1), 101-128.

27.   Kilbourn, M. R.; Huizenga, J. R.; Nuclear, N. R. C. C. o.; Radiochemistry; Sciences, N. R. C. B. o. C.; Technology; National Research Council . Commission on Physical Sciences, M.; Applications, *Fluorine-18 Labeling of Radiopharmaceuticals*. National Academy Press: 1990.

28.   Miller, P. W.; Long, N. J.; Vilar, R.; Gee, A. D., Synthesis of 11C, 18F, 15O, and 13N Radiolabels for Positron Emission Tomography. *Angewandte Chemie International Edition* **2008,** *47* (47), 8998-9033.

29.   Cole, E. L.; Stewart, M. N.; Littich, R.; Hoareau, R.; Scott, P. J. H., Radiosyntheses using Fluorine-18: the Art and Science of Late Stage Fluorination. *Current topics in medicinal chemistry* **2014,** *14* (7), 875-900.

30.   Kim, D. W.; Jeong, H.-J.; Lim, S. T.; Sohn, M.-H., Recent Trends in the Nucleophilic [(18)F]-radiolabeling Method with No-carrier-added [(18)F]fluoride. *Nuclear Medicine and Molecular Imaging* **2010,** *44* (1), 25-32.

31.   Stewart, M. N.; Hockley, B. G.; Scott, P. J., Green approaches to late-stage fluorination: radiosyntheses of (18)F-labelled radiopharmaceuticals in ethanol and water. *Chem Commun (Camb)* **2015,** *51* (79), 14805-8.

32.   Kim, D. W.; Jeong, H. J.; Lim, S. T.; Sohn, M. H.; Katzenellenbogen, J. A.; Chi, D. Y., Facile nucleophilic fluorination reactions using tert-alcohols as a reaction medium: significantly enhanced reactivity of alkali metal fluorides and improved selectivity. *The Journal of organic chemistry* **2008,** *73* (3), 957-62.

33.   Sergeev, M. E.; Morgia, F.; Lazari, M.; Wang, C.; van Dam, R. M., Titania-Catalyzed Radiofluorination of Tosylated Precursors in Highly Aqueous Media. *Journal of the American Chemical Society* **2015,** *137* (17), 5686-5694.

34.   Chun, J.-H.; Telu, S.; Lu, S.; Pike, V. W., Radiofluorination of diaryliodonium tosylates under aqueous-organic and cryptand-free conditions. *Organic & biomolecular chemistry* **2013,** *11* (31), 5094-5099.

35.   Mossine, A. V.; Brooks, A. F.; Ichiishi, N.; Makaravage, K. J.; Sanford, M. S.; Scott, P. J. H., Development of Customized [(18)F]Fluoride Elution Techniques for the Enhancement of Copper-Mediated Late-Stage Radiofluorination. *Scientific Reports* **2017,** *7*, 233.

36.   Dollé, F.; Helfenbein, J.; Hinnen, F.; Mavel, S.; Mincheva, Z.; Saba, W.; Schöllhorn-Peyronneau, M.-A.; Valette, H.; Garreau, L.; Chalon, S.; Halldin, C.; Madelmont, J.-C.; Deloye, J.-B.; Bottlaender, M.; Le Gailliard, J.; Guilloteau, D.; Emond, P., One-step radiosynthesis of [18F]LBT-999: a selective radioligand for the visualization of the dopamine transporter with PET. *Journal of Labelled Compounds and Radiopharmaceuticals* **2007,** *50* (8), 716-723.

37.	Grierson, J. R.; Shields, A. F., Radiosynthesis of 3′-deoxy-3′-[18F]fluorothymidine: [18F]FLT for imaging of cellular proliferation in vivo. *Nuclear Medicine and Biology* **2000,** *27* (2), 143-156.

38.	Hamacher, K.; Coenen, H. H.; Stocklin, G., Efficient stereospecific synthesis of no-carrier-added 2-[18F]-fluoro-2-deoxy-D-glucose using aminopolyether supported nucleophilic substitution. *J Nucl Med* **1986,** *27* (2), 235-8.

39.	Mori, T.; Kasamatsu, S.; Mosdzianowski, C.; Welch, M. J.; Yonekura, Y.; Fujibayashi, Y., Automatic synthesis of 16α-[18F]fluoro-17β-estradiol using a cassette-type [18F]fluorodeoxyglucose synthesizer. *Nuclear Medicine and Biology* **2006,** *33* (2), 281-286.

40.	Wang, M.; Yin, D.; Li, S.; Wang, Y., Synthesis of O-(2-[18F]fluoroethyl)-L-tyrosine and its biological evaluation in B16 melanoma-bearing mice as PET tracer for tumor imaging. *Science in China Series B: Chemistry* **2007,** *50* (2), 276-283.

41.	Balz, G.; Schiemann, G., Über aromatische Fluorverbindungen, I.: Ein neues Verfahren zu ihrer Darstellung. *Berichte der deutschen chemischen Gesellschaft (A and B Series)* **1927,** *60* (5), 1186-1190.

42.	Wallach, O., Ueber die Einwirkung von Phosphorpentachlorid auf Säureamide. *Justus Liebigs Annalen der Chemie* **1882,** *214* (1-2), 193-256.

43.	Chun, J.-H.; Morse, C. L.; Chin, F. T.; Pike, V. W., No-carrier-added [(18)F]fluoroarenes from the radiofluorination of diaryl sulfoxides. *Chemical communications (Cambridge, England)* **2013,** *49* (21), 2151-2153.

44.	Tredwell, M.; Gouverneur, V., 18F Labeling of Arenes. *Angewandte Chemie International Edition* **2012,** *51* (46), 11426-11437.

45.	Sun, H.; DiMagno, S. G., Competitive demethylation and substitution in N,N,N-trimethylanilinium fluorides. *Journal of Fluorine Chemistry* **2007,** *128* (7), 806-812.

46.	Neumann, C. N.; Ritter, T., Late-Stage Fluorination: Fancy Novelty or Useful Tool? *Angewandte Chemie International Edition* **2015,** *54* (11), 3216-3221.

47.	Ross, T. L.; Ermert, J.; Hocke, C.; Coenen, H. H., Nucleophilic 18F-Fluorination of Heteroaromatic Iodonium Salts with No-Carrier-Added [18F]Fluoride. *Journal of the American Chemical Society* **2007,** *129* (25), 8018-8025.

48.	Cardinale, J.; Ermert, J.; Humpert, S.; Coenen, H. H., Iodonium ylides for one-step, no-carrier-added radiofluorination of electron rich arenes, exemplified with 4-(([18F]fluorophenoxy)-phenylmethyl)piperidine NET and SERT ligands. *RSC Advances* **2014,** *4* (33), 17293-17299.

49.	Rotstein, B. H.; Stephenson, N. A.; Vasdev, N.; Liang, S. H., Spirocyclic hypervalent iodine(III)-mediated radiofluorination of non-activated and hindered aromatics. *Nature Communications* **2014,** *5*, 4365.

50.	Lee, E.; Kamlet, A. S.; Powers, D. C.; Neumann, C. N.; Boursalian, G. B.; Furuya, T.; Choi, D. C.; Hooker, J. M.; Ritter, T., A Fluoride-derived Electrophilic Late-Stage Fluorination Reagent for PET Imaging. *Science (New York, N.Y.)* **2011,** *334* (6056), 639-642.

51.	Brooks, A. F.; Topczewski, J. J.; Ichiishi, N.; Sanford, M. S.; Scott, P. J. H., Late-stage [18F]fluorination: new solutions to old problems. *Chemical Science* **2014,** *5* (12), 4545-4553.

52.	Lee, E.; Hooker, J. M.; Ritter, T., Nickel-Mediated Oxidative Fluorination for PET with Aqueous [(18)F] Fluoride. *Journal of the American Chemical Society* **2012,** *134* (42), 17456-17458.

53.	Tredwell, M.; Preshlock, S. M.; Taylor, N. J.; Gruber, S.; Huiban, M.; Passchier, J.; Mercier, J.; Génicot, C.; Gouverneur, V., A General Copper-Mediated Nucleophilic 18F Fluorination of Arenes. *Angewandte Chemie International Edition* **2014,** *53* (30), 7751-7755.

54.	Ichiishi, N.; Canty, A. J.; Yates, B. F.; Sanford, M. S., Mechanistic Investigations of Cu-Catalyzed Fluorination of Diaryliodonium Salts: Elaborating the CuI/CuIII Manifold in Copper Catalysis. *Organometallics* **2014,** *33* (19), 5525-5534.

55. Ye, Y.; Schimler, S. D.; Hanley, P. S.; Sanford, M. S., Cu(OTf)2-Mediated Fluorination of Aryltrifluoroborates with Potassium Fluoride. *Journal of the American Chemical Society* **2013,** *135* (44), 16292-16295.

56. Zlatopolskiy, B. D.; Zischler, J.; Krapf, P.; Zarrad, F.; Urusova, E. A.; Kordys, E.; Endepols, H.; Neumaier, B., Copper-Mediated Aromatic Radiofluorination Revisited: Efficient Production of PET Tracers on a Preparative Scale. *Chemistry – A European Journal* **2015,** *21* (15), 5972-5979.

57. Mossine, A. V.; Brooks, A. F.; Makaravage, K. J.; Miller, J. M.; Ichiishi, N.; Sanford, M. S.; Scott, P. J. H., Synthesis of [18F]Arenes via the Copper-Mediated [18F]Fluorination of Boronic Acids. *Organic Letters* **2015,** *17* (23), 5780-5783.

58. Allen, S. J.; Watson, J. J.; Shoemark, D. K.; Barua, N. U.; Patel, N. K., GDNF, NGF and BDNF as therapeutic options for neurodegeneration. *Pharmacology & Therapeutics* **2013,** *138* (2), 155-175.

59. Marios, G. L.; Anna, K. B.; Konstantinos, A. C.; Alexandros, E. B., The Role of Neurotrophins in Axonal Growth, Guidance, and Regeneration. *Current Neurovascular Research* **2007,** *4* (2), 143-151.

60. Barbara, L. H., Dissecting the Diverse Actions of Pro- and Mature Neurotrophins. *Current Alzheimer Research* **2006,** *3* (1), 19-24.

61. Reichardt, L. F., Neurotrophin-regulated signalling pathways. *Philosophical Transactions of the Royal Society B: Biological Sciences* **2006,** *361* (1473), 1545-1564.

62. Levi-Montalcini, R., The nerve growth factor 35 years later. *Science* **1987,** *237* (4819), 1154.

63. Barde, Y. A.; Edgar, D.; Thoenen, H., Purification of a new neurotrophic factor from mammalian brain. *The EMBO Journal* **1982,** *1* (5), 549-553.

64. Maisonpierre, P. C.; Belluscio, L.; Squinto, S.; Ip, N. Y.; Furth, M. E.; Lindsay, R. M.; Yancopoulos, G. D., Neurotrophin-3: a neurotrophic factor related to NGF and BDNF. *Science* **1990,** *247* (4949), 1446.

65. Hallböök, F.; Ibáñez, C. F.; Persson, H., Evolutionary studies of the nerve growth factor family reveal a novel member abundantly expressed in xenopus ovary. *Neuron* **1991,** *6* (5), 845-858.

66. Seidah, N. G.; Benjannet, S.; Pareek, S.; Chrétien, M.; Murphy, R. A., Cellular processing of the neurotrophin precursors of NT3 and BDNF by the mammalian proprotein convertases. *FEBS Letters* **1996,** *379* (3), 247-250.

67. Hempstead, B. L., Deciphering Proneurotrophin Actions. In *Neurotrophic Factors*, Lewin, G. R.; Carter, B. D., Eds. Springer Berlin Heidelberg: Berlin, Heidelberg, 2014; pp 17-32.

68. Bradshaw, R. A.; Blundell, T. L.; Lapatto, R.; McDonald, N. Q.; Murray-Rust, J., Nerve growth factor revisited. *Trends in Biochemical Sciences* **1993,** *18* (2), 48-52.

69. Kaplan, D. R.; Miller, F. D., Signal transduction by the neutrophin receptors. *Current Opinion in Cell Biology* **1997,** *9* (2), 213-221.

70. Martin-Zanca, D.; Hughes, S. H.; Barbacid, M., A human oncogene formed by the fusion of truncated tropomyosin and protein tyrosine kinase sequences. *Nature* **1986,** *319* (6056), 743-748.

71. Barbacid, M.; Lamballe, F.; Pulido, D.; Klein, R., The trk family of tyrosine protein kinase receptors. *Biochimica et Biophysica Acta (BBA) - Reviews on Cancer* **1991,** *1072* (2), 115-127.

72. Stoleru, B.; Popescu, A. M.; Tache, D. E.; Neamtu, O. M.; Emami, G.; Tataranu, L. G.; Buteica, A. S.; Dricu, A.; Purcaru, S. O., Tropomyosin-Receptor-Kinases Signaling in the Nervous System. *Mædica* **2013,** *8* (1), 43-48.

73. Chao, M. V., Neurotrophins and their receptors: A convergence point for many signalling pathways. *Nat Rev Neurosci* **2003,** *4* (4), 299-309.

74. Vaishnavi, A.; Le, A. T.; Doebele, R. C., TRKing Down an Old Oncogene in a New Era of Targeted Therapy. *Cancer Discovery* **2015,** *5* (1), 25.

75. Banfield, M. J.; Naylor, R. L.; Robertson, A. G. S.; Allen, S. J.; Dawbarn, D.; Brady, R. L., Specificity in Trk Receptor:Neurotrophin Interactions. *Structure 9* (12), 1191-1199.

76. Schneider, R.; Schweiger, M., A novel modular mosaic of cell adhesion motifs in the extracellular domains of the neurogenic trk and trkB tyrosine kinase receptors. *Oncogene* **1991,** *6* (10), 1807-11.

77.	Urfer, R.; Tsoulfas, P.; O'Connell, L.; Shelton, D. L.; Parada, L. F.; Presta, L. G., An immunoglobulin-like domain determines the specificity of neurotrophin receptors. *The EMBO Journal* **1995,** *14* (12), 2795-2805.
78.	Bibel, M.; Barde, Y. A., Neurotrophins: key regulators of cell fate and cell shape in the vertebrate nervous system. *Genes & development* **2000,** *14* (23), 2919-37.
79.	Barbacid, M., Structural and Functional Properties of the TRK Family of Neurotrophin Receptors. *Annals of the New York Academy of Sciences* **1995,** *766* (1), 442-458.
80.	Barker, P. A.; Lomen-Hoerth, C.; Gensch, E. M.; Meakin, S. O.; Glass, D. J.; Shooter, E. M., Tissue-specific alternative splicing generates two isoforms of the trkA receptor. *Journal of Biological Chemistry* **1993,** *268* (20), 15150-15157.
81.	Haapasalo, A.; Sipola, I.; Larsson, K.; Åkerman, K. E. O.; Stoilov, P.; Stamm, S.; Wong, G.; Castrén, E., Regulation of TRKB Surface Expression by Brain-derived Neurotrophic Factor and Truncated TRKB Isoforms. *Journal of Biological Chemistry* **2002,** *277* (45), 43160-43167.
82.	Haapasalo, A.; Koponen, E.; Hoppe, E.; Wong, G.; Castrén, E., Truncated trkB.T1 Is Dominant Negative Inhibitor of trkB.TK+-Mediated Cell Survival. *Biochemical and Biophysical Research Communications* **2001,** *280* (5), 1352-1358.
83.	Brodeur, G. M.; Minturn, J. E.; Ho, R.; Simpson, A. M.; Iyer, R.; Varela, C. R.; Light, J. E.; Kolla, V.; Evans, A. E., Trk Receptor Expression and Inhibition in Neuroblastomas. *Clinical Cancer Research* **2009,** *15* (10), 3244-3250.
84.	Lamballe, F.; Tapley, P.; Barbacid, M., trkC encodes multiple neurotrophin-3 receptors with distinct biological properties and substrate specificities. *The EMBO Journal* **1993,** *12* (8), 3083-3094.
85.	Patapoutian, A.; Reichardt, L. F., Trk receptors: mediators of neurotrophin action. *Current Opinion in Neurobiology* **2001,** *11* (3), 272-280.
86.	Huang, E. J.; Reichardt, L. F., Neurotrophins: roles in neuronal development and function. *Annual Review Of Neuroscience* **2001,** *24*, 677-736.
87.	Vaishnavi, A.; Le, A. T.; Doebele, R. C., TRKing Down an Old Oncogene in a New Era of Targeted Therapy. *Cancer Discovery* **2015,** *5* (1), 25-34.
88.	Khotskaya, Y. B.; Holla, V. R.; Farago, A. F.; Mills Shaw, K. R.; Meric-Bernstam, F.; Hong, D. S., Targeting TRK family proteins in cancer. *Pharmacology & Therapeutics* **2017,** *173*, 58-66.
89.	Zheng, Z.; Liebers, M.; Zhelyazkova, B.; Cao, Y.; Panditi, D.; Lynch, K. D.; Chen, J.; Robinson, H. E.; Shim, H. S.; Chmielecki, J.; Pao, W.; Engelman, J. A.; Iafrate, A. J.; Le, L. P., Anchored multiplex PCR for targeted next-generation sequencing. *Nature Medicine* **2014,** *20*, 1479.
90.	Vaishnavi, A.; Capelletti, M.; Le, A. T.; Kako, S.; Butaney, M.; Ercan, D.; Mahale, S.; Davies, K. D.; Aisner, D. L.; Pilling, A. B.; Berge, E. M.; Kim, J.; Sasaki, H.; Park, S.-i.; Kryukov, G.; Garraway, L. A.; Hammerman, P. S.; Haas, J.; Andrews, S. W.; Lipson, D.; Stephens, P. J.; Miller, V. A.; Varella-Garcia, M.; Jänne, P. A.; Doebele, R. C., Oncogenic and drug-sensitive NTRK1 rearrangements in lung cancer. *Nature Medicine* **2013,** *19*, 1469.
91.	Ardini, E.; Bosotti, R.; Borgia Andrea, L.; De Ponti, C.; Somaschini, A.; Cammarota, R.; Amboldi, N.; Raddrizzani, L.; Milani, A.; Magnaghi, P.; Ballinari, D.; Casero, D.; Gasparri, F.; Banfi, P.; Avanzi, N.; Saccardo Maria, B.; Alzani, R.; Bandiera, T.; Felder, E.; Donati, D.; Pesenti, E.; Sartore-Bianchi, A.; Gambacorta, M.; Pierotti Marco, A.; Siena, S.; Veronese, S.; Galvani, A.; Isacchi, A., The TPM3-NTRK1 rearrangement is a recurring event in colorectal carcinoma and is associated with tumor sensitivity to TRKA kinase inhibition. *Molecular Oncology* **2014,** *8* (8), 1495-1507.
92.	Wiesner, T.; He, J.; Yelensky, R.; Esteve-Puig, R.; Botton, T.; Yeh, I.; Lipson, D.; Otto, G.; Brennan, K.; Murali, R.; Garrido, M.; Miller, V. A.; Ross, J. S.; Berger, M. F.; Sparatta, A.; Palmedo, G.; Cerroni, L.; Busam, K. J.; Kutzner, H.; Cronin, M. T.; Stephens, P. J.; Bastian, B. C., Kinase fusions are frequent in Spitz tumours and spitzoid melanomas. *Nat Commun* **2014,** *5*, 3116.

93.   Greco, A.; Miranda, C.; Pagliardini, S.; Fusetti, L.; Bongarzone, I.; Pierotti Marco, A., Chromosome I rearrangements involving the genes TPR and NTRK1 produce structurally different thyroid-specific TRK oncogenes. *Genes, Chromosomes and Cancer* **1998,** *19* (2), 112-123.

94.   Tognon, C.; Knezevich, S. R.; Huntsman, D.; Roskelley, C. D.; Melnyk, N.; Mathers, J. A.; Becker, L.; Carneiro, F.; MacPherson, N.; Horsman, D.; Poremba, C.; Sorensen, P. H. B., Expression of the ETV6-NTRK3 gene fusion as a primary event in human secretory breast carcinoma. *Cancer Cell* **2002,** *2* (5), 367-376.

95.   Eguchi, M.; Eguchi-Ishimae, M.; Tojo, A.; Morishita, K.; Suzuki, K.; Sato, Y.; Kudoh, S.; Tanaka, K.; Setoyama, M.; Nagamura, F.; Asano, S.; Kamada, N., Fusion of ETV6 to neurotrophin-3 receptor TRKC in acute myeloid leukemia with t(12;15)(p13;q25). *Blood* **1999,** *93* (4), 1355-63.

96.   Stransky, N.; Cerami, E.; Schalm, S.; Kim, J. L.; Lengauer, C., The landscape of kinase fusions in cancer. *Nature Communications* **2014,** *5*, 4846.

97.   Brodeur, G. M.; Nakagawara, A.; Yamashiro, D. J.; Ikegaki, N.; Liu, X.-G.; Azar, C. G.; Lee, C. P.; Evans, A. E., Expression of TrkA, TrkB and TrkC in human neuroblastomas. *Journal of Neuro-Oncology* **1997,** *31* (1), 49-56.

98.   Brodeur, G. M., Neuroblastoma: biological insights into a clinical enigma. *Nat Rev Cancer* **2003,** *3* (3), 203-216.

99.   Geiger, T. R.; Peeper, D. S., The neurotrophic receptor TrkB in anoikis resistance and metastasis: a perspective. *Cancer research* **2005,** *65* (16), 7033-6.

100.   Dolle, L.; Adriaenssens, E.; El Yazidi-Belkoura, I.; Le Bourhis, X.; Nurcombe, V.; Hondermarck, H., Nerve growth factor receptors and signaling in breast cancer. *Current cancer drug targets* **2004,** *4* (6), 463-70.

101.   Weeraratna, A. T.; Dalrymple, S. L.; Lamb, J. C.; Denmeade, S. R.; Miknyoczki, S.; Dionne, C. A.; Isaacs, J. T., Pan-trk inhibition decreases metastasis and enhances host survival in experimental models as a result of its selective induction of apoptosis of prostate cancer cells. *Clinical cancer research : an official journal of the American Association for Cancer Research* **2001,** *7* (8), 2237-45.

102.   Starr, C.; McMillan, B., *Human Biology*. Cengage Learning: 2015.

103.   Michalski, M. H.; Chen, X., Molecular imaging in cancer treatment. *European journal of nuclear medicine and molecular imaging* **2011,** *38* (2), 358-377.

104.   Tao, J. J.; Schram, A. M.; Hyman, D. M., Basket Studies: Redefining Clinical Trials in the Era of Genome-Driven Oncology. *Annual Review of Medicine* **2018,** *69* (1), 319-331.

105.   Gerbaudo, V. H.; Kim, C. K., PET Imaging-Based Phenotyping as a Predictive Biomarker of Response to Tyrosine Kinase Inhibitor Therapy in Non-small Cell Lung Cancer: Are We There Yet? *Nucl Med Mol Imaging* **2017,** *51* (1), 3-10.

106.   Amatu, A.; Sartore-Bianchi, A.; Siena, S., NTRK gene fusions as novel targets of cancer therapy across multiple tumour types. *ESMO Open* **2016,** *1* (2).

107.   Laetsch, T. W.; DuBois, S. G.; Mascarenhas, L.; Turpin, B.; Federman, N.; Albert, C. M.; Nagasubramanian, R.; Davis, J. L.; Rudzinski, E.; Feraco, A. M.; Tuch, B. B.; Ebata, K. T.; Reynolds, M.; Smith, S.; Cruickshank, S.; Cox, M. C.; Pappo, A. S.; Hawkins, D. S., Larotrectinib for paediatric solid tumours harbouring NTRK gene fusions: phase 1 results from a multicentre, open-label, phase 1/2 study. *The Lancet Oncology* **2018**.

108.   Drilon, A.; Laetsch, T. W.; Kummar, S.; DuBois, S. G.; Lassen, U. N.; Demetri, G. D.; Nathenson, M.; Doebele, R. C.; Farago, A. F.; Pappo, A. S.; Turpin, B.; Dowlati, A.; Brose, M. S.; Mascarenhas, L.; Federman, N.; Berlin, J.; El-Deiry, W. S.; Baik, C.; Deeken, J.; Boni, V.; Nagasubramanian, R.; Taylor, M.; Rudzinski, E. R.; Meric-Bernstam, F.; Sohal, D. P. S.; Ma, P. C.; Raez, L. E.; Hechtman, J. F.; Benayed, R.; Ladanyi, M.; Tuch, B. B.; Ebata, K.; Cruickshank, S.; Ku, N. C.; Cox, M. C.; Hawkins, D. S.; Hong, D. S.; Hyman, D. M., Efficacy of Larotrectinib in TRK Fusion–Positive Cancers in Adults and Children. *New England Journal of Medicine* **2018,** *378* (8), 731-739.

109.   Drilon, A.; Nagasubramanian, R.; Blake, J. F.; Ku, N.; Tuch, B. B.; Ebata, K.; Smith, S.; Lauriault, V.; Kolakowski, G. R.; Brandhuber, B. J.; Larsen, P. D.; Bouhana, K. S.; Winski, S. L.; Hamor, R.; Wu, W.-I.; Parker, A.; Morales, T. H.; Sullivan, F. X.; DeWolf, W. E.; Wollenberg, L. A.; Gordon, P. R.; Douglas-Lindsay, D. N.; Scaltriti, M.; Benayed, R.; Raj, S.; Hanusch, B.; Schram, A. M.; Jonsson, P.; Berger, M. F.; Hechtman, J. F.; Taylor, B. S.; Andrews, S.; Rothenberg, S. M.; Hyman, D. M., A Next-Generation TRK Kinase Inhibitor Overcomes Acquired Resistance to Prior TRK Kinase Inhibition in Patients with TRK Fusion–Positive Solid Tumors. *Cancer Discovery* **2017**.

110.   Zhai, D.; Deng, W.; Huang, J.; Rogers, E.; Cui, J. J., Abstract 3161: TPX-0005, an ALK/ROS1/TRK inhibitor, overcomes multiple resistance mechanisms by targeting SRC/FAK signaling. *Cancer research* **2017,** *77* (13 Supplement), 3161.

111.   Drilon, A.; Siena, S.; Ou, S. I.; Patel, M.; Ahn, M. J.; Lee, J.; Bauer, T. M.; Farago, A. F.; Wheler, J. J.; Liu, S. V.; Doebele, R.; Giannetta, L.; Cerea, G.; Marrapese, G.; Schirru, M.; Amatu, A.; Bencardino, K.; Palmeri, L.; Sartore-Bianchi, A.; Vanzulli, A.; Cresta, S.; Damian, S.; Duca, M.; Ardini, E.; Li, G.; Christiansen, J.; Kowalski, K.; Johnson, A. D.; Patel, R.; Luo, D.; Chow-Maneval, E.; Hornby, Z.; Multani, P. S.; Shaw, A. T.; De Braud, F. G., Safety and Antitumor Activity of the Multitargeted Pan-TRK, ROS1, and ALK Inhibitor Entrectinib: Combined Results from Two Phase I Trials (ALKA-372-001 and STARTRK-1). *Cancer Discov* **2017,** *7* (4), 400-409.

112.   Cunha, L.; Szigeti, K.; Mathe, D.; Metello, L. F., The role of molecular imaging in modern drug development. *Drug Discov Today* **2014,** *19* (7), 936-48.

113.   Zhu, A.; Lee, D.; Shim, H., Metabolic PET Imaging in Cancer Detection and Therapy Response. *Seminars in oncology* **2011,** *38* (1), 55-69.

114.   Slobbe, P.; Poot, A. J.; Windhorst, A. D.; van Dongen, G. A. M. S., PET imaging with small-molecule tyrosine kinase inhibitors: TKI-PET. *Drug Discovery Today* **2012,** *17* (21), 1175-1187.

115.   Bernard-Gauthier, V.; Aliaga, A.; Aliaga, A.; Boudjemeline, M.; Hopewell, R.; Kostikov, A.; Rosa-Neto, P.; Thiel, A.; Schirrmacher, R., Syntheses and Evaluation of Carbon-11- and Fluorine-18-Radiolabeled pan-Tropomyosin Receptor Kinase (Trk) Inhibitors: Exploration of the 4-Aza-2-oxindole Scaffold as Trk PET Imaging Agents. *ACS Chemical Neuroscience* **2015,** *6* (2), 260-276.

116.   Bernard-Gauthier, V.; Bailey, J. J.; Mossine, A. V.; Lindner, S.; Vomacka, L.; Aliaga, A.; Shao, X.; Quesada, C. A.; Sherman, P.; Mahringer, A.; Kostikov, A.; Grand'Maison, M.; Rosa-Neto, P.; Soucy, J.-P.; Thiel, A.; Kaplan, D. R.; Fricker, G.; Wängler, B.; Bartenstein, P.; Schirrmacher, R.; Scott, P. J. H., A Kinome-Wide Selective Radiolabeled TrkB/C Inhibitor for in Vitro and in Vivo Neuroimaging: Synthesis, Preclinical Evaluation, and First-in-Human. *Journal of Medicinal Chemistry* **2017,** *60* (16), 6897-6910.

117.   Bernard-Gauthier, V.; Mossine, A. V.; Mahringer, A.; Aliaga, A.; Bailey, J. J.; Shao, X.; Stauff, J.; Arteaga, J.; Sherman, P.; Grand'Maison, M.; Rochon, P.-L.; Wängler, B.; Wängler, C.; Bartenstein, P.; Kostikov, A.; Kaplan, D. R.; Fricker, G.; Rosa-Neto, P.; Scott, P. J. H.; Schirrmacher, R., Identification of [18F]TRACK, a Fluorine-18-Labeled Tropomyosin Receptor Kinase (Trk) Inhibitor for PET Imaging. *Journal of Medicinal Chemistry* **2018,** *61* (4), 1737-1743.

118.   Shewchuk, L. M.; Hassell, A. M.; Holmes, W. D.; Veal, J. M.; Emmerson, H. K.; Musso, D. L.; Chamberlain, S. D.; Peckham, G. E. Crystal structure of liganded cFMS kinase domain. 2004.

119.   James G. Conway, a.; Brad McDonald, a.; Janet Parham, a.; Barry Keith, a.; David W. Rusnak, a.; Eva Shaw, a.; Marilyn Jansen, a.; Peiyuan Lin, a.; Alan Payne, a.; Renae M. Crosby, a.; Jennifer H. Johnson, a.; Lloyd Frick, a.; Min-Hwa Jasmine Lin, a.; Scott Depee, a.; Sarva Tadepalli, a.; Bart Votta, a.; Ian James, a.; Karen Fuller, a.; Timothy J. Chambers, a.; Frederick C. Kull, a.; Stanley D. Chamberlain, a.; Jeff T. Hutchins, a.; Joseph Schlessinger, a., Inhibition of Colony-Stimulating-Factor-1 Signaling in vivo with the Orally Bioavailable cFMS Kinase Inhibitor GW2580. *Proceedings of the National Academy of Sciences of the United States of America* **2005,** (44), 16078.

120.   Conway, J. G.; Pink, H.; Bergquist, M. L.; Han, B.; Depee, S.; Tadepalli, S.; Lin, P.; Crumrine, R. C.; Binz, J.; Clark, R. L.; Selph, J. L.; Stimpson, S. A.; Hutchins, J. T.; Chamberlain, S. D.; Brodie, T. A., Effects of

the cFMS kinase inhibitor 5-(3-methoxy-4-((4-methoxybenzyl)oxy)benzyl)pyrimidine-2,4-diamine (GW2580) in normal and arthritic rats. *The Journal Of Pharmacology And Experimental Therapeutics* **2008,** *326* (1), 41-50.

121.   Lin, E. Y.; Nguyen, A. V.; Russell, R. G.; Pollard, J. W., Colony-Stimulating Factor 1 Promotes Progression of Mammary Tumors to Malignancy. *The Journal of Experimental Medicine* **2001,** *193* (6), 727.

122.   Kacinski, B. M., CSF-1 and its receptor in ovarian, endometrial and breast cancer. *Annals Of Medicine* **1995,** *27* (1), 79-85.

123.   Chitu, V.; Stanley, E. R., Colony-stimulating factor-1 in immunity and inflammation. *Current opinion in immunology* **2006,** *18* (1), 39-48.

124.   Stanley, E. R.; Chitu, V., CSF-1 Receptor Signaling in Myeloid Cells. *Cold Spring Harbor Perspectives in Biology* **2014,** *6* (6), a021857.

125.   Lewis, C. E.; Pollard, J. W., Distinct Role of Macrophages in Different Tumor Microenvironments. *Cancer research* **2006,** *66* (2), 605-612.

126.   Pollard, J. W., Trophic macrophages in development and disease. *Nature reviews. Immunology* **2009,** *9* (4), 259-70.

127.   Zhu, Y.; Knolhoff, B. L.; Meyer, M. A.; Nywening, T. M.; West, B. L.; Luo, J.; Wang-Gillam, A.; Goedegebuure, S. P.; Linehan, D. C.; DeNardo, D. G., CSF1/CSF1R blockade reprograms tumor-infiltrating macrophages and improves response to T-cell checkpoint immunotherapy in pancreatic cancer models. *Cancer research* **2014,** *74* (18), 5057-69.

128.   Cannarile, M. A.; Weisser, M.; Jacob, W.; Jegg, A.-M.; Ries, C. H.; Rüttinger, D., Colony-stimulating factor 1 receptor (CSF1R) inhibitors in cancer therapy. *Journal for ImmunoTherapy of Cancer* **2017,** *5* (1), 53.

129.   Karaman, M. W.; Herrgard, S.; Treiber, D. K.; Gallant, P.; Atteridge, C. E.; Campbell, B. T.; Chan, K. W.; Ciceri, P.; Davis, M. I.; Edeen, P. T.; Faraoni, R.; Floyd, M.; Hunt, J. P.; Lockhart, D. J.; Milanov, Z. V.; Morrison, M. J.; Pallares, G.; Patel, H. K.; Pritchard, S.; Wodicka, L. M., A quantitative analysis of kinase inhibitor selectivity. *Nature Biotechnology* **2008,** *26* (1), 127-132.

130.   Schwaid, A. G.; Cornella-Taracido, I., Causes and Significance of Increased Compound Potency in Cellular or Physiological Contexts. *Journal of Medicinal Chemistry* **2018,** *61* (5), 1767-1773.

131.   Fabian, M. A.; Biggs Iii, W. H.; Treiber, D. K.; Atteridge, C. E.; Azimioara, M. D.; Benedetti, M. G.; Carter, T. A.; Ciceri, P.; Edeen, P. T.; Floyd, M.; Ford, J. M.; Galvin, M.; Gerlach, J. L.; Grotzfeld, R. M.; Herrgard, S.; Insko, D. E.; Insko, M. A.; Lai, A. G.; Lélias, J.-M.; Mehta, S. A.; Milanov, Z. V.; Velasco, A. M.; Wodicka, L. M.; Patel, H. K.; Zarrinkar, P. P.; Lockhart, D. J., A small molecule–kinase interaction map for clinical kinase inhibitors. *Nature Biotechnology* **2005,** *23*, 329.

132.   Bertrand, T.; Kothe, M.; Liu, J.; Dupuy, A.; Rak, A.; Berne, P. F.; Davis, S.; Gladysheva, T.; Valtre, C.; Crenne, J. Y.; Mathieu, M., The Crystal Structures of TrkA and TrkB Suggest Key Regions for Achieving Selective Inhibition. *Journal of Molecular Biology* **2012,** *423* (3), 439-453.

133.   Stachel, S. J.; Sanders, J. M.; Henze, D. A.; Rudd, M. T.; Su, H.-P.; Li, Y.; Nanda, K. K.; Egbertson, M. S.; Manley, P. J.; Jones, K. L. G.; Brnardic, E. J.; Green, A.; Grobler, J. A.; Hanney, B.; Leitl, M.; Lai, M.-T.; Munshi, V.; Murphy, D.; Rickert, K.; Riley, D.; Krasowska-Zoladek, A.; Daley, C.; Zuck, P.; Kane, S. A.; Bilodeau, M. T., Maximizing Diversity from a Kinase Screen: Identification of Novel and Selective pan-Trk Inhibitors for Chronic Pain. *Journal of Medicinal Chemistry* **2014,** *57* (13), 5800-5816.

134.   Bernard-Gauthier, V.; Schirrmacher, R., 5-(4-((4-[(18)F]Fluorobenzyl)oxy)-3-methoxybenzyl)pyrimidine-2,4-diamine: a selective dual inhibitor for potential PET imaging of Trk/CSF-1R. *Bioorg Med Chem Lett* **2014,** *24* (20), 4784-90.

135.   Tetko, I. V. G., J.; Todeschini, R.; Mauri, A.; Livingstone, D.; Ertl, P.; Palyulin, V. A.; Radchenko, E. V.; Zefirov, N. S.; Makarenko, A. S.; Tanchuk, V. Y.; Prokopenko, V. V., Virtual computational chemistry laboratory - design and description. *J. Comput. Aid. Mol. Des* **2005,** *19*, 453-463.

136.   VCCLAB, Virtual Computational Chemistry Laboratory. http://www.vcclab.org.
137.   Molinspiration Property Calculation Service, www.molinspiration.com. **2002**.
138.   Zhang, L.; Villalobos, A.; Beck, E. M.; Bocan, T.; Chappie, T. A.; Chen, L.; Grimwood, S.; Heck, S. D.; Helal, C. J.; Hou, X.; Humphrey, J. M.; Lu, J.; Skaddan, M. B.; McCarthy, T. J.; Verhoest, P. R.; Wager, T. T.; Zasadny, K., Design and Selection Parameters to Accelerate the Discovery of Novel Central Nervous System Positron Emission Tomography (PET) Ligands and Their Application in the Development of a Novel Phosphodiesterase 2A PET Ligand. *Journal of Medicinal Chemistry* **2013,** *56* (11), 4568-4579.
139.   Chan, D. C. M.; Fu, H.; Forsch, R. A.; Queener, S. F.; Rosowsky, A., Design, Synthesis, and Antifolate Activity of New Analogues of Piritrexim and Other Diaminopyrimidine Dihydrofolate Reductase Inhibitors with ω-Carboxyalkoxy or ω-Carboxy-1-alkynyl Substitution in the Side Chain. *Journal of Medicinal Chemistry* **2005,** *48* (13), 4420-4431.
140.   Ishiyama, T.; Murata, M.; Miyaura, N., Palladium(0)-Catalyzed Cross-Coupling Reaction of Alkoxydiboron with Haloarenes: A Direct Procedure for Arylboronic Esters. *The Journal of organic chemistry* **1995,** *60* (23), 7508-7510.
141.   Zischler, J.; Kolks, N.; Modemann, D.; Neumaier, B.; Zlatopolskiy, B. D., Alcohol-Enhanced Cu-Mediated Radiofluorination. *Chemistry – A European Journal* **2017,** *23* (14), 3251-3256.
142.   Preshlock, S.; Calderwood, S.; Verhoog, S.; Tredwell, M.; Huiban, M.; Hienzsch, A.; Gruber, S.; Wilson, T. C.; Taylor, N. J.; Cailly, T.; Schedler, M.; Collier, T. L.; Passchier, J.; Smits, R.; Mollitor, J.; Hoepping, A.; Mueller, M.; Genicot, C.; Mercier, J.; Gouverneur, V., Enhanced copper-mediated (18)F-fluorination of aryl boronic esters provides eight radiotracers for PET applications. *Chem Commun (Camb)* **2016,** *52* (54), 8361-4.
143.   Mossine, A. V.; Brooks, A. F.; Bernard-Gauthier, V.; Bailey, J. J.; Ichiishi, N.; Schirrmacher, R.; Sanford, M. S.; Scott, P. J. H., Automated synthesis of PET radiotracers by copper-mediated 18F-fluorination of organoborons: Importance of the order of addition and competing protodeborylation. *Journal of Labelled Compounds and Radiopharmaceuticals*, n/a-n/a.
144.   Bernard-Gauthier, V.; Schirrmacher, R., 5-(4-((4-[18F]fluorobenzyl)oxy)-3-methoxybenzyl)pyrimidine-2,4-diamine: A selective dual inhibitor for potential PET imaging of Trk/CSF-1R. *Bioorganic & Medicinal Chemistry Letters* **2014,** *24* (20), 4784-4790.
145.   Englebienne, P.; Moitessier, N., Docking ligands into flexible and solvated macromolecules. 5. Force-field-based prediction of binding affinities of ligands to proteins. *J Chem Inf Model* **2009,** *49* (11), 2564-71.
146.   Therrien, E.; Englebienne, P.; Arrowsmith, A. G.; Mendoza-Sanchez, R.; Corbeil, C. R.; Weill, N.; Campagna-Slater, V.; Moitessier, N., Integrating Medicinal Chemistry, Organic/Combinatorial Chemistry, and Computational Chemistry for the Discovery of Selective Estrogen Receptor Modulators with Forecaster, a Novel Platform for Drug Discovery. *Journal of Chemical Information and Modeling* **2012,** *52* (1), 210-224.
147.   Corbeil, C. R.; Englebienne, P.; Yannopoulos, C. G.; Chan, L.; Das, S. K.; Bilimoria, D.; L'Heureux, L.; Moitessier, N., Docking Ligands into Flexible and Solvated Macromolecules. 2. Development and Application of Fitted 1.5 to the Virtual Screening of Potential HCV Polymerase Inhibitors. *Journal of Chemical Information and Modeling* **2008,** *48* (4), 902-909.
148.   Inc, A. S., Discovery Studio Modeling Environment, Release 2017. *San Diego: Accelrys Software Inc* **2007**.

Appendix

Chemical procedure for the synthesis of non-radioactive standards **3.0** and **3.1**

3-Fluoro-4-methoxybenzyl alcohol (4.1). To a solution of 3-fluoro-4-methoxybenzoic acid (**4.0**) (3.0 g, 17 mmol, 1.0 equiv) in THF (50 mL) at 0 $^{\circ}$C was added LiAlH$_4$ (1.3 g, 34 mmol, 2.0 equiv) over 5 minutes. The reaction was warmed to rt then stirred for 12 h. The mixture was then cooled to 5 $^{\circ}$C and quenched with H$_2$O (30 mL) and EtOAc (30 mL). The combined mixture was poured into sat. Rochelle's salt solution. The phases were separated and the aqueous layer was extracted with EtOAc (3 × 100 mL). The combined organic phases were washed with water and brine, then dried over anhydrous Na$_2$SO$_4$, filtered, and concentrated *in vacuo*. The crude product was purified by flash chromatography (50 % EtOAc/hexane) to afford 2.51 g of compound **4.1** as a colorless oil (93 %). R$_f$ 0.35 (50 % EtOAc/hexane)

^{1}H NMR (498 MHz, CDCl$_3$) δ = 7.00 (dd, J = 12.0, 2.0 Hz, 1H), 6.96 (d, J = 8.7 Hz, 1H), 6.87 (t, J = 8.3 Hz, 1H), 4.47 (s, 2H), 3.82 (s, 3H) ppm. ^{13}C NMR (125 MHz, CDCl$_3$) δ = 152.2 (d, $^1J_{CF}$ = 245.4 Hz, 1C), 146.8 (d, $^2J_{CF}$ =10.8 Hz, 1C), 134.0 (d, $^3J_{CF}$ = 5.7 Hz, 1C), 122.7 (br d, $^3J_{CF}$ = 3.6 Hz, 1C), 114.8 (d, $^2J_{CF}$ =18.3 Hz, 1C), 113.2, 63.9, 56.2 ppm

3-Fluoro-4-methoxybenzyl chloride (4.2). 3-Fluoro-4-methoxybenzyl alcohol (**4.1**) (1.0 g, 6.4 mmol, 1.0 equiv) was dissolved in DMSO (7 mL) and cooled to 5 $^{\circ}$C. Cyanuric chloride (0.76 g, 4.2 mmol, 0.65 equiv) was added to the stirred solution in 3 batches under N$_2$. The reaction was warmed to rt and stirred for additional 10 min. Upon completion of the reaction, Et$_2$O (100 mL) was added and the reaction mixture was washed with H$_2$O (4 × 50 mL), dried over anhydrous Na$_2$SO$_4$, filtered, and concentrated *in vacuo*. The crude mixture was eluted through a silica plug with Et$_2$O and concentrated *in vacuo* to afford 1.0 g of compound **4.2** as a yellow liquid (90 %). R$_f$ 0.76 (50 % EtOAc/hexane)

^{1}H NMR (498 MHz, CDCl$_3$) δ = 7.13 (dd, J = 11.7, 2.2 Hz, 1H), 7.09 (td, J = 8.6, 1.5 Hz, 1H), 6.92 (t, J = 8.5 Hz, 1H), 4.52 (s, 2H), 3.87 (s, 3H) ppm. ^{13}C NMR (125 MHz, CDCl$_3$) δ = 152.1 (d, $^1J_{CF}$ = 246.5 Hz, 1C), 147.8 (d, $^2J_{CF}$ = 10.8 Hz, 1C), 130.3 (d, $^3J_{CF}$ = 6.5 Hz, 1C), 124.6 (br d, $^3J_{CF}$ = 3.6 Hz, 1C), 116.4 (br d, $^2J_{CF}$ = 18.8 Hz, 1C), 113.2, 113.3, 56.1, 45.5 ppm

4-((3-Fluoro-4-methoxybenzyl)oxy)-3-methoxybenzaldehyde (4.3a). To a heterogeneous mixture of 4-hydroxy-3-methoxybenzaldehyde (100 mg, 0.34 mmol, 1.0 equiv) and K_2CO_3 (218 mg, 1.6 mmol, 2.4 equiv) in DMF (3 mL) at room temperature was added 3-fluoro-4-methoxybenzyl chloride (**4.2**) (121 mg, 0.70 mmol, 1.06 equiv) dropwise. The mixture was stirred at room temperature overnight under N_2. Upon completion of the reaction, Et_2O (70 mL) was added and washed with water (2 × 40 mL). The aqueous layer was combined and extracted with Et_2O (50 mL) and DCM (2 × 50 mL). The combined organic phases were washed with water (30 mL) and brine (30 mL), then dried over anhydrous Na_2SO_4, filtered, and concentrated *in vacuo*. The product was purified by flash chromatography using (50 % EtOAc/hexane) to afford 126 mg of compound **4.3a** as a white solid (66 %). R_f 0.45 (50 % EtOAc/hexane)

^{1}H NMR (498 MHz, CDCl$_3$) δ = 9.89 - 9.83 (m, 1H), 7.45 (d, *J*=1.8 Hz, 1H), 7.42 (dd, *J* = 8.1, 1.8 Hz, 1H), 7.21 (dd, *J* = 11.7, 2.1 Hz, 1H), 7.16 (d, *J* = 8.1 Hz, 1H), 7.01 - 6.96 (m, 2H), 5.16 (s, 2H), 3.96 (s, 3H), 3.91 (s, 3H) ppm. ^{13}C NMR (125 MHz, CDCl$_3$) δ = 190.8, 153.3, 152.4 (d, [1]J_{CF} = 246.5 Hz, 1C), 150.1, 147.7, 147.6 (d, [2]J_{CF} = 10.6 Hz, 1C), 130.4, 128.9 (d, [3]J_{CF} = 5.7 Hz, 1C), 126.4, 123.3 (d, [3]J_{CF} = 3.6 Hz, 1C), 115.4 (d, [2]J_{CF} = 18.8 Hz, 1C), 113.5, 112.4, 109.4, 70.1, 56.3, 56.0 ppm. HRMS (ESI) calcd for $C_{16}H_{15}FO_4$ (M+H)$^+$ 291.10344, found 291.10160

2-(4-((3-Fluoro-4-methoxybenzyl)oxy)-3-methoxybenzyl)-3-morpholinoacrylonitrile (4.4a)
4-((3-Fluoro-4-methoxybenzyl)oxy)-3-methoxybenzaldehyde (**4.3a**) (500 mg, 1.72 mmol, 1.0 equiv) and 3-morpholinopropronitrile (0.256 mL, 1.85 mmol, 1.1 equiv) was added to DMSO (5 mL) at room temperature. The mixture was heated to 48 °C until homogenization then cooled to 40 °C. After cooling, sodium methoxide (1.04 mL from 0.5 M in MeOH, 0.52 mmol, 0.3 equiv) was added. The mixture was heated to 75 °C for 20 min and cooled to room temperature. Brine (40 mL) and DCM (40 mL) were added to the mixture and the organic phase was separated. The aqueous phase was extracted once with DCM (40 mL). The combined organic phases were dried over anhydrous Na_2SO_4, filtered, and concentrated *in vacuo*. The crude mixture was purified by flash chromatography (50 % EtOAc/hexane) to afford 512 mg of compound **4.4a** as a clear yellow oil (62 %). R_f 0.42 (65 % EtOAc/hexane)

^{1}H NMR (400 MHz, CDCl$_3$) δ = 7.17 (dd, J = 11.9, 2.0 Hz, 1H), 7.12 (br d, J = 8.7 Hz, 1H), 6.92 (t, J = 8.5 Hz, 1H), 6.80 (d, J = 8.1 Hz, 1H), 6.77 (d, J = 1.8 Hz, 1H), 6.70 (dd, J = 8.1, 2.0 Hz, 1H), 6.21 (s, 1H), 5.01 (s, 2H), 3.87 (s, 3H), 3.79 (s, 3H) 3.73 - 3.64 (m, 4H), 3.48 - 3.42 (m, 4H), 3.30 (s, 2H) ppm. ^{13}C NMR (101 MHz, CDCl$_3$) δ = 152.3 (d, $^1J_{CF}$ = 245.7 Hz, 1C), 149.7, 148.8, 146.7 (d, $^2J_{CF}$ = 10.3 Hz, 1C), 132.9, 130.2 (d, $^3J_{CF}$ = 6.2 Hz, 1C), 123.3 (d, $^3J_{CF}$ = 3.7 Hz, 1C), 121.6, 120.2, 115.4 (d, $^2J_{CF}$ = 18.9 Hz, 1C), 114.4, 113.3, 112.3, 75.3, 70.4, 66.2, 56.2, 56.0, 49.48, 38.9 ppm. HRMS (ESI) calcd for C$_{23}$H$_{25}$FN$_2$O$_4$ (M+H)$^+$ 413.18784, found 413.18636

2-(4-((3-Fluoro-4-methoxybenzyl)oxy)-3-methoxybenzyl)-3-(phenylamino)acrylonitrile (4.5a). 2-(4-((3-Fluoro-4-methoxybenzyl)oxy)-3-methoxybenzyl)-3-morpholinoacrylonitrile **(4.4a)** (400 mg, 0.97 mmol, 1.0 equiv) was suspended in isopropanol (6 mL) to form a cloudy solution. Aniline hydrochloride (138 mg, 1.06 mmol, 1.1 equiv) was added to the mixture and then heated at reflux for 30 minutes. The reaction mixture was cooled to room temperature and quenched with water (2 mL) followed by cooling in an ice bath for 30 minutes. The resulting precipitate was collected to afford 382 mg of brownish/white powder (94 %). The crude compound **4.5a** was used directly in the next step without further purification.

4-(4-((3-Fluoro-4-methoxybenzyl)oxy)-3-methoxybenzyl)pyrimidine-2,4-diamine (3.0). 2-(4-((3-Fluoro-4-methoxybenzyl)oxy)-3-methoxybenzyl)-3-(phenylamino)acrylonitrile **(4.5a)** (300 mg, 0.72 mmol, 1.0 equiv) and guanidine hydrochloride (103 mg, 1.08 mmol, 1.5 equiv) was suspended in EtOH (5 mL). Sodium ethoxide (0.403 mL, of 21 % wt in ethanol solution, 1.08 mmol, 1.5 equiv) was added to the reaction mixture drop wise at room temperature then stirred at reflux overnight. The mixture was cooled to room temperature and sodium hydroxide (2.0 mL, 2.0 M solution) was added. The mixture was cooled to 5 °C and allowed to precipitate for 15 minutes. The precipitate was filtered and washed with a cold mixture of ethanol/water (1:1), EtOAc, hexane and dried *in vacuo.* The crude compound was purified by flash chromatography to obtain 140 mg of compound 3.0 as a white powder (51 %) R$_f$ 0.58 (50 % MeOH/DCM)

^{1}H NMR (400 MHz, DMSO-d$_6$) δ = 7.43 (s, 1H), 7.22 (dd, J = 12.3, 1.5 Hz, 1H), 7.17 - 7.08 (m, 2H), 6.87 (d, J = 8.2 Hz, 1H), 6.84 (d, J = 1.7 Hz, 1H), 6.64 (dd, J = 8.2, 1.7 Hz, 1H), 6.00 (s, 2H), 5.63 (s, 2H), 4.91 (s, 2H), 3.79 (s, 3H), 3.69 (s, 3H), 3.48 (s, 2H) ppm. ^{13}C NMR (126 MHz,

DMSO-d$_6$) δ = 162.2, 162.15 155.5, 151.2 (d, $^1J_{CF}$ = 243.8 Hz, 1C), 148.9, 146.6 (d, $^2J_{CF}$ = 10.6 Hz, 1C), 145.8, 133.1, 130.1 (d, $^3J_{CF}$ = 5.9 Hz, 1C), 124.2 (d, $^3J_{CF}$ =3.4 Hz, 1C), 120.1, 115.4 (d, $^2J_{CF}$ = 18.3 Hz, 1C), 113.9, 113.6 (d, $^4J_{CF}$ = 1.5 Hz, 1C), 112.8, 105.9, 69.2, 55.9, 55.5, 32.2 ppm. HRMS (ESI) calcd for C$_{20}$H$_{21}$FN$_4$O$_3$ (M+H)$^+$ 385.16777, found 385.16724

4-Hydroxy-5-methoxy-2-methylbenzaldehyde (4.7) 2-Methoxy-5-methylphenol (**4.6**) (2.5 g, 18.1 mmol, 1.0 equiv) was dissolved in DCM then cooled to 0 $^{\circ}$C. Titanium tetrachloride (3.96 mL, 36.2 mmol, 2.0 equiv) was added to the mixture drop wise under N$_2$. Afterwards, dichloromethyl methyl ether (2.7 mL, 29.7 mmol, 1.6 equiv) was also added to the mixture drop wise under N$_2$. The mixture was stirred for 1.5 hours slowly warming up to room temperature. The precipitate was filtered and discarded. Remaining filtrate was dissolved in DCM (50 mL) and washed with water (50 mL). The organic phase was collected, dried over anhydrous Na$_2$SO$_4$, filtered, and concentrated *in vacuo*. Crude compound was collected and recrystallized with EtOAc to afford 1.86 g of the compound **4.7** as abrown crystal needles (61 %). R$_f$ 0.55 (50 % EtOAc/hexane)

^{1}H NMR (498MHz, CDCl$_3$) δ = 10.21 (s, 1H), 7.37 (s, 1H), 6.80 (s, 1H), 6.11 (s, 1H), 3.96 (s, 3H), 2.61 (s, 3H) ^{13}C NMR (125MHz, CDCl$_3$) δ = 190.0, 150.8, 145.1, 136.7, 126.9, 117.21, 110.9, 56.1, 17.8 HRMS (ESI) calcd for C$_9$H$_{10}$O$_3$ (M+H)$^+$ 167.0699 found 167.0703

4-((3-Fluoro-4-methoxybenzyl)oxy)-5-methoxy-2-methylbenzaldehyde (4.3b) To a heterogeneous mixture of 4-Hydroxy-5-methoxy-2-methylbenzaldehyde (**4.7**) (363 mg, 2.16 mmol, 1.0 equiv) and K$_2$CO$_3$ (716 mg, 5.18 mmol, 2.4 equiv) in DMF (10 mL) at room temperature was added 3-fluoro-4-methoxybenzyl chloride (**4.2**) (400 mg, 2.29 mmol, 1.06 equiv) dropwise. The mixture was stirred at room temperature overnight under N$_2$. Upon completion of the reaction, Et$_2$O (50 mL) was added and washed with water (2 × 50 mL). The aqueous layer was combined and extracted with Et$_2$O (50 mL) and DCM (2 × 50 mL). The combined organic phases were washed with water (30 mL), brine (30 mL), dried over anhydrous Na$_2$SO$_4$, filtered and concentrated *in vacuo.* The product was purified by flash chromatography using (50 % EtOAc/hexane) to afford 395 mg of compound **4.3b** as a white solid (57 %). R$_f$ 0.63 (50 % EtOAc/hexane)

^{1}H NMR (498MHz, CDCl$_3$) δ = 10.23 (s, 1H), 7.38 (s, 1H), 7.21 (dd, J = 11.8, 2.1 Hz, 1H), 7.17 (d, J = 8.4 Hz, 1H), 6.98 (t, J = 8.4 Hz, 1H), 6.73 (s, 1H), 5.14 (s, 2H), 3.93 (s, 3H), 3.92 - 3.91 (m, 3H), 2.61 (s, 3H), 1.57 (s, 2H) ^{13}C NMR (126MHz, CDCl$_3$) δ = 190.2, 152.6, 152.4 (d, $^1J_{CF}$ = 245.4 Hz, 1C), 174.9, 147.6 (d, $^2J_{CF}$ = 10.6 Hz, 1C), 135.5, 129.0 ($^3J_{CF}$ = 5.9 Hz, 1C), 127.4, 123.3 ($^3J_{CF}$ = 3.6 Hz, 1C), 115.6, 115.4 ($^2J_{CF}$ = 19.1 Hz, 1C), 113.4 ($^4J_{CF}$ =1.8 Hz, 1C), 111.8, 70.0, 56.33, 56.1, 18.1 HRMS (ESI) calcd for C$_{17}$H$_{17}$FO$_4$ (M+H)$^+$ 305.1177 found 305.1184

2-(4-((3-Fluoro-4-methoxybenzyl)oxy)-5-methoxy-2-methylbenzyl)-3 morpholinoacrylonitrile (4.4b) 4-((3-Fluoro-4-methoxybenzyl)oxy)-5-methoxy-2-methylbenzaldehyde (**4.3b**) (350 mg, 1.15 mmol, 1.0 equiv) and 3-morpholinoproprionitrile (0.10 mL, 1.27 mmol, 1.1 equiv) was added to DMSO (5 mL) at room temperature. The mixture was heated to 48 °C until homogenization then cooled to 40 °C. After cooling, sodium methoxide (0.7 mL from 0.5 M in MeOH, 0.52 mmol, 0.3 equiv) was added. The mixture was heated to 75 °C for 20 min and cooled to room temperature. Brine (40 mL) and DCM (40 mL) was added to the mixture and the organic phase was separated. The aqueous phase was extracted once with DCM (40 mL). The combined organic phases were dried over anhydrous Na$_2$SO$_4$, filtered, and concentrated *in vacuo*. The crude mixture was purified by flash chromatography (50 % EtOAc/hexane) to afford 436 mg of compound **4.4b** as a clear yellow oil (88 %). R$_f$ 0.26 (50 % EtOAc/hexane)

^{1}H NMR (498MHz, CDCl$_3$) δ = 7.21 (dd, J = 11.9, 2.1 Hz, 1H), 7.16 (br d, J = 9.1 Hz, 1H), 6.96 (t, J = 8.4 Hz, 1H), 6.76 (s, 1H), 6.71 (s, 1H), 6.04 (s, 1H), 5.04 (s, 2H), 3.91 (s, 3H), 3.89 (s, 3H), 3.74 - 3.67 (m, 4H), 3.50 - 3.43 (m, 4H), 3.34 (s, 2H), 2.21 (s, 3H) ^{13}C NMR (126MHz, CDCl$_3$) δ = 152.4 ($^1J_{CF}$ = 245.9 Hz, 1C), 148.5, 147.9, 147.2 ($^2J_{CF}$ = 10.8 Hz, 1C), 146.6, 130.3 ($^3J_{CF}$ = 6.2 Hz, 1C), 129.6, 128.4, 123.3 ($^3J_{CF}$ = 3.6 Hz, 1C), 121.7, 116.9, 115.4 ($^2J_{CF}$ = 18.8 Hz, 1C), 113.9, 113.3 ($^4J_{CF}$ = 1.8 Hz, 1C), 74.6, 70.5, 66.3, 56.3, 49.6, 36.1, 18.9 HRMS (ESI) calcd for C$_{24}$H$_{27}$FN$_2$O$_4$ (M+H)$^+$ 427.2016 found 427.2028

2-(4-((3-Fluoro-4-methoxybenzyl)oxy)-5-methoxy-2-methylbenzyl)-3-(phenylamino)acrylonitrile **(4.5b)** 2-(4-((3-Fluoro-4-methoxybenzyl)oxy)-5-methoxy-2-methylbenzyl)-3 morpholinoacrylonitrile (**4.4b**) (500 mg, 1.72 mmol, 1.0 equiv) was suspended in isopropanol (5 mL) to form a cloudy solution. Aniline hydrochloride (172 mg, 1.33 mmol, 1.1 equiv) was added to the mixture then heated at reflux for 30 minutes. The reaction mixture was cooled to room temperature and quenched with water (2 mL) followed by cooling in an ice bath for 30 minutes. Resulting precipitate was collected to afford 391 mg of brownish/white powder (77 %). The crude compound **4.5b** was used directly in the next step without further purification.

5-(4-((3-Fluoro-4-methoxybenzyl)oxy)-5-methoxy-2-methylbenzyl)pyrimidine-2,4-diamine **(3.1)** 2-(4-((3-Fluoro-4-methoxybenzyl)oxy)-5-methoxy-2-methylbenzyl)-3-(phenylamino)acrylonitrile (**4.5b**) (300 mg, 0.69 mmol, 1.0 equiv) and guanidine hydrochloride (100 mg, 1.04 mmol, 1.5 equiv) was suspended in EtOH (5 mL). Sodium ethoxide (0.388 mL, of 21 % wt in ethanol solution, 1.084mmol, 1.5 equiv) was added to the reaction mixture drop wise at room temperature then stirred at reflux overnight. The mixture was cooled to room temperature and sodium hydroxide (2 mL, 2 M solution) was added. The mixture was cooled to 5 °C and allowed to precipitate for 15 minutes. The precipitate was filtered and washed with a cold mixture of ethanol/water (1:1), EtOAc, hexane and dried *in vacuo.* The crude compound was purified by flash chromatography to produce 125 mg of compound **3.1** as a white powder (46 %) R_f 0.58 (50 % MeOH/DCM)

^{1}H NMR (498MHz, DMSO-d_6) δ = 7.25 (dd, J = 12.2, 1.9 Hz, 1H), 7.21 - 7.18 (m, 1H), 7.16 - 7.12 (m, 1H), 7.03 (s, 1H), 6.86 (s, 1H), 6.68 (s, 1H), 6.18 (s, 2H), 5.70 (s, 2H), 4.95 (s, 2H), 3.82 (s, 3H), 3.65 (s, 3H), 3.43 (s, 2H), 2.13 (s, 3H), ^{13}C NMR (126MHz, DMSO-d_6) δ = 162.8, 162.1, 154.3, 151.6 ($^1J_{CF}$ = 243.8 Hz, 1C), 147.5, 147.1 ($^2J_{CF}$ = 10.6 Hz, 1C), 146.3, 130.6 ($^3J_{CF}$ = 5.9 Hz, 1C), 130.1, 128.6, 124.7 ($^3J_{CF}$ = 3.4 Hz, 1C), 116.7, 115.9 ($^2J_{CF}$ = 18.3 Hz, 1C), 114.5, 114.1 ($^4J_{CF}$ = 1.5 Hz, 1C), 105.2, 69.7, 56.4, 56.2, 30.6, 18.8 HRMS (ESI) calcd for $C_{21}H_{23}FN_4O_3$ (M+H)$^+$ 399.1836 found 399.1827

Synthesis of Boc-protected standards: **4.8a** and **4.8b**

di-*tert*-Butyl   (5-(4-((3-fluoro-4-methoxybenzyl)oxy)-3-methoxybenzyl)pyrimidine-2,4-diyl)bis(*tert*-butoxycarbonylcarbamate)   (4.8a)   4-(4-((3-Fluoro-4-methoxybenzyl)oxy)-3-methoxybenzyl)pyrimidine-2,4-diamine (**3.0**) (65 mg, 0.17 mmol, 1.0 equiv), di-tert-butyl dicarbonate (369 mg, 1.70 mmol, 10.0 equiv), 4-dimethylaminopyridine (4.0 mg, 0.034 mmol, 0.2 equiv), and triethylamine (0.094 mL, 0.68 mmol, 4.0 equiv) were added to THF (10 mL) under N_2. The mixture was stirred for 4 days until completion of the reaction and then diluted with EtOAc (100 mL). The organic phase was washed with water (40 mL), brine (40 mL), dried over anhydrous Na_2SO, filtered, and concentrated *in vacuo*. The resulting precipitate was purified by flash chromatography to afford 276 mg of compound **4.8a** as a yellowish powder (67 %). R_f 0.35 (50 % EtOAc/hexane)

^{1}H NMR (400MHz, CDCl$_3$) δ = 8.54 (s, 1H), 7.23 - 7.16 (m, 1H), 7.15 - 7.10 (m, 1H), 6.95 (t, J = 8.4 Hz, 1H), 6.80 (d, J = 8.2 Hz, 1H), 6.71 (d, J = 2.1 Hz, 1H), 6.64 (dd, J = 8.1, 2.1 Hz, 1H), 5.04 (s, 2H), 3.89 (s, 3H), 3.84 (s, 3H), 3.83 - 3.81 (m, 2H), 1.46 (s, 18H), 1.39 (s, 18H) ppm. ^{13}C NMR (126MHz, CDCl$_3$) δ = 160.8, 159.5, 157.0, 152.4 ($^1J_{CF}$ = 246.2 Hz, 1C), 150.6, 149.9, 149.6, 147.3 ($^2J_{CF}$ = 10.8 Hz, 1C), 146.9, 130.3, 130.1 ($^3J_{CF}$ = 6.2 Hz, 1C), 129.6, 123.2 ($^3J_{CF}$ = 3.6 Hz, 1C), 121.1, 115.4 ($^2J_{CF}$ = 18.8 Hz, 1C), 114.4, 113.3 ($^4J_{CF}$ = 1.8 Hz, 1C), 112.8, 83.8, 83.3, 70.3, 56.3, 55.9, 56.1, 33.9, 27.8, 27.7 HRMS (ESI) calcd for $C_{40}H_{53}FN_4O_{11}$ (M+H)$^+$ 785.37749, found 785.37578

di-*tert*-Butyl   (5-(4-((4-fluorobenzyl)oxy)-3-methoxybenzyl)pyrimidine-2,4-diyl)bis(*tert*-butoxycarbonylcarbamate)   (4.8b)   5-(4-((4-Fluorobenzyl)oxy)-3-methoxybenzyl)pyrimidine-2,4-diamine (**1.23**) (500 mg, 1.41 mmol, 1.0 equiv), di-*tert*-butyl dicarbonate (2.2 g, 10.1 mmol, 10 equiv), 4-dimethylaminopyridine (34 mg, 0.28 mmol, 0.2 equiv), and triethylamine (0.789 mL, 2.76 mmol, 4.0 equiv) were added to THF (10 mL) under N_2. The mixture was stirred for 4 days until completion of the reaction and diluted with EtOAc (100 mL). The organic phase was washed with water (40 mL), brine (40 mL), dried over anhydrous Na_2SO, filtered and concentrated *in vacuo*. The crude product was purified by flash chromatography (30 % EtOAc/hexane) to afford 423 mg of compound **4.8b** as a yellowish foam (40 %). R_f 0.43 (50 % EtOAc/hexane)

^{1}H NMR (498MHz, CDCl$_3$) δ = 8.54 (s, 1H), 7.40 (dd, J = 8.4, 5.4 Hz, 2H), 7.05 (t, J = 8.7 Hz, 2H), 6.80 (d, J = 8.2 Hz, 1H), 6.71 (d, J = 1.9 Hz, 1H), 6.65 (dd, J = 8.1, 1.8 Hz, 1H), 5.08 (s, 2H), 3.84 (s, 3H), 3.83 (s, 2H), 1.46 (s, 18H), 1.39 (s, 18H) ^{13}C NMR (126MHz, CDCl$_3$) δ = 163.4, 161.4, 160.8, 158.2 ($^1J_{CF}$ = 313.4 Hz, 1C), 150.6, 149.9, 149.6, 147.0, 132.8 ($^3J_{CF}$ = 3.1 Hz, 1C), 130.3, 129.6, 129.1 ($^3J_{CF}$ = 8.2 Hz, 1C), 121.2, 115.4 ($^2J_{CF}$ = 21.7 Hz, 1C), 114.4, 112.9, 83.8, 83.3, 70.5, 55.9, 33.9, 27.8, 27.7 HRMS (ESI) calcd for C$_{39}$H$_{51}$FN$_4$O$_{10}$ (M+H)$^+$ 755.3630, found 755.3662

Boc-protected Bpin precursor synthesis: **4.17a** and **4.17b**

3-Iodo-4-methoxybenzyl chloride (4.11). 2-Iodoanisole (**4.9**) (1.5 mL, 11.5 mmol, 1.0 equiv) and chloromethyl methyl ether (2.0 mL, 27 mmol, 2.3 equiv) were added to acetic acid (40 mL) and stirred at 55 °C for 3 days. The mixture was cooled to room temperature and then poured into ice water (50 mL). The aqueous phase extracted with DCM (2 × 100 mL) and washed with water (2 × 75 mL). The organic layer was dried over anhydrous Na$_2$SO$_4$, filtered, and concentrated *in vacuo*. The crude product was purified by flash chromatography (20 % EtOAc/hexane) to afford 2.12 g of compound **4.11** as a clear oil (65 %) R$_f$ 0.40 (30 % EtOAc/hexane)

^{1}H NMR (498MHz, CDCl$_3$) δ = 7.83 (d, J = 2.2 Hz, 1H), 7.35 (dd, J = 8.4, 2.2 Hz, 1H), 6.81 (d, J = 8.4 Hz, 1H), 4.53 (s, 2H), 3.90 (s, 3H) ppm. ^{13}C NMR (125MHz, CDCl$_3$) δ = 158.2, 139.7, 131.6, 129.9, 110.7, 85.9, 56.4, 45.0 ppm

4-((3-Iodo-4-methoxybenzyl)oxy)-3-methoxybenzaldehyde (4.12a). To a heterogeneous mixture of 4-Hydroxy-3-methoxybenzaldehyde (1.5 g, 9.85 mmol, 1.0 equiv) and K$_2$CO$_3$ (3.26 g, 23.6 mmol, 2.4 equiv) in DMF (3 mL) at room temperature was added 3-Iodo-4-methoxybenzyl chloride (**4.11**) (3.0 g, 10.84 mmol, 1.1 equiv) dropwise. The mixture was stirred at room temperature overnight under N$_2$. Upon completion of the reaction, the reaction was diluted with Et$_2$O (100 mL) and washed with water (2 × 50 mL). The aqueous layers were combined and extracted with Et$_2$O (100 mL) and DCM (2 × 150 mL). The combined organic phases were washed with water (100 mL), brine (100 mL), dried over anhydrous Na$_2$SO$_4$, filtered and concentrated *in*

vacuo. The product was purified by flash chromatography using (50 % EtOAc/hexane) to afford 2.82 g of compound **4.12a** as a white solid (72 %). R_f 0.59 (50 % EtOAc/hexane)

^{1}H NMR (498 MHz, CDCl$_3$) δ = 9.87 (s, 1H), 7.88 (d, J = 2.1 Hz, 1H), 7.46 - 7.39 (m, 3H), 7.01 (d, J = 8.1 Hz, 1H), 6.84 (d, J = 8.4 Hz, 1H), 5.14 (s, 2H), 3.96 (s, 3H), 3.90 (s, 3H) ppm. ^{13}C NMR (125 MHz, CDCl$_3$) δ = 190.8, 153.4, 150.1, 138.7, 130.4, 130.0, 129.0, 126.4, 112.5, 110.8, 109.48, 86.1, 69.8, 56.4, 56.0 ppm. HRMS (ESI) calcd for C$_{16}$H$_{15}$IO$_4$ (M+H)$^+$ 399.0095, found 399.00846

2-(4-((3-Iodo-4-methoxybenzyl)oxy)-3-methoxybenzyl)-3-morpholinoacrylonitrile (4.13a). 4-((3-Iodo-4-methoxybenzyl)oxy)-3-methoxybenzaldehyde (**4.12a)** (500 mg, 1.26 mmol, 1.0 equiv) and 3-morpholinoproronitrile (0.186 mL, 1.38 mmol, 1.1 equiv) were added to DMSO (2 mL) at room temperature. The mixture was heated to 48 $^\circ$C until homogenization then cooled to 40 $^\circ$C and sodium methoxide (0.76 from 0.5 M in MeOH, 0.38 mmol, 0.3 equiv) was added dropwise. The mixture was heated to 75 $^\circ$C for 20 min and cooled to room temperature. Brine (75 mL) and DCM (75 mL) were added to the mixture and the organic phase was extracted. The aqueous phase was extracted once with DCM (40 mL). The combined organic phases were dried over anhydrous Na$_2$SO$_4$, filtered, and concentrated *in vacuo*. The crude mixture was purified by flash chromatography (50 % EtOAc/hexane) to afford 510 mg of compound **4.13a** as a clear white solid (78 %). R_f 0.24 (50 % EtOAc/hexane)

^{1}H NMR (498 MHz, CDCl$_3$) δ = 7.88 - 7.84 (m, 1H), 7.39 (d, J = 8.2 Hz, 1H), 6.86 - 6.78 (m, 3H), 6.72 (br d, J = 8.1 Hz, 1H), 6.22 (s, 1H), 5.01 (s, 2H), 3.89 (s, 3H), 3.88 (s, 3H), 3.74 - 3.67 (m, 4H), 3.47 (t, J = 4.8 Hz, 4H), 3.32 (s, 2H) ppm. ^{13}C NMR (125MHz, CDCl$_3$) δ = 157.8, 149.8, 148.3, 146.8, 138.7, 132.9, 131.4, 129.0, 121.6, 120.3, 114.6 (br d, J = 13.2 Hz, 1C), 112.3, 110.8, 85.9, 75.4, 70.2, 66.3, 56.4, 56.0, 49.5, 38.9 HRMS (ESI) calcd for C$_{23}$H$_{15}$IN$_2$O$_4$ (M+H)$^+$ 521.0939, found 521.09531

2-(4-((3-Iodo-4-methoxybenzyl)oxy)-3-methoxybenzyl)-3-(phenylamino)acrylonitrile (4.14a). 2-(4-((3-Iodo-4-methoxybenzyl)oxy)-3-methoxybenzyl)-3-morpholinoacrylonitrile (**4.13a)** (450 mg, 0.86 mmol, 1.0 equiv) was added to isopropanol (5 mL) to form a cloudy solution. Aniline hydrochloride (123 mg, 0.95 mmol, 1.1 equiv) was added to the mixture then heated at reflux for 30 minutes. The mixture was cooled to room temperature and quenched with water (2 mL) and put

in an ice bath for 30 minutes. The resulting precipitate was collected to afford 320 mg compound **4.14a** as a brownish/white powder (71%). The crude precipitate was used directly in the next step without further purification.

4-(4-((3-Iodo-4-methoxybenzyl)oxy)-3-methoxybenzyl)pyrimidine-2,4-diamine (4.15a). 2-(4-((3-Iodo-4-methoxybenzyl)oxy)-3-methoxybenzyl)-3-(phenylamino)acrylonitrile **(4.14a)** (600 mg, 1.14 mmol, 1.0 equiv) and guanidine hydrochloride (163 mg, 1.71 mmol, 1.5 equiv) was added to EtOH (5 mL). Sodium ethoxide (0.638 mL from 21%wt in ethanol solution, 1.71 mmol, 1.5 equiv) was added to the reaction mixture drop wise at room temperature then stirred at reflux overnight. The mixture was cooled to room temperature and sodium hydroxide (3 mL, 2N solution) was added. The mixture was cooled to 5 ^{0}C and allowed to precipitate for 15 minutes. The precipitate was filtered and washed with cold mixture of ethanol/water (1:1), EtOAc, hexane and dried *in vacuo.* The crude mixture was purified by flash chromatography (10% MeOH/DCM) to afford 210 mg of compound **4.15a** as a white solid (38%). R_f 0.47 (50% MeOH/DCM)

^{1}H NMR (498 MHz, DMSO-d$_6$) δ = 7.81 (d, J = 2.1 Hz, 1H), 7.45 (s, 1H), 7.39 (d, J = 8.3 Hz, 1H), 6.98 (d, J = 8.4 Hz, 1H), 6.89 (d, J = 8.2 Hz, 1H), 6.86 (s, 1H), 6.66 (dd, J = 8.1, 1.9 Hz, 1H), 6.02 (s, 2H), 5.65 (s, 2H), 4.91 (s, 2H), 3.80 (s, 3H), 3.70 (s, 3H), 3.52 - 3.46 (m, 2H) ppm. ^{13}C NMR (125 MHz, DMSO-d$_6$) δ = 162.6, 157.8, 155.8, 149.4, 146.3, 138.9, 133.9, 131.9, 130.0, 120.6, 114.7, 114.5, 113.3, 111.8, 106.4, 86.2, 69.3, 56.8, 55.9, 32.7 ppm. HRMS (ESI) calcd for C$_{20}$H$_{21}$IN$_4$O$_3$ (M+H)$^+$ 493.0741, found 493.0731

di-*tert*-Butyl (5-(4-((3-iodo-4-methoxybenzyl)oxy)-3-methoxybenzyl)pyrimidine-2,4-diyl)bis(*tert*-butoxycarbonylcarbamate) (4.16a) 4-(4-((3-Iodo-4-methoxybenzyl)oxy)-3-methoxybenzyl)pyrimidine-2,4-diamine **(4.15a)** (200 mg, 0.41 mmol, 1.0 equiv), di-tert-butyl dicarbonate (890 g, 4.1 mmol, 10.0 equiv), 4-dimethylaminopyridine (10 mg, 0.082 mmol, 0.2 equiv), triethylamine (0.229 mL, 1.64 mmol, 4.0 equiv) were added to THF (15 mL) under N$_2$. The mixture was stirred at room temperature for 5 days. THF was removed under reduced pressure and the crude product was re-dissolved in EtOAc (100 mL). The organic phase was washed with water

(50 mL), 1M HCl (20 mL), brine (50 mL), and dried over anhydrous Na_2SO_4. The crude product was purified using flash chromatography (20 % EtOAc/hexane) to afford 242 mg of compound **4.16a** as yellow crystals (67 %). R_f 0.51 (50 % EtOAc/hexane)

^{1}H NMR (498 MHz, $CDCl_3$) δ = 8.54 (s, 1H), 7.86 (d, J = 2.1 Hz, 1H), 7.43 - 7.32 (m, 1H), 7.28 (s, 1H), 6.81 (d, J = 8.3 Hz, 2H), 6.71 (d, J = 1.9 Hz, 1H), 6.69 - 6.59 (m, 1H), 5.01 (s, 2H), 3.89 (s, 3H), 3.84 (s, 3H), 3.83 (s, 2H), 1.46 (s, 18H), 1.40 (s, 18H) ppm. ^{13}C NMR (125 MHz, DMSO-d_6) δ = 162.6, 157.8, 155.87 149.4, 146.3, 138.9, 133.9, 131.9, 130.0, 120.6, 114.7, 114.5, 113.3, 111.8, 106.4, 86.2, 69.3, 56.8, 55.9, 32.7 ppm. HRMS (ESI) calcd for $C_{40}H_{53}IN_4O_{11}$ (M+H)[+] 893.28355, found 893.28386

di-*tert*-Butyl (5-(3-methoxy-4-((4-methoxy-3-(4,4,5,5-tetramethyl-1,3,2-dioxaborolan-2-yl)benzyl)oxy)benzyl)pyrimidine-2,4-diyl)bis(*tert*-butoxycarbonylcarbamate) (4.17a) di-*tert*-Butyl (5-(4-((3-iodo-4-methoxybenzyl)oxy)-3-methoxybenzyl)pyrimidine-2,4-diyl)bis(*tert*-butoxycarbonylcarbamate) (**4.16a**) (350 mg, 0.39 mmol, 1.0 equiv), bis(pinacolato)diboron (124 mg, 0.50 mmol, 1.25 equiv), 1,1'-bis(diphenylphosphino)ferrocene-palladium(II)dichloride (57 mg, 0.078 mg, 0.2 equiv), and potassium acetate (76 mg, 0.78 mmol, 2.0 equiv) were added to DMSO (6 mL) under N_2. The mixture was heated to 60 °C for 1 hour while purging with N_2 then stirred overnight at 80 °C. The mixture was cooled to room temperature and EtOAc (100 mL) was added. The organic phase was washed with water (50 mL), brine (50 mL) and dried over Na_2SO_4. The resulting precipitate was purified by flash chromatography to afford 180 mg of compound **4.17a** as a yellowish foam (51 %). R_f 0.36 (50 % EtOAc/hexane)

^{1}H NMR (498MHz, $CDCl_3$) δ = 8.53 (s, 1H), 7.72 (d, J = 2.3 Hz, 1H), 7.48 (dd, J = 8.5, 2.3 Hz, 1H), 6.87 - 6.82 (m, 2H), 6.70 (d, J= 1.9 Hz, 1H), 6.66 - 6.62 (m, 1H), 5.04 (s, 2H), 3.84 (s, 3H), 3.82 (s, 3H), 1.45 (s, 18H), 1.39 (s, 18H), 1.36 (s, 12H) ppm. ^{13}C NMR (125MHz, $CDCl_3$) δ = 164.0, 161.7, 160.8, 159.9, 157.4, 150.5, 149.9, 149.6, 147.5, 136.2, 132.1, 129.6, 129.7, 128.4, 121.2, 114.5, 112.9, 110.6, 110.7, 83.8, 83.5, 83.3, 75.0, 71.0, 55.9, 55.9, 33.8, 27.8, 27.7, 27.7, 24.8, 24.8 ppm. HRMS (ESI) calcd for $C_{40}H_{53}IN_4O_{11}$ (M+H)[+] 893.47212, found 893.47573

4-((4-Iodobenzyl)oxy)-3-methoxybenzaldehyde (4.12b) 4-Hydroxy-3-methoxybenzaldehyde (1.0 g, 6.57 mmol, 1.0 equiv) and K_2CO_3 (2.17 g, 15.77 mmol, 2.5 equiv) was added to DMF (25 mL) at room temperature. 1-(Bromomethyl)-4-iodobenzene (**4.10**) (300 mg, 1.0 mmol, 1.05 equiv) was added drop wise to the heterogeneous mixture and stirred at room temperature overnight under N_2. Upon completion of the reaction, Et_2O (100 mL) was added and the organic phase was washed with water (2 × 50 mL). The aqueous layers were combined and extracted with Et_2O (50 mL) and DCM (2 × 50 mL). The combined organic phases were washed with water (30 mL), brine (30 mL), dried over anhydrous Na_2SO_4, filtered and concentrated *in vacuo*. The product was purified by flash chromatography using (50 % EtOAc/hexane) to afford 289 mg compound **4.12b** as a white solid (83 %). R_f 0.33 (30 % EtOAc/hexane)

^{1}H NMR (498 MHz, CDCl$_3$) δ = 9.87 (s, 1H), 7.77 - 7.72 (m, 2H), 7.46 (d, *J*= 1.8 Hz, 1H), 7.41 (d, *J* = 7.8 Hz, 1H), 7.21 (d, *J* = 8.4 Hz, 2H), 6.97 (d, *J* = 8.2 Hz, 1H), 5.20 (s, 2H), 3.97 (s, 3H) ^{13}C NMR (125 MHz, CDCl$_3$) δ = 190.8, 153.2, 150.1, 137.8, 135.7, 130.5, 129.0, 126.4, 112.4, 109.5, 93.7, 70.2, 56.0. HRMS (ESI) calcd for $C_{15}H_{13}IO_3$ (M+H)$^+$ 368.99821, found 369.9982

2-(4-((4-Iodobenzyl)oxy)-3-methoxybenzyl)-3-morpholinoacrylonitrile (4.13b) 4-((4-Iodobenzyl)oxy)-3-methoxybenzaldehyde (**4.12b**) (1.3 g, 3.53 mmol, 1.0 equiv) and 3-morpholinopropronitrile (0.525 mL, 3.88 mmol, 1.1 equiv) were added to DMSO (10 mL) at room temperature. The mixture was heated to 48 °C until homogenization and cooled to 40 °C. Sodium methoxide (2.12 mL 0.5 M in MeOH, 0.809 mmol, 0.3 equiv) was added drop wise to the reaction and heated to 75 °C for 20 min then cooled to room temperature. Brine (50 mL) and DCM (50 mL) were added to the mixture and the organic phase was separated. The aqueous phase was extracted once with DCM (100 mL). The combined organic phases were dried over anhydrous Na_2SO_4, filtered and concentrated *in vacuo*. The crude mixture was purified by flash chromatography (50 % EtOAc/hexane) to afford 1.49 g of compound **4.13b** as a clear yellow oil (86 %). R_f 0.28 (50 % EtOAc/hexane)

^{1}H NMR (498MHz, CDCl$_3$) δ = 7.73 - 7.68 (m, 2H), 7.20 (d, *J* = 7.9 Hz, 2H), 6.82 - 6.78 (m, 2H), 6.72 (dd, *J* = 8.1, 2.0 Hz, 1H), 6.22 (s, 1H), 5.08 (s, 2H), 3.94 - 3.87 (m, 3H), 3.79 - 3.66 (m, 4H), 3.52 - 3.45 (m, 4H), 3.33 (s, 2H) ^{13}C NMR (125MHz, CDCl$_3$) δ = 149.7, 148.7, 146.7, 137.6,

137.0, 132.9, 129.1, 121.6, 120.3, 114.3, 112.3, 90.2, 75.5, 70.5, 66.3, 56.0, 49.5, 38.9. HRMS (ESI) calcd for $C_{22}H_{23}IN_2O_3$ $(M+H)^+$ 491.0826, found 491.0844

2-(4-((4-Iodobenzyl)oxy)-3-methoxybenzyl)-3-(phenylamino)acrylonitrile (4.14b) 2-(4-((4-Iodobenzyl)oxy)-3-methoxybenzyl)-3-morpholinoacrylonitrile (**4.13b**) (1.35 g, 2.75 mmol, 1.0 equiv) was added to isopropanol (10 mL) to form a cloudy solution. Aniline hydrochloride (0.393 g, 3.03 mmol, 1.1 equiv) was added to the mixture then heated at reflux for 30 minutes. The mixture was cooled to room temperature and quenched with water (2 mL) and placed in an ice bath for 30 minutes. The resulting precipitate was collected to afford 0.82 g of compound **4.14b** as a yellowish powder (60 %). The crude precipitate was used directly in the next step without further purification. R_f 0.78 (50 % EtOAc/hexane)

5-(4-((4-Iodobenzyl)oxy)-3-methoxybenzyl)pyrimidine-2,4-diamine (4.15b) 2-(4-((4-Iodobenzyl)oxy)-3-methoxybenzyl)-3-(phenylamino)acrylonitrile (**4.14b**) (700 mg, 1.41 mmol, 1.0 equiv) and guanidine hydrochloride (200 mg, 2.11 mmol, 1.5 equiv) were added to EtOH (5 mL). Sodium ethoxide (0.403 mL, 1.08mmol from 21% wt in ethanol solution, 1.5 equiv) was added to the reaction mixture drop wise at room temperature then stirred at reflux overnight. The mixture was cooled to room temperature and sodium hydroxide (2.0 mL, 2.0 M solution) was added. The mixture was cooled to 5 °C and allowed to precipitate for 15 minutes. The precipitate was filtered and purified by flash chromatography (10% MeOH/DCM) to produce 350 mg of compound **4.15b** as a white powder (53%) R_f 0.53 (50% MeOH/DCM)

^1H NMR (498 MHz, DMSO-d_6) δ = 7.74 - 7.69 (m, 2H), 7.45 (s, 1H), 7.21 (d, J = 8.4 Hz, 2H), 6.87 (d, J = 6.7 Hz, 1H), 6.86 (s, 1H), 6.65 (dd, J = 8.1, 2.0 Hz, 1H), 6.00 (s, 2H), 5.62 (s, 2H), 4.97 (s, 2H), 3.74 - 3.70 (m, 3H), 3.52 - 3.46 (m, 2H) ^{13}C NMR (126 MHz, DMSO-d_6) δ = 162.1, 155.5, 148.9, 145.7, 137.1, 137.0, 133.2, 129.8, 120.1, 113.8, 112.8, 105.9, 93.6, 69.3, 55.5, 32.2. HRMS (ESI) calcd for $C_{19}H_{19}IN_4O_2$ $(M+H)^+$ 463.0625, found 463.0604

Di-*tert*-Butyl (5-(4-((4-iodobenzyl)oxy)-3-methoxybenzyl)pyrimidine-2,4-diyl)bis((*tert*-butoxycarbonyl)carbamate) (4.16b) 5-(4-((4-Iodobenzyl)oxy)-3-methoxybenzyl)pyrimidine-

2,4-diamine (**4.15b**) (320 mg, 0.69 mmol, 1.0 equiv), di-*tert*-butyl dicarbonate (1.5 g, 6.90 mmol, 10 equiv), 4-dimethylaminopyridine (17 mg, 0.14 mmol, 0.2 equiv), and triethylamine (0.385 mL, 2.76 mmol, 4.0 equiv) were added to THF (10 mL) under N_2. The mixture was stirred for 4 days until completion of the reaction and diluted with EtOAc (100 mL). The organic phase was washed with water (40 mL), brine (40 mL), dried over anhydrous Na_2SO, filtered, and concentrated *in vacuo*. The crude product was purified by flash chromatography (30 % EtOAc/hexane) to afford 431 mg of compound **4.16b** as a yellowish foam (72 %). R_f 0.35 (50 % EtOAc/hexane)

^{1}H NMR (498 MHz, CDCl$_3$) δ = 7.70 (d, J = 8.2 Hz, 2H), 7.28 (s, 1H), 7.21 - 7.16 (m, 2H), 6.77 (d, J = 8.1 Hz, 1H), 6.72 (m, 1H), 6.64 (m, 1H), 5.08 (m, 2H), 3.85 (s, 3H), 3.84 - 3.82 (m, 2H), 1.47 (s, 18H), 1.40 (s, 18H). ^{13}C NMR (126 MHz, CDCl$_3$) δ = 160.8, 159.5, 157.0, 150.6, 149.9, 149.6, 146.8, 137.6, 136.2, 130.4, 129.6, 129.1, 121.2, 114.3, 112.9, 93.3, 83.8, 83.3, 70.4, 55.9, 33.8, 27.8, 27.7. HRMS (ESI) calcd for $C_{39}H_{51}IN_4O_{10}$ (M+H)$^+$ 863.2723 found 863.2719

Di-*tert*-Butyl (5-(3-methoxy-4-((4-(4,4,5,5-tetramethyl-1,3,2-dioxaborolan-2-yl)benzyl)oxy)benzyl)pyrimidine-2,4-diyl)bis((*tert*-butoxycarbonyl)carbamate) (4.17b) Di-*tert*-butyl (5-(4-((4-Iodobenzyl)oxy)-3-methoxybenzyl)pyrimidine-2,4-diyl)bis((*tert*-butoxycarbonyl)carbamate) (**4.16b**) (400 mg, 0.46 mmol, 1.0 equiv), bis(pinacolato)diboron (147 mg, 0.58 mmol, 1.25 equiv), 1,1'-bis(diphenylphosphino)ferrocene-palladium(II)dichloride (67 mg, 0.092 mg, 0.2 equiv), and potassium acetate (90 mg, 0.92 mmol, 2.0 equiv) were added to DMSO (10 mL) under N_2. The mixture was heated to 60 $^\circ$C for 1 hour while purging with N_2 then stirred overnight at 80 $^\circ$C. The mixture was cooled to room temperature and diluted with EtOAc (100 mL). The organic phase was washed with water (50 mL), brine (50 mL) and dried over anhydrous Na_2SO_4. The resulting precipitate was purified by flash chromatography (30 % EtOAc/hexane) to afford 204 mg of compound **4.17b** as a yellowish foam (51 %). R_f 0.54 (50 % EtOAc/hexane)

^{1}H NMR (498 MHz, CDCl$_3$) δ = 8.53 (s, 1H), 7.81 (d, J = 8.0 Hz, 2H), 7.43 (d, J = 7.9 Hz, 2H), 6.80 - 6.75 (m, J = 8.1 Hz, 1H), 6.73 - 6.69 (m, 1H), 6.62 (br d, J = 8.1 Hz, 1H), 5.17 (s, 2H), 3.86 (s, 3H), 3.83 - 3.80 (m, 2H), 1.46 (s, 18H), 1.39 (s, 18H), 1.38 - 1.33 (m, 12H). ^{13}C NMR (126 MHz, CDCl$_3$) δ = 160.8, 159.5, 157.0, 150.5, 149.7, 147.1, 146.8, 137.6, 136.2, 130.4, 129.6, 129.1,

121.2, 114.3, 112.9, 93.3, 83.8, 83.3, 70.4, 55.9, 33.8, 27.8, 27.7. HRMS (ESI) calcd for $C_{45}H_{63}BN_4O_{12}$ (M+H)$^+$ 862.4645 found 863.4632

Protodeboronated side product synthesis: **4.21**

3-Methoxy-4-phenethylbenzaldehyde (4.18). To a heterogeneous mixture of 4-Hydroxy-3-methoxybenzaldehyde (1.5 g, 10 mmol, 1.0 equiv) and K_2CO_3 (3.3 mg, 24 mmol, 2.4 equiv) in DMF (20 mL) at room temperature was added benzyl chloride (1.37 g, 11 mmol, 1.1 equiv) dropwise. The mixture was stirred at room temperature overnight under N_2. Upon completion of the reaction, Et_2O (100 mL) was added and washed with water (2 × 100 mL). The aqueous layers were combined and extracted with Et_2O (100 mL) and DCM (2 × 50 mL). The combined organic phases were washed with water (50 mL), brine (50 mL), dried over anhydrous Na_2SO_4, filtered and concentrated *in vacuo*. The product was purified by flash chromatography using (50 % EtOAc/hexane) to afford 1.73 g of compound **4.18** as a white solid (71 %). R$_f$ 0.53 (50 % EtOAc/hexane)

^{1}H NMR (498MHz, CDCl$_3$) δ = 9.95 - 9.77 (m, 1H), 7.47 - 7.44 (m, 3H), 7.43 - 7.38 (m, 3H), 7.37 - 7.32 (m, 1H), 7.01 (d, *J* = 8.2 Hz, 1H), 5.27 (s, 2H), 3.97 (s, 3H) ^{13}C NMR (125MHz, CDCl$_3$) δ = 190.8, 153.6, 150.1, 136.0, 130.4, 128.7, 128.2, 127.2, 126.5, 112.4, 109.4, 70.9, 56.0 HRMS (ESI) calcd for $C_{15}H_{15}O_3$ (M+H)$^+$ 243.10720 found 243.1067

2-(3-Methoxy-4-phenethylbenzyl)-3-morpholinoacrylonitrile **(4.19)** 3-Methoxy-4-phenethylbenzaldehyde (**4.18**) (313 mg, 1.29 mmol, 1.0 equiv) and 3-morpholinopropronitrile (0.200 mL, 1.42 mmol, 1.1 equiv) was added to DMSO (5 mL) at room temperature. The mixture was heated to 48 °C until homogenization then cooled to 40 °C. After cooling, sodium methoxide (0.77 mL from 0.5 M in MeOH, 0.387 mmol, 0.3 equiv) was added. The mixture was heated to 75 °C for 20 min and cooled to room temperature. Brine (40 mL) and DCM (40 mL) was added to the mixture and the organic phase was separated. The aqueous phase was extracted once with DCM (40 mL). The combined organic phases were dried over anhydrous Na_2SO_4, filtered, and concentrated *in vacuo*. The crude mixture was purified by flash chromatography (50 %

EtOAc/hexane) to afford 450 mg of compound **4.19** as a clear yellow oil (58 %). R_f 0.43 (50% EtOAc/hexane)

^{1}H NMR (400MHz, CDCl$_3$) δ = 7.48 - 7.42 (m, 2H), 7.40 - 7.34 (m, 2H), 7.33 - 7.28 (m, 1H), 6.85 (d, J = 8.1 Hz, 1H), 6.80 (d, J = 2.0 Hz, 1H), 6.72 (dd, J = 8.1, 2.1 Hz, 1H), 6.22 (s, 1H), 5.14 (s, 2H), 3.90 (s, 3H), 3.72 - 3.68 (m, 4H), 3.49 - 3.45 (m, 4H), 3.32 (s, 2H) ^{13}C NMR (101MHz, CDCl$_3$) δ = 149.7, 148.8, 147.0, 137.3, 132.6, 128.5, 127.8, 127.2, 121.7, 120.3, 114.2, 112.3, 75.4, 71.1, 66.3, 56.1, 49.5, 38.9 HRMS (ESI) calcd for C$_{22}$H$_{24}$N$_2$O$_3$ (M+H)$^+$ 365.186 found 365.18597

2-(3-Methoxy-4-phenethylbenzyl)-3-(phenylamino)acrylonitrile (4.20) 2-(3-Methoxy-4-phenethylbenzyl)-3-morpholinoacrylonitrile (**4.19**) (450 mg, 1.23 mmol, 1.0 equiv) was suspended in isopropanol (10 mL) to form a cloudy solution. Aniline hydrochloride (176 mg, 1.36 mmol, 1.1 equiv) was added to the mixture then heated at reflux for 30 minutes. The reaction mixture was cooled to room temperature and quenched with water (4 mL) followed by cooling in an ice bath for 30 minutes. Resulting precipitate was collected to afford 312 mg of brownish/white powder (87 %). The crude compound **4.20** was used directly in the next step without further purification.

5-(4-(Benzyloxy)-3-methoxybenzyl)pyrimidine-2,4-diamine (4.21) 2-(4-((3-Fluoro-4-**2-(3-**methoxy-4-phenethylbenzyl)-3-(phenylamino)acrylonitrile (**4.20**) (300 mg, 0.809 mmol, 1.0 equiv) and guanidine hydrochloride (115 mg, 1.21 mmol, 1.5 equiv) was suspended in EtOH (5 mL). Sodium ethoxide (0.451 mL, of 21 % wt in ethanol solution, 1.21 mmol, 1.5 equiv) was added to the reaction mixture drop wise at room temperature then stirred at reflux overnight. The mixture was cooled to room temperature and sodium hydroxide (2.0 mL, 2.0 M solution) was added. The mixture was cooled to 5 °C and allowed to precipitate for 15 minutes. The precipitate was filtered and washed with a cold mixture of ethanol/water (1:1), EtOAc, hexane and dried *in vacuo.* The crude compound was purified by flash chromatography to produce 153 mg of compound **4.21** as a white powder (56 %) R_f 0.62 (50 % MeOH/DCM)

^{1}H NMR (498MHz, DMSO-d$_6$) δ = 7.45 (s, 1H), 7.42 - 7.38 (m, 2H), 7.38 - 7.33 (m, 2H), 7.32 - 7.27 (m, 1H), 6.90 (d, J = 8.2 Hz, 1H), 6.86 (d, J = 2.0 Hz, 1H), 6.66 (dd, J = 8.2, 2.0 Hz, 1H),

6.06 (br s, 2H), 5.68 (s, 2H), 5.00 (s, 2H), 3.71 (s, 3H), 3.50 (s, 2H) ^{13}C NMR (126MHz, DMSO-d_6) δ = 162.1, 161.9, 155.0, 148.9, 146.0, 137.2, 132.9, 128.3, 127.6, 127.6, 120.1, 113.7, 112.8, 106.0, 70.0, 55.5, 32.1. HRMS (ESI) calcd for $C_{19}H_{20}N_4O_2$ (M+H)$^+$ 377.1674 found 377.1659

Calibration curve of **1.23** based on UV absorbance
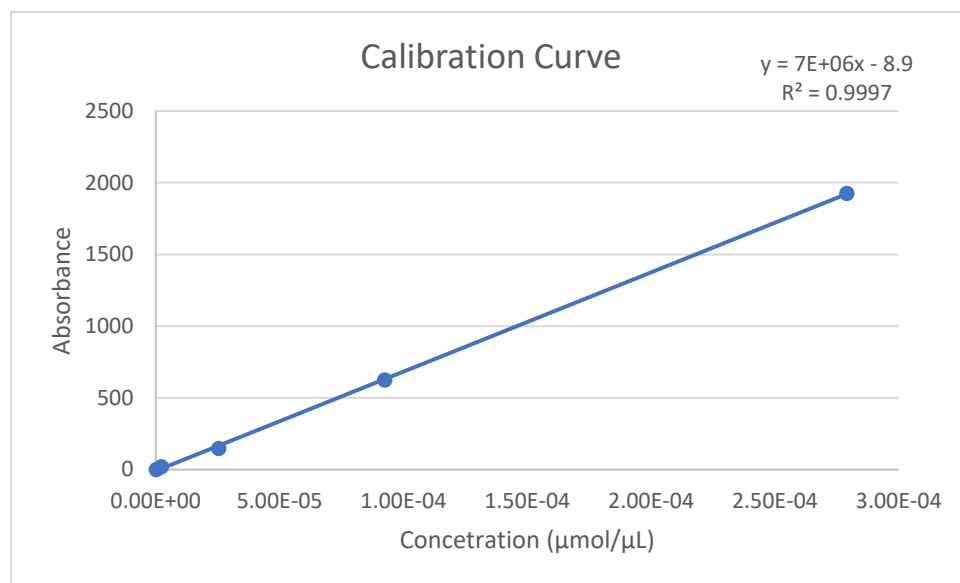
Appendix 1. Calibration curve of **1.23** used to determine the molar activity of [^{18}F]**1.23**